A SYSTEMATIC SIX-DIMENSIONAL SCALING SOLUTION SEARCH

A Systematic Scaling Solution Search in Six-Dimensional Inflation

By Jared J.H. Enns, BSc (Hons)

A Thesis Submitted to the School of Graduate Studies
in Partial Fulfillment of the Requirements for the
Degree of Master of Science

McMaster University MASTER OF SCIENCE (2016) Hamilton, Ontario (Physics)

TITLE: A Systematic Scaling Solution Search in Six-Dimensional Inflation AUTHOR: Jared J.H. Enns, BSc (Hons) (University of Winnipeg) SUPERVISOR: Professor Clifford P. Burgess NUMBER OF PAGES: xxiv, 138

MCMASTER UNIVERSITY

Lay Abstract

Faculty of Science
Department of Physics and Astronomy

Master of Science

A Systematic Scaling Solution Search in Six-Dimensional Inflation

by Jared J.H. Enns

When looking out at the night sky, we see a universe that is extremely flat and looks the same no matter what direction we stare. However, these present-day observations require the universe to have begun under very specific circumstances, which is not something that naturally occurs; think about what is necessary to hit a hole-in-one with a golf club: a very precise and specific shot is required. The theory of Cosmological Inflation—a period of rapid expansion in the early universe—is the current leading theory proposed to explain these observations. In our exploration, we aim to study inflation from a higher-dimensional perspective in which two extra spatial dimensions are added to our usual three. Ultimately, we find three classes of solutions, two of which exist outside of the regimes usually studied, that have the potential both to explain current observations, and also be useful tools in future explorations.

MCMASTER UNIVERSITY

Abstract

Faculty of Science
Department of Physics and Astronomy

Master of Science

A Systematic Scaling Solution Search in Six-Dimensional Inflation

by Jared J.H. Enns

We explore the mechanics of inflation within simplified extra-dimensional models involving an inflaton interacting with a Einstein-Maxwell system in two extra dimensions. The models are complicated enough to include a stabilization mechanism for the extra-dimensional radius, but simple enough to solve the full six-dimensional field equations. After performing a consistent truncation, which guarantees our six-dimensional equations are equivalently satisfied by the four-dimensional equations of motion, we explore (numerically and analytically) the power-law solutions evident in our initial parameter search. After a comprehensive search for potential power-law scaling solutions in both six and four dimensions, we find two that give rise to interesting inflationary dynamics. They both can generically exist outside of the usual four dimensional effective theory, and yet, we still trust them since our truncation is consistent. One of these is a dynamical attractor whose features are relatively insensitive to initial conditions, but whose slow-roll parameters cannot be arbitrarily small; the other is not an attractor but can roll much more slowly, until eventually transitioning to another solution due to its unstable nature. We present a numerical and analytic discussion of these two solutions. Four of the appendices contain calculations in more explicit detail than are performed in the main text, while a fifth contains a representative *Mathematica* worksheet and the sixth contains the general results of the systematic sweep for scaling solutions.

Acknowledgements

I thank, first and foremost, my supervisor, professor, and one helluva guy, Dr. Cliff Burgess, for his academic and financial support during this project. Additionally, I would like to acknowledge my collaborators on this project: Dr. Subodh Patil for giving this project the breath of life, and Peter Hayman for being a very willing sounding board and accomplice. I am grateful for the insight and feedback provided by members of my supervisory committee as well: Dr. Sung-Sik Lee and Dr. Peter Sutherland. Nick Reid first taught me how to use *Mathematica* (or at least takes the credit for it) and so I guess I owe him thanks. I would also like to thank my undergraduate supervisor and mentor, Dr. Andrew Frey, who encouraged me to both pursue a graduate degree and get out of Winnipeg.[1] Thanks for the push.

Computational and nutritional sustenance was partially provided by the Perimeter Institute for Theoretical Physics. Driver *extraordinaire* Werner Friesendorf provided semi-weekly transportation, entertainment, and an unending stream of wisdom. Thanks to you, the hour-long trek between Hamilton and Waterloo was always a joy. Additional financial, spatial, computational, and social supports were provided by the Department of Physics and Astronomy at McMaster University. The administrative team (Cheryl, Tina, and Rose) made life—particularly the bureaucratic aspects—at McMaster as easy as possible.

Finally, I coudn't've completed this degree without the support of my fmaily around me. I can never thank enough my parents, John and Sandi Enns, who never stopped encouraging or supporting me during my educational pursuits. And then, of course I wish to acknowledge the ceaseless support of my wife, Tonya Enns, who was willing to both follow me on this adventure, and work so I could enjoy the luxurious life of a graduate student in theoretical physics. You made sure I had a lunch everyday, a supper every night, clean clothes every week, and a home every second. You are my momentum, the source of my energy, the love of my life.

[1] While potentially surprising to the general reader, those of us born in this city do often need an external force to displace us.

Table of Contents

List of Figures

List of Tables

List of Abbreviations

2D	**2** (two)-**D**imension(s)(al)
4D	**4** (four)-**D**imension(s)(al)
4DEF	**4D E**instein **F**rame
6D	**6** (six)-**D**imension(s)(al)
CMB	**C**osmic **M**icrowave **B**ackground
EFEs	**E**instein **F**ield **E**quation**s**
EOM(s)	**E**quation(**s**) **O**f **M**otion
FRW	**F**riedmann-**R**obertson-**W**alker
GR	**G**eneral Theory of **R**elativity
KK	**K**aluza-**K**lein
LHS	**L**eft-**H**and **S**ide
RHS	**R**eft-**H**and **S**ide
UV	**U**ltra**V**iolet

Physical Constants

speed of light in vacuum	$c = 2.997\,924\,58 \times 10^{8}\,\mathrm{m\,s^{-1}}$
Newtonian constant of gravitation	$G = 6.674\,08(31) \times 10^{-11}\,\mathrm{Nm^2/kg^2}$
Planck constant	$h = 6.626\,070\,040(81) \times 10^{-31}\,\mathrm{J\,s}$
	$= 4.135\,667\,662(25) \times 10^{-15}\,\mathrm{eV\,s}$
(Reduced) Planck constant	$\hbar = 1.054\,571\,800(13) \times 10^{-34}\,\mathrm{J\,s}$
	$= 6.582\,119\,514(40) \times 10^{-16}\,\mathrm{eV\,s}$
fine-structure constant	$\alpha = 1/137.035\,999\,139(31)$
elementary charge $\sqrt{4\pi\alpha\epsilon_0\hbar c}$	$e = 1.602\,176\,620\,8(98) \times 10^{-19}\,\mathrm{C}$
Planck mass $\sqrt{\hbar c/G}$	$M_p = 2.176\,470(51) \times 10^{-8}\,\mathrm{kg}$
	$= 1.220\,910(29) \times 10^{19}\,\mathrm{GeV}/c^2$
Planck length $\sqrt{\hbar G/c^3}$	$L_p = 1.616\,229(38) \times 10^{-35}\,\mathrm{m}$
Planck time $\sqrt{\hbar G/c^5}$	$T_p = 5.391\,16(13) \times 10^{-44}\,\mathrm{s}$

Notes:

- All numerical values are taken from CODATA 2014 [2].
- The speed of light in a vacuum is exact due to the SI definition of the metre.
- Numbers in parentheses indicate the uncertainty in the last digits.
  For example, $1.007\,12(69) = 1.007\,12 \pm 0.000\,69$.
- This thesis utilizes natural unit conventions as decribed in the Introduction.

Declaration of Academic Achievement

I, Jared J.H. Enns, declare that this thesis titled, "A Systematic Scaling Solution Search in Six-Dimensional Inflation" and the work presented in it are my own. The following outlines the contributions of others to this thesis:

- Chapter 1 presents background information relevant to the thesis. While the knowledge is common, the presentation is original.
- The 6D action first mentioned in (2.1) was proposed by Cliff Burgess. The subsequent derivation of the field equations and truncation are original.
- Section 3.2 follows a calculation first performed by Peter Hayman, which itself is based on one previously performed by Subodh Patil. The discussion of Section 3.2.1 was first proposed by Peter Hayman.
- The existence of the Cradle Solution presented in Section 3.3 was first discovered by Peter Hayman, but the particular solutions presented in this thesis are original.
- The relationship in (4.5) was first noted by Peter Hayman.
- The solutions to the stability calculations presented in Appendix F follow an *ansatz* proposed by Peter Hayman, particularly (F.5). The stability of the Attractor Solution was first shown by Peter Hayman.

Portions of this thesis have been accepted for publication in [3].

To my wife, Tonya.

Introduction

We begin the thesis with a brief introduction to our study's place in the field of extra-dimensional cosmic inflationary models. This introduction provides the context, and motivation for, many of the unique and important features of our work. While we outline the important features here, later chapters of the thesis expand upon these ideas in much greater detail, cementing their relevance to our project.

This thesis has its roots in a collaborative project whose aim is to investigate the features of a six-dimensional inflationary universe. The results of the overall project can be found in [3]. While this Introduction provides context and motivation for the project at large, this thesis focuses on the power-law solutions we discoverand the numerics since these areas are the focus of this author and constitute the major contributions thereto.

We close with a brief outline of the Notations and Conventions used throughout the thesis.

Cosmological Context and Motivation

In the beginning, our universe formed as the result of the most incredibly fine-tuned system perhaps to ever evolve… or so it would seem given the glimpses into this history we have received thus far. These special and very finely-tuned initial conditions are unnatural in the sense that it is highly improbable that nature, in all her random glory, would be so precise. In an effort to explain this unnatural start to our universe, a sufficiently long period of accelerated expansion—known as inflationary acceleration or *cosmic inflation* [4–6]—is required. While other models exist (involving crunches and bounces [7–13]), models of cosmic inflation seem, at present, to be the most successful explanation due to the context they provide to study the evolution of the early universe.

However, the theory of cosmic inflation is not without its own issues [14–16], most of which are due to the fact that it would occur during an epoch when our universe was at extremely high temperatures and energies. Typically, it is necessary to describe these problems from the perspective of an effective theory, a theory which

is valid below a certain cut-off energy. The act of passing from the low-energy effective theory to the higher general theory is known as ultraviolet (UV) completion. So, we strive to present simple (but not too simple) models of inflation that are well-poised to answer UV questions using extra dimensions.

It is natural to treat these issues within an extra-dimensional context because extra dimensions form a natural part of any UV-complete theory, usually in a more distinctly stringy context. We work within the simplest extra-dimensional framework that still produces results which can be generalized to higher dimensions: two extra dimensions modeled as a sphere. We avoid working with only one dimension for two main reasons. The first is that analyses involving one extra dimension contain many features which often do not necessarily generalize to higher dimensions. Additionally, models with only one extra dimension have been actively studied in cosmology [17–21], and so, by committing to two extra dimensions, we avoid searching under this already-well-explored lamppost.

Theories with more than one extra dimension have not been well-explored. Even in a few cases that do exist [22–28], these are usually approached from a string theory perspective. However, our studies differ in that most other treatments study only an effective four-dimensional (4D) theory. This typically involves restricting analysis to energy scales below a natural high energy scale, the Kaluza-Klein (KK) scale, m_{KK}.[1] While there is nothing inherently wrong with this approach, it restricts the study to regimes in which solutions are not trusted when parameters (Hubble's in particular) are greater than m_{KK}, since, in an effective theory, one does not trust anything above the cutoff scale (in this case, m_{KK}). Thus, this approach only looks for inflationary solutions through a narrower-than-necessary spyglass. We widen our lens by solving all the 6D field equations explicitly. This is one of the important distinctions of our models.

A second important feature of the models we investigate is that we include a mechanism for modulus stabilization, where the modulus is a quantity related to the size of the extra dimensions. Since the development of modulus stabilization mechanisms, such as the flux stabilization [29, 30] that we employ in our analysis, modulus stabilization has become a critical component of inflationary models that wish to be taken seriously.

Another attractive feature of our models is that they are *Goldilocks* models. This does not mean that they trespass into the homes of forest animals, eat their breakfasts, break their chairs, and sleep in their beds, but rather they are named for the

[1] The KK scale, m_{KK} is the energy scale associated with the size of the extra dimensions, so $m_{KK} = 1/b$, where b is the radius of extra dimensions.

items of the littlest bear whose possessions are consistently "just right". Our models are "just right" in the sense that they are complicated enough to include features such as flux stabilization, while simple enough to avoid complicated string physics, which can often accompany such extra-dimensional inflationary tales. We accomplish this balance by working in a system with only two dimensions, which, as aforementioned, is complicated enough to avoid the non-generalizable features of a single extra dimension, but simple enough in the sense that we have included the bare minimum number of fields needed to achieve both inflation and modulus stabilization.

The final interesting property of our analysis came as a revelation during the analysis itself, as opposed to a motivating, attractive feature. We find our power-law solutions give rise to an alluring relationship between the duration of inflationand the size of the extra dimensions. This is appealing since it is a relationship between two characters that we would not naïvely expect to be related to each other. One the one side, we have inflation: a theory that predicts a large universe; one the other side, we have another physical scale: that of the extra dimensions, which can also be large. This perhaps hints at a fundamental connection between the two parameters.

The above four properties highlight the attractive, general features of these models: they solve exactly the general 6D field equations, they include flux stabilization, they are Goldilocks models, and they revealed an interesting numerological relationship between the inflation of the 4D universe and the size of the extra dimensions. For these reasons, we hope these models can be of use in the future study of extra-dimensional inflation.

Our Study

The system we study is an Einstein-Maxwell-Scalar system. The Einstein component is necessary due to the fundamental role gravity plays in any cosmological study. The Maxwell field is used to thread (only) the extra dimensions with flux to provide a means by which the radion can be stabilized, and the scalar field, ϕ, is performing the role of an extra-dimensional inflaton. While we begin with the general theory in the full 6D, we eventually pare it down into a 4D representation. We do this by dimensionally-reducing the extra dimensions; this leaves us with a new 4D potential that intuitively captures the dynamics of the extra-dimensions in the form of the radion, ψ. This is referred to as a *truncation* of our 6D action. Moreover, we actually perform a *consistent truncation*, which means that our 4D theory is not

merely an effective theory, but exactly equivalent to the 6D theory: essentially, we have not lost anything by choosing to work in the 4D theory. We situate ourselves in the 4D realm for a number of reasons: the first (already mentioned) reason is the gain of an intuitive 4D potential. Two other important reasons are the fact that we find ourselves living in a 4D world, making the analysis more intuitive, and for numerical simplicity during the actual numerical integration.

Once we arrive in 4D, we use *Mathematica* [31] to numerically integrate our equations of motion (EOMs) to study the behaviour of the fields at play. Our initial integrations reveal many regions that seemed to follow power-law relationships (which we will also refer to as scaling solutions) and so we perform a systematic power-law analysis on the system. This analysis reveals two different, interesting classes of scaling solutions,[2] which we outline and discuss in great detail in Chapter 4 of the main text.

We hope that these Goldilocks scaling solutions, with interesting numerology, provide new shovels so that the extra-dimensional-cosmic-inflationary sandbox may be dug up in new ways. The systematic scaling solution search performed by this author not only enables us to better understand the solutions we see numerically, but ultimately reveals two of the three interesting solutions, one of which we would never have been found numerically due to its unstable nature.

Outline

The thesis is divided into four chapters: Chapter 1 details relevant background information on cosmology and inflation. Chapter 2 introduces the 6D model we use, as described above, and shows how we reduce it into an equivalent 4D model so that we can numerically integrate it in Chapter 3. Then, Chapter 4 describes the bulk of the work performed by this author: the results of the systematic power-law analysis. The main text of the thesis ends with a chapter of Conclusions that summarize the project and its main points.

We close the thesis with six appendices. Appendices A, B, C, and F contain more mathematically detailed analyses of calculations in the main text. Appendix D summarizes our systematic power-law analysis and details through all the cases

[2] Our numerical integration also yields a solution we refer to as a Cradling solution, since the radion's potential acts as a cradle by gentling bringing it to settle on its minimum while the inflation is still inflating. While this solution has some interesting properties discussed in [3], it will only be briefly mentioned in this thesis, since this author's focus was on the power-law analysis and solutions.

that are relevant to the main discussion, explaining why this is the case in each situation. Finally, Appendix E contains raw *Mathematica* files used in our numerical analysis and itemizes the specific numerical values required to produce all the figures in the main text.

Notation and Conventions

Throughout this thesis, we use natural units, in that the speed of light and the reduced Planck constant to unity—i.e., $c = \hbar = 1$—and use Planck masses that include a factor of 8π, the so-called *reduced* Planck mass:

$$M_p = \sqrt{\frac{\hbar c}{8\pi G}} \quad \text{or} \quad M_p = \frac{1}{\sqrt{8\pi G}}, \text{ in our notation.}$$

Lower-case Latin indices from the first half of the alphabet—usually i, j, k, l—generally run over the regular spatial dimensions (1, 2, 3). Lower-case Latin indices like m, n, r, s from the second half of the alphabet are reserved for extra-dimensional coordinate labels (4, 5). Greek indices such as μ, ν, ρ, σ generally label the usual four spacetime dimensions (0, 1, 2, 3), where 0 is the time coordinate. Capital Latin indices (M, N, ...) are fully general and can refer to any coordinate label.

Einstein's summation convention, in which repeated indices are summed, is exploited throughout. We use the East Coast, or "mostly plus", metric signature, which renders the Minkowski metric as $\mathrm{d}s^2 = \eta_{\mu\nu}\mathrm{d}x^\mu \mathrm{d}x^\nu = -\mathrm{d}t^2 + \delta_{ij}\mathrm{d}x^i\mathrm{d}x^j$, and Weinberg curvature conventions [32] so that the Riemann tensor and Einstein equations are:

$$R^\mu{}_{\nu\rho\sigma} = \Gamma^\mu_{\nu\rho,\sigma} - \Gamma^\mu_{\nu\sigma,\rho} + \Gamma^\mu_{\sigma\lambda}\Gamma^\lambda_{\nu\rho} - \Gamma^\mu_{\rho\lambda}\Gamma^\lambda_{\nu\sigma}\,, \qquad \text{and} \qquad G_{MN} + \kappa^2 T_{MN} = 0\,,$$

where G_{MN} is the Einstein tensor, a comma subscript indicates a derivative:

$$A_{,M} := \partial_M A = \frac{\partial A}{\partial x^M}\,,$$

and a semi-colon subscript denotes a covariant derivative: $T^{\mu\nu}{}_{;\mu} := \nabla_\mu T^{\mu\nu}$.

Where ambiguities may arise, we distinguish 6D quantities from their 4D counterparts with a caret ($\hat{}$). Additionally, primes ($'$) denote derivatives with respect to

6D Friedmann-Robertson-Walker (FRW) time while overdots ($\dot{}$) denote derivatives with respect to 4D FRW time. Explicitly,

$$x' := \frac{\mathrm{d}x}{\mathrm{d}\hat{t}} \qquad \text{versus} \qquad \dot{x} := \frac{\mathrm{d}x}{\mathrm{d}t}\,.$$

Chapter 1

Background Information: Cosmic Inflation

Before attacking our model, we must arm ourselves with weapons to understand cosmic inflation: critical background information needed to understand the bulk of the project. Not surprisingly, this consists of a brief introduction to two topics: cosmology and inflation.

Since it was first proposed, the Big Bang Theory has held up quite well to observational tests. However, in order to be a successful description of our universe's origins, a fine-tuned and particular set of initial conditions are required to explain the current observed state of the universe. The two problems that collectively describe the necessary fine-tuned initial conditions of our universe are the Horizon Problem and the Flatness Problem. Enter the theory of Cosmic Inflation. Cosmic Inflation is a proposed period of continuous accelerated expansion in the universe's early history, originally designed as a means to solve the two aforementioned problems [4]. However, it has held its ground continuously against observations since its original postulation.

We start this chapter with an explanation of the structure of our universe and the energy content we dump into it. This provides us our first glance at power-law relationships, which play a critical role in the bulk of this thesis. We follow this introduction to cosmology with a brief description of the Horizon and Flatness Problems and conclude with a description of Cosmic Inflation and how it is well-positioned to solve the above problems.

1.1 A Friedmann-Robertson-Walker Universe

Einstein's General Theory of Relativity (GR) presents a beautiful relationship between energy content and geometry; his equations describe the effect matter has

on the geometry of spacetime and how that geometry in turn affects the motion of matter:

$$G_{\mu\nu} := R_{\mu\nu} - \frac{1}{2}Rg_{\mu\nu} = -\kappa^2 T_{\mu\nu}\,, \tag{1.1}$$

where $G_{\mu\nu}$ is the Einstein tensor, $R_{\mu\nu}$ and R are the Ricci tensor and scalar respectively that describe the curvature of spacetime, $\kappa = 1/M_p = 1/\sqrt{8\pi G}$ with G Newton's constant, and $T_{\mu\nu}$ is the stress-energy tensor that specifies the energy content of the universe. We pick a geometry first using the so-called Cosmological Principle: an assumption that the universe is spatially homogeneous and isotropic.[1]

In GR, we use a metric to define infinitesimal distances in our spacetime. The most general metric consistent with the our assumptions of isotropy and homogeneity is the Friedmann-Robertson-Walker (FRW) metric:

$$\mathrm{d}s^2 = -\mathrm{d}t^2 + a^2(t)\left[\frac{\mathrm{d}r^2}{1-kr^2} + r^2\mathrm{d}\Omega^2\right], \tag{1.2}$$

where $\mathrm{d}\Omega^2 = \mathrm{d}\theta^2 + \sin^2\theta\mathrm{d}\phi^2$ is the metric on a two-sphere, $a(t)$ is the scale factor, a dimensionless quantity that describes the expansion of the universe such that the proper distance between two objects during some period of time, t, is given by $d(t) = a(t)d_0$ (clearly $a_0 := a(t_0) = 1$; usually, t_0 is taken as the present time) and k is a quantity that sets the curvature of the spatial slices with $k \in \{-1, 0, 1\}$. The case $k = 0$ corresponds to no curvature (i.e., flat slices), $k = -1$ describes negative curvature—hyperbolic surfaces, often called open—while the $k = 1$ case gives us positive curvature wherein spatial slices are described by spheres. Similarly, we call this geometry closed.

In order to do cosmology, we wish to understand the time-evolution of the scale-factor. This can be determined by dumping an appropriate geometry and matter content into (1.1). Presently, we only have one of these ingredients: we have a description of the geometry of the universe given by (1.2), but we still need to introduce some matter, or energy content, into our universe. We choose the most general stress-energy tensor consistent with our assumptions of isotropy and

[1] While originally a simplifying and conceptually pleasing assumption, the Cosmological Principle has also been upheld by recent observations. The most successful observation is perhaps the radiation of the Cosmic Microwave Background (CMB), which is observed to have a uniform temperature to one part in 10^5.

homogeneity, that of a perfect fluid:

$$T_{\mu\nu} = \begin{pmatrix} \rho & 0 \\ 0 & p\, g_{ij} \end{pmatrix}, \tag{1.3}$$

where ρ and p are the energy density and pressure of the fluid respectively. Recall that Latin indices run only over spatial coordinates.

So, now that we have both a geometry (FRW) and matter content (a perfect fluid), we are ready to dump our ingredients into Einstein's equations. This gives

$$\left(\frac{\dot{a}}{a}\right)^2 = \frac{\rho}{3M_p^2} - \frac{k}{a^2}, \tag{1.4}$$

for the 00-component where overdots refer to derivative with respect to time, t, while the spatial components yield[2]

$$2\,\frac{\ddot{a}}{a} + \left(\frac{\dot{a}}{a}\right)^2 = -\left(\frac{p}{M_p^2} + \frac{k}{a^2}\right). \tag{1.5}$$

Subtracting (1.4) from (1.5) to eliminate the first order terms in the spatial equation, we arrive at the more common rendering of the second equation

$$\frac{\ddot{a}}{a} = -\frac{1}{6M_p^2}\,(\rho + 3p)\,. \tag{1.6}$$

Together, (1.4) and (1.6) are known as the Friedmann equations.[3] If the relationship between ρ and a is known, the Friedmann equation is sufficient to solve for $a(t)$.

The easiest way to pursue this is by exploiting conservation of energy. In GR, this takes the form of $T^{\mu\nu}{}_{;\mu} = 0$. If we look at the zeroth component (i.e., $\nu = 0$) of this equation, we have

$$\dot{\rho} = -3H(\rho + p)\,, \tag{1.7}$$

where $H := \dot{a}/a$ is the Hubble parameter.

[2] Note that we only have one distinct equation for the spatial coordinates (instead of three) due to the isotropy of the FRW metric.

[3] It is common practice to refer to the first of these, (1.4), as *the* Friedmann equation. We follow this convention here, but, when necessary, refer to (1.6) as the *second* Friedmann equation.

Now that we have two differential equations—(1.4) and (1.7)—that tell us how the scale factor a evolves for a given matter content ρ, what's the matter? We will examine the four energy contents that are commonly considered in cosmological studies: non-relativistic matter, radiation (which includes relativistic matter), curvature, and vacuum-energy (also referred to as dark energy). This exploration is particularly relevant to our project since it introduces the concept of power-law relationships (which play a fundamental role in later chapters): we show that ρ depends on a to various powers.

The first thing we do is model our perfect fluid as one that abides by an equation of state

$$p = w\rho\,, \tag{1.8}$$

where w, a constant, defines the ratio of pressure to density. Then, using the equation of state, the conservation of energy equation, (1.7), becomes

$$\frac{\dot{\rho}}{\rho} = -3H\,(1+w)\,, \tag{1.9}$$

which we can integrate to find

$$\rho = \rho_0\, a^{-3(1+w)}\,. \tag{1.10}$$

To see what values of w are allowed, we investigate the properties of our universe's constituents.

A matter-dominated universe is made up of non-relativistic particles that are, essentially, a collection of collisionless particles. As such, we expect very little pressure: $p_M \approx 0$. To see this, recall that the ideal gas law says $p \propto T/V$. Then, since $\rho = m/V$, we see $w_M = p/\rho \propto T/m \approx 0$ since, for non-relativistic matter, $m \gg T$. Using $w_M = 0$ in (1.10), we find

$$\rho_M \propto a^{-3}\,. \tag{1.11}$$

This is an intuitive result: as a matter-dominated universe expands, the number density of particles will just decrease as the volume of the universe increases.

When discussing a radiation-dominated universe, we refer not only to photons, but any particle moving relativistically. We can find the ratio of p_R/ρ_R by comparing the traces of the stress-energy tensor. For a Maxwell Lagrangian, the associated

stress-energy tensor is traceless.[4] Modeling radiation as a perfect fluid, we should also be able to take the trace of (1.3) and set this equal to zero, so

$$T = T^{\mu}{}_{\mu} = g^{\mu\alpha}T_{\alpha\mu} = -\rho + 3p = 0 \implies p_R = \frac{1}{3}\rho_R \implies w_R = \frac{1}{3}. \tag{1.12}$$

So, this tells us that the energy density of radiation scales as

$$\rho_R \propto a^{-4}, \tag{1.13}$$

again, a result for which we have an intuition. As the the volume of the universe increases, the number density of photons (and other relativistic particles) decreases, just like in the matter case. However, the extra a^{-1} comes from additional loss of energy due to the redshift of the photons: $E_\gamma = \omega = 1/\lambda$, but wavelengths increase as the universe expands, and so $E \propto a^{-1}$.

We can also observe the energy density contributed by the curvature of the universe.[5] In this case, the relationship can be deduced from the Friedmann equation (1.4). Since the energy density in (1.4) is the sum over all the fluid components—i.e., $\rho = \sum \rho_i$—it is convenient to classify k/a^2 as an energy density as well. To this end, we define

$$\rho_C = -\frac{3kM_p^2}{a^2} \implies \rho_C \propto a^{-2} \implies w_C = -\frac{1}{3}. \tag{1.14}$$

Finally, we discuss a vacuum-energy-dominated universe: an energy density due to the empty space of the vacuum itself. In this case, we demand that the vacuum be Lorentz invariant, which means it needs a Lorentz invariant stress-energy tensor. This requires $T_{\mu\nu} \propto g_{\mu\nu}$ since $g_{\mu\nu}$ is the only Lorentz invariant tensor with two lower indices. This forces $p_\Lambda = -\rho_\Lambda$ and so $w_\Lambda = -1$. This provides us the relationship between ρ_Λ and a:

$$\rho_\Lambda \propto a^0, \tag{1.15}$$

showing that the energy density of the vacuum is constant.

[4] Proof: $L_{\text{EM}} = \frac{1}{4}F^{\mu\nu}F_{\mu\nu}$, and the stress-energy tensor is defined as $T_{AB} := 2\frac{\delta L}{\delta g^{AB}} - g_{AB}L$. So, $T^{\text{EM}}_{\mu\nu} = F_{\mu\alpha}F_{\nu}{}^{\alpha} - \frac{1}{4}g_{\mu\nu}F_{\alpha\beta}F^{\alpha\beta} \implies T^{\text{EM}} = F_{\mu\alpha}F^{\mu\alpha} - \frac{1}{4}(4)F_{\alpha\beta}F^{\alpha\beta} = 0$. Hence, $T^{\text{EM}}_{\mu\nu}$ is traceless.

[5] Note that the curvature itself does not contribute energy to the universe, but rather its term k/a^2, as it appears in the Friedmann equation, contributes something analogous to an energy density.

Now that we understand how ρ relates to a for various fluids, it is pertinent to examine the dependence of a on t. If we assume ρ depends on a in the form of (1.10), we can substitute this into the Friedmann and integrate. We also make the well-supported assumption that the universe is dominated by only one fluid at any given time and so we do not have to worry about summing over multiple ρ_i. This procedure shows us

$$a = a_0 \left(\frac{t}{t_0}\right)^{2/n}, \tag{1.16}$$

where a_0 and t_0 are constants of integration, and $n = 3(1+w)$. In other words, $a \propto t^{2/n}$ if $\rho \propto a^{-n}$. We can use this last proportionality to conveniently track how a is related to the important cosmological quantity $(aH)^{-1}$ using the Friedmann equation (without curvature):

$$\rho \propto a^{-n} \implies H \propto \sqrt{\rho} \propto a^{-n/2} \implies aH \propto a^{1-n/2} \implies (aH)^{-1} \propto a^{n/2-1}. \tag{1.17}$$

Note that the above two equations are only valid for $n \neq 0$. In the case of vacuum-energy domination, we have $w_\Lambda = -1$ which implies $n = 0$. The Friedmann equation shows that, if ρ_Λ is constant, H is constant as well and we can easily integrate:

$$\frac{\dot{a}}{a} = H = \text{const.} \implies \frac{\mathrm{d}a}{a} = H\,\mathrm{d}t \implies a \propto e^{Ht} \implies (aH)^{-1} \propto e^{-Ht}. \tag{1.18}$$

A summary of all the power-law relationships for the various fluids can be found in Table 1.1. We can combine these results into a single equation which describes the total energy density of the universe by summing up the contributions from each fluid:

$$\rho(a) = \rho_{\Lambda,0} + \rho_{C,0}\left(\frac{a}{a_0}\right)^{-2} + \rho_{M,0}\left(\frac{a}{a_0}\right)^{-3} + \rho_{R,0}\left(\frac{a}{a_0}\right)^{-4}, \tag{1.19}$$

where $\rho_{i,0}$ is the initial energy density of each fluid.

1.2 A Finely-Tuned Universe

While the previous section provides a reliable description of the universe according to present observations, the universe rudely demands special initial conditions

Energy Content	w	n
Matter	0	3
Radiation	$\frac{1}{3}$	4
Curvature	$-\frac{1}{3}$	2
Vacuum	-1	0

TABLE 1.1: In this table, we summarize the power-laws, given a particular dominating form of energy. Here, $w = p/\rho$, and $-n$ is the power on the scale factor. For $n \neq 0$, $\rho \propto a^{-3(1+w)} = a^{-n}$, where $a \propto t^{2/n}$. As described in the main text, the case $n = 0$ corresponds to $a \propto e^{Ht}$.

for it to actually present itself as we observe it: it demands to be incredibly flat (the Flatness Problem) and incredibly homogeneous (the Horizon Problem). This section describes these two problems, both of which a period of Cosmic Inflation in the early universe is well-poised to solve.

1.2.1 Flatness Problem

The Flatness Problem, perhaps unsurprisingly, asks "why is the universe so flat?" Or, perhaps more accurately, "how was the early universe so specifically and specially poised to create a universe that we measure to be so flat today?" Let's paint the picture.

We start by defining the critical density, ρ_c, such that a flat universe ($k = 0$) has $\rho = \rho_c$. From (1.4), we see that $\rho_c = 3M_p H^2$. Next, we define the density parameter as the ratio of the energy density to the critical density, $\Omega = \rho/\rho_c$, which can be used to rewrite the Friedmann equation as

$$\Omega - 1 = \frac{k}{(aH)^2}\,. \tag{1.20}$$

From the above, we find the following conditions on Ω:

$$\begin{aligned} k = 0 \quad &\text{(flat)} \quad \Longrightarrow \quad \Omega = 1\,, \\ k < 0 \quad &\text{(open)} \quad \Longrightarrow \quad \Omega < 1\,, \\ k > 0 \quad &\text{(closed)} \quad \Longrightarrow \quad \Omega > 1\,. \end{aligned} \tag{1.21}$$

In a matter- or radiation-dominated universe, we previously showed that $\rho_M \propto a^{-3}$ and $\rho_R \propto a^{-4}$. Because a grows in an expanding universe, these both fall *faster* than the curvature term in the Friedmann equation, which follows $\rho_C \propto a^{-2}$. So, given *any* spatial curvature in the early universe, the curvature term becomes more and more significant as time goes on. Because observations tell us $\Omega_{\text{now}} \sim 1$,[6] to within about 10%, Ω would have had to be even more incredibly close to unity in the past. We can perform a quick order of magnitude calculation to demonstrate this.

Let's check what $\Omega(t_{\text{eq}}) = \Omega_{\text{eq}}$ would have had to be at the time of matter-radiation equality. Working backwards in time, we are leaving a period of matter-domination. Checking (1.17) and referring back to Table 1.1, we see that

$$aH \propto a^{1-3/2} = a^{-1/2} \implies (aH)^{-2} \propto a\,. \tag{1.22}$$

Using this result with (1.20), we can compute the deviation of Ω_{eq} from unity. Working backwards from today at which time observations show $\Omega_0 - 1 \approx 0.1$, we find

$$\Omega_{\text{eq}} - 1 \propto a_{\text{eq}} \implies \Omega_{\text{eq}} - 1 = (\Omega_0 - 1)\, a_{\text{eq}} \approx \frac{0.1}{3600} \sim 10^{-5}\,, \tag{1.23}$$

where we have used $a_{\text{eq}} \approx 1/3600$, which is just found by extrapolating backwards from today to $\rho_R = \rho_M$ and solving for $a = a_{\text{eq}}$. But let's go further back!

Continuing back in time to a period of known as Big Bang Nucleosynthesis,[7] the earliest era for which explicit observational evidence exists, the universe was radiation-dominated. Again, (1.17) tells us $(aH)^{-2} \propto a^2$. In this era, $a_{\text{BBN}} \sim 10^{-10}$, again assuming $a_0 = 1$, which comes from tracking temperatures backwards in time. Following the same procedure as above, we can count backwards from the radiation-matter equilibrium era:

$$\Omega_{\text{BBN}} - 1 = (\Omega_{\text{eq}} - 1)\left(\frac{a_{\text{BBN}}}{a_{\text{eq}}}\right)^2 \sim \left(10^{-5}\right)\left(\frac{3600}{10^{10}}\right)^2 \sim 10^{-18}\,, \tag{1.24}$$

which is an incredibly restrictive constraint on Ω.

[6] This comes from summing up the fluid content of our universe: $\Omega_\Lambda + \Omega_M + \Omega_R = 1 - \Omega_c$. The constraints on the measured values of the dark energy, radiation, and matter contributions to the energy density of the universe in turn constrain Ω_c.

[7] While it is not relevant to the overall picture we wish to paint here, Big Bang Nucleosynthesis is the epoch during which protons and neutrons combined to form some of the lightest atomic nuclei: hence, nucleosynthesis.

The point of these calculations is to demonstrate that the further back in time we go, the tighter the constraints on Ω become in order to describe the presently-observed flatness of the universe. Why the universe demands this strict imposition on the initial curvature of the universe is the essence of the Flatness Problem.

1.2.2 Horizon Problem

In addition to requiring the universe to be incredibly flat at early times, present observations also demand that the universe be extremely homogeneous at early times. Simply phrased, the Horizon Problem asks why does the universe look the same in all directions? Let's expand on this.

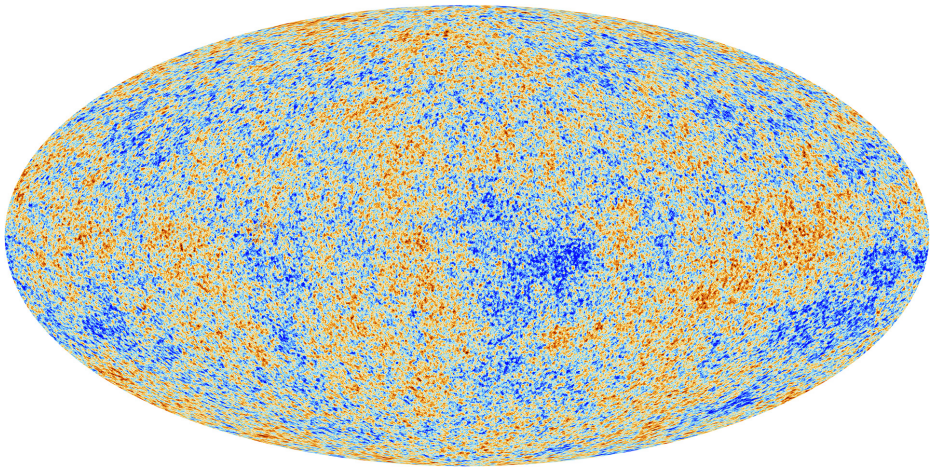

FIGURE 1.1: The Cosmic Microwave Background as measured by the Planck collaboration [1]: the "all sky map" shows temperature fluctuations (where $\delta T/T \sim 10^{-5}$) in the early universe. The plot shows how uniform the temperatures in the early universe are, even though most of the sky is causally-disconnected.

The Cosmic Microwave Background (CMB) radiation is leftover radiation from a period of time known as recombination, when neutral atoms are first formed approximately $\sim$ 3–4 $\times$ 10^5 yr after the Big Bang. It is the radiation that escaped the hot "particle soup" of the early universe once the universe cooled sufficiently so neutral atoms could form. The formation of neutral atoms caused the universe to become transparent to electromagnetic radiation at microwave frequencies ($\sim$ GHz). This occurs because the photons no longer care to interact with neutral

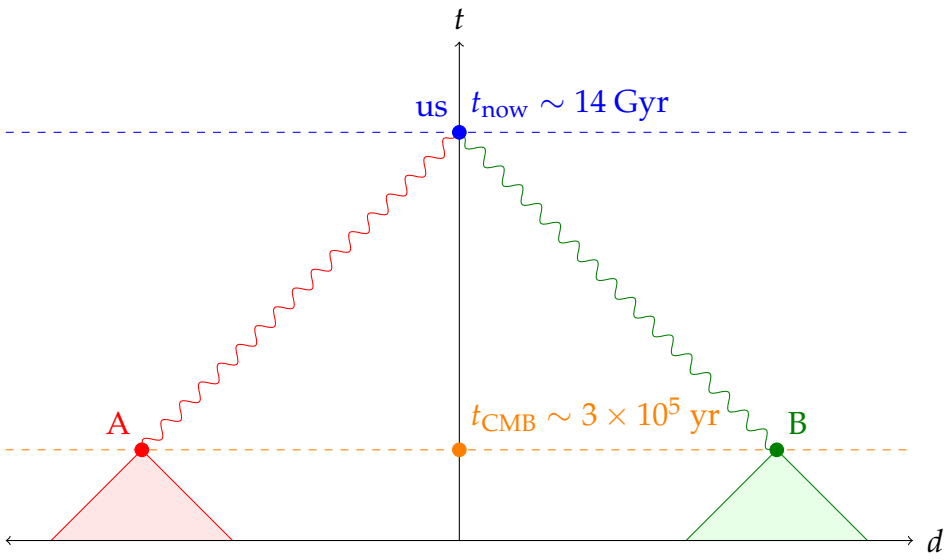

FIGURE 1.2: A spacetime diagram of two spacelike-separated points A and B that emitted microwaves (the curvy lines at 45° angles) at the time of the CMB. The past light cones (shaded regions in the figure) of A and B do not overlap indicating they were never in causal contact and thus should not be able to be at the same temperature. The proper distance axis, d, lines up with $t_0 \gtrsim 0$, i.e., *just* after the Big Bang. The time axis coincides with our world line and is *not* drawn to scale.

atoms and instead are free to travel unimpeded to our detectors on and around Earth.[8] This epoch is known as recombination because it is the era when atoms *combined* (the prefix "re-" is a bit of a misnomer). We can use the CMB to demonstrate the Horizon Problem explicitly. Points on the CMB are measured to have extremely uniform temperature: Figure 1.1 shows both the uniformity of the night sky, and the (very tiny) variations in the measured temperature which is approximately 2.7 ± 0.005 K [1].[9] The temperature fluctuations are measured to be even smaller at $\delta T/T \sim 10^{-5}$. The problem arises due to the fact that information cannot have passed to the entire night sky during the current age of the universe; so, why is the sky not measured to have varying temperatures? Figure 1.2 uses a spacetime diagram to demonstrate this explicitly. Essentially, since two points far enough apart on the CMB have past light cones that do not overlap (we refer to these points as causally-disconnected or acausally-connected), information by means of electromagnetic radiation could not have made it from one point to the other.

As an analogy, consider Investors Group Field, a stadium in Winnipeg, Manitoba that can seat just over 30 000 people. Let us invite 20 000 of our closest friends and then take a picture capturing the colours of their shirts. While small groups of people may have coordinated their outfits, there would generically be no long-range correlation in outfit colour. The Horizon Problem would be analogous to all 20 000 attendees showing up at Investors Group Field for the same event, wearing the same colour shirt. How did each person know what colour shirt to wear?[10] Returning to the case at hand, how do causally-disconnected points on the CMB know to all be at 2.7 K given their lack of communication?

Points on the surface of last scattering that are separated by more than about two degrees will be acausally-connected [33]. This means there are approximately 20 000 patches on the sky, each with area two degrees squared, that could not have shared information with each other. The vast number of points that are acausally-connected all but rules out a coincidence that each point just showed up at the CMB at the exact same temperature.

[8] For this reason, it is sometimes referred to as the surface of last scattering, since it is the last point in time at which light scattered off of charged particles.

[9] The magnitude of this error is the result of Earth moving in some preferred direction. Temperatures we measure will be Doppler-shifted due to the speed of the Earth, with $\delta T \sim \delta\nu \propto v_{\text{Earth}}$.

[10] In this contrived scenario, we are ignoring the fact that many events held at stadia may actually have large-scale shirt-colour-correlation due to the patriotic nature of sports fans et cetera. Let's say we invited all our soon-to-be-ex friends for a timeshare presentation.

1.3 Inflation to the Rescue

Now that we have outlined a couple problems that speak to the finely-tuned beginning of our universe, we need to provide a solution. Inflation was originally proposed as a means by which these special initial conditions become less special and more natural. While it was initially designed to solve these problems, it has since been applied to other cosmological observations; a period of Cosmic Inflation can be used to explain how the temperature fluctuations in the CMB, seen in Figure 1.1, become the large-scale structure of the universe today. This section demonstrates how a period of accelerated expansion in the early history of the universe can solve the two problems discussed in the previous section.

Introducing a period of accelerated expansion in the early universe corresponds to an epoch with $\ddot{a} > 0$. This implies $\dot{a} = aH$ is *increasing* (or, equivalently, $(aH)^{-1}$ is *decreasing*). So, how do we arrange our universe so that aH increases with time? Recall from (1.17) that $aH \propto a^{1-n/2}$ and from (1.16) that $a \propto t^{2/n}$. Putting these together, we have

$$aH \propto t^{2/n-1}\,, \tag{1.25}$$

which only increases in time if $2/n - 1 > 0$, or, $n < 2$. This excludes us from using curvature, matter, or radiation to dominate the universe during a period of inflation. Of the four choices previously discussed, we are left with vacuum-energy as the dominating fluid. In fact, (1.18) shows us that aH will grow exponentially with time, since H is a constant, during any vacuum-energy dominating period of time. We assume a very large, constant, energy density $\rho = M_I^4$, where $M_I \sim M_p/10^4$ (the subscript I refers to the inflationary period) [23]. We now outline how the exponential growth of aH solves both the Flatness and Horizon Problems.

1.3.1 Flatness Problem Revisited...and Resolved?

Recall the Friedmann equation in the form of (1.20). If aH is exponentially increasing in time, the curvature term, $k/(aH)^2$ diminishes very rapidly, driving away any initial curvature. In other words, the present-day flatness of our universe is no longer caused by a highly fine-tuned initial condition. We are able to explain away the no-longer-finely-tuned initial flatness. So, how much inflation is necessary to explain the presently-observed flatness? Let's assume that the universe expands from a temperature of order $T_i \sim M_I$ up to BBN (at which point $T_{\text{BBN}} \sim$ MeV).

Since $T \propto a^{-1}$ for relativistic particles,[11] as the universe cooled it would have expanded by a factor of

$$\frac{a_{\text{BBN}}}{a_i} = \frac{T_i}{T_{\text{BBN}}} \approx \frac{10^{15}\,\text{GeV}}{\text{MeV}} = 10^{18}\,. \tag{1.26}$$

Following (1.24),

$$\Omega_i - 1 = (\Omega_{\text{BBN}} - 1)\left(\frac{a_i}{a_{\text{BBN}}}\right)^2 \sim \left(10^{-18}\right)\left(10^{-18}\right)^2 \sim 10^{-54}\,, \tag{1.27}$$

which is an incredibly precise initial condition. However, we can account for this by having our inflationary period last for a sufficient number of e-foldings, $\mathrm{d}N_e := H\,\mathrm{d}t$. We have $\Omega_i - 1 \propto (aH)^{-2}$, with $(aH) \propto \exp(H\,\Delta t) = \exp N_e$: putting it altogether, we have

$$\Omega_i - 1 = e^{-2N_e} \implies N_e \sim \frac{1}{2}\ln\left(10^{54}\right) \sim 60\,. \tag{1.28}$$

Thus, the small initial condition of (1.27) could be justified if there existed a period of inflation lasting approximately 60 e-foldings prior to the radiation-dominated phase. Note that we choose $T_i \sim 10^{15}$ GeV since this is about the energy scale of Grand Unified theories (above which the strong and electro-weak forces become one), and also because it is roughly the temperature required to solve the Horizon Problem.

1.3.2 Horizon Problem Revisited...and Rectified?

In addition to solving the Flatness Problem, inflation is an attractive theory because it simultaneously solves the Horizon Problem.

Since $a(t)$ is exponentially increasing, while H^{-1} remains constant, physical distances—governed by $d(t) = a(t)d_0$—clearly grow at a much faster rate than the Hubble length, H^{-1}. Since the Hubble length describes the distance light can travel in an expanding universe, the fact that physical distances are growing *faster*

[11] A quick way to see this is to note that temperature is related to the average kinetic energy of the particles: $T \sim E$. By calculating the geodesic equation (which governs the motion of all particles in a given geometry) for the FRW metric (1.2), one can show $P \propto 1/a$, where P is the 3-momentum of a particle. For relativistic particles, $E = P$, and therefore $E \propto 1/a$ and so $T \propto 1/a$. For non-relativistic particles, $E \propto P^2$ implying $T \propto 1/a^2$ in that case. For the details, see [34].

than this implies the expansion of the universe is faster than the speed of light, or super-luminal. Super-luminal expansion makes it possible for events to have been in causal contact in the distant past, but appear to be acausally-connected presently. Figure 1.3 shows how the spacetime diagram we saw in Figure 1.2 changes under the addition of an inflationary period. The period of inflation causes the two points to have past worldlines at angles less than 45° which is the super-luminal expansion of the universe. Tracking this backwards, we see that there exists a period of time in the histories of points A and B wherein the points were in causal contact. This mechanism can be used to explain the isotropy of the radiation from the CMB: provided a period of exponential expansion in the distant past, points that are presently acausally-disconnected, were in causal contact at very early times and so could have communicated amongst themselves to all show up at 2 K some 300 000 years later.

While the calculation is not relevant to the story we are telling here (though [23, 33] perform it in a clear and concise manner), it turns out that a similar amount of inflation, $N_e \sim 60$, is required to solve the Horizon problem and explain the correlations observed in the CMB radiation.

1.3.3 A Bit of Inflationary Vocabulary, or Inflabulary

Finally, after having resolved all of the universe's problems, we briefly outline some of the parameters we use in our inflationary analysis, or inflalysis.

First, we define two parameters (often called the *slow-roll* parameters) that are used to interpret our inflationary solutions:

$$\epsilon := -\frac{\dot{H}}{H^2}\,, \qquad \text{and} \qquad \eta := \frac{\dot{\epsilon}}{H\epsilon}\,. \tag{1.29}$$

The first of these, ϵ, is less than one if $(aH)^{-1}$ is decreasing (i.e., accelerated expansion is occurring):

$$\frac{\mathrm{d}}{\mathrm{d}t}(aH)^{-1} = -\frac{\dot{a}H + a\dot{H}}{(aH)^2} = -\frac{1}{a}(1-\epsilon) < 0 \implies \epsilon < 1\,. \tag{1.30}$$

Therefore, it provides a useful check on an inflationary solution: if $\epsilon < 1$, then the universe is inflating.

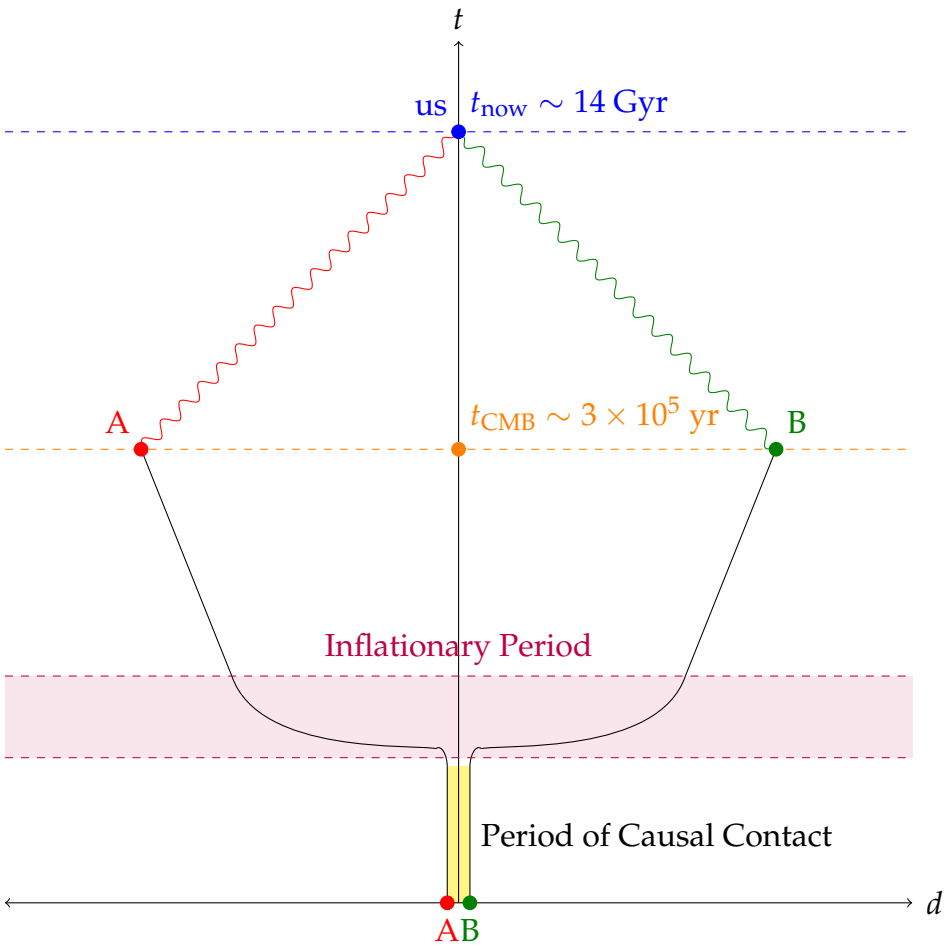

FIGURE 1.3: The spacetime diagram from Figure 1.2 revisited: in this version, we draw how the diagram changes given the addition of a period of inflationary expansion (shaded region) in the distant past. We can see from the past world lines of A and B that, because they have slopes less than one, the universe is expanding at speeds greater than c. This allows points A and B to be in causal contact at very early times, even though this does not seem possible when we observe them today. Again, the scales are greatly exaggerated for clarity.

The second parameter, η, measures how long inflation lasts:

$$\eta = \frac{\mathrm{d}\ln\epsilon}{\mathrm{d}N_e} = \frac{1}{H}\frac{\mathrm{d}\ln\epsilon}{\mathrm{d}t} = \frac{\dot{\epsilon}}{H\epsilon}, \tag{1.31}$$

where $\mathrm{d}N_e := H\,\mathrm{d}t$ is the number of e-foldings of inflation as above. From (1.31), we can see that if $|\eta| \ll 1$, the rate at which ϵ is changing as a function of N_e is slow, implying that ϵ will stay below one for many e-foldings, of which approximately 60 are necessary as described in the previous section. So, for this reason, we seek out solutions with very small η.

1.3.4 Primordial Spectra

It is also useful to relate the theory of Cosmic Inflation to what can actually be observed. Detailed derivations of the various spectra can be found in resources such as [23, 33], but we merely quote some of the important results here since the specific details are not relevant to our overall story.

An understanding of density perturbations in an inflationary regime are crucial to describing the evolution of the universe as a whole. It is predicted that these perturbations may have caused the large-scale structure we observe in the distribution of galaxies today. So what are these density perturbations? They are small perturbations in the scalar field, ϕ, due to the fact that the vacuum of an accelerating universe has non-zero energy. This produces small fluctuations in the energy density of the universe. When anisotropic radiation Thompson scatters, it creates linearly polarized radiation. This radiation can be decomposed into scalar and tensor components (usually referred to as E- and B-modes in analogy to electromagnetic radiation: E-modes a curl-free component, and B-modes the curl component) [35]. It is common to discuss these perturbations in terms of *power spectra*, which are Fourier transforms of the fractional density perturbations $\delta\rho/\rho$. The transform is then averaged over all spatial locations.

We introduce the dimensionless power spectra, in the slow-roll approximation ($\dot{\phi}^2 \ll V(\phi)$, $\ddot{\phi} \ll 3H\dot{\phi}$), given by

$$\Delta_s^2(k) = \frac{1}{8\pi^2}\frac{H^2}{M_p^2}\frac{1}{\epsilon}, \tag{1.32}$$

for scalar fluctuations in the inflaton field, and

$$\Delta_t^2(k) = \frac{2}{\pi^2}\frac{H^2}{M_p^2}\,, \tag{1.33}$$

for tensor fluctuations in the background metric, where k is the co-moving wavenumber of the fluctuations, related to the wavelength, λ, by $k = 2\pi a/\lambda$. So why do we label the power spectra Δ_i as functions of k? It is theoretically convenient to track the spectra as power-laws of k:

$$\Delta_s^2 \propto k^{n_s-1}, \qquad \text{and} \qquad \Delta_t^2 \propto k^{n_t}\,. \tag{1.34}$$

where the n_i are the spectral indices of the scalar and tensor perturbations. Inflation predicts a slight k-dependence in the spectra which we can quantify by evaluating

$$n_s - 1 := \frac{\mathrm{d}\ln\Delta_s^2}{\mathrm{d}\ln k}, \tag{1.35}$$

once the power spectrum is measured. If $n_s = 1$, we see that the scalar perturbations are scale-independent since they would not depend on k. In the slow-roll approximation, we can compute the relationship between n_s and the inflationary parameters, ϵ and η:

$$n_s - 1 = -6\epsilon + 2\eta\,. \tag{1.36}$$

(Note that our analysis does not consider tensor modes since they have yet to be observed.)

Recent measurements of the polarization of the CMB radiation have placed constraints on the ratio of these power spectra, r, known as the tensor-to-scalar ratio, which is then given by

$$r := \frac{\Delta_t^2(k)}{\Delta_s^2(k)} = 16\epsilon\,, \tag{1.37}$$

where the second equality comes from (1.32) and (1.33) and is only valid during slow-roll inflationary regimes. Inflation predicts the existence of primordial gravitational waves, which realize as tensor perturbations of the metric. These perturbations contain both E-modes and B-modes and so are usually classified by r, since power spectra features can be determined directly from the polarization. Because the temperature and polarization perturbations are correlated, a measurement of the temperature anisotropies (as in Figure 1.1) indirectly tells us information about

the polarization, which ultimately tells us information about the density perturbations in the scalar field via the E-modes.

To date, no B-modes have been observed, and so a constraint is placed on the tensor-to-scalar ratio of $r \lesssim 0.07$ [36]. So, in order for any of our models to be consistent with observations, we seek inflationary parameters, ϵ and η, that agree with this limit.

Note that the above analysis is only valid for slow-roll regimes in a standard 4D effective theory (i.e., one in which $H < m_{KK}$). Since some of our models lie outside this realm, new fluctuation spectra may be required to properly describe these models.

Chapter 2

The Model

We begin our journey by introducing our six-dimensional sandbox: the Einstein-Maxwell-Scalar action (and its associated field equations) we use in our study. We start with the general six-dimensional theory and derive the full field equations which we can use to study our cosmology. However, because we live in a four-dimensional world, analysis is more meaningful when we look at the system from a so-called dimensionally-reduced perspective. Therefore, we *truncate* our system by integrating out the extra two dimensions. This leaves us with an intuitive 4D potential and equations of motion (EOMs) we can then numerically integrate, which are performed explicitly in the next chapter.

2.1 6D Action and Field Equations

In this section we introduce the 6D action of interest to our studies. We then outline the derivation of the 6D field equations. For a more detailed mathematical derivation, see Appendix A.

The system we are analyzing is a 6D Einstein-Maxwell-Scalar field theory, with action

$$S = -\int \mathrm{d}^6x \sqrt{-g_{(6)}} \left(\frac{\mathcal{R}}{2\kappa^2} + L_{\mathrm{mat}} \right) , \tag{2.1}$$

and matter content

$$L_{\mathrm{mat}} = \frac{1}{4} F_{MN} F^{MN} + \frac{1}{2} \partial_M \phi \, \partial^M \phi + V(\phi) , \tag{2.2}$$

where $F_{MN} = \partial_M A_N - \partial_N A_M$ is an Abelian gauge Maxwell field strength, ϕ is the scalar field, while $g_{(6)}$ and $\mathcal{R} = g^{MN}\mathcal{R}_{MN}$ are the determinant and Ricci scalar for the 6D metric, g_{MN}, respectively. Where explicitness is necessary (and in our

numerics), we model the scalar potential as a sum of exponentials of the form

$$V(\phi) = V_0\left(e^{-\beta_1\phi} - e^{-\beta_2\phi}\right) + \Lambda\,, \tag{2.3}$$

which (for $V_0, \beta_i > 0$) is minimized by

$$\phi_\star = \frac{1}{\beta_1 - \beta_2}\,\ln\left(\frac{\beta_1}{\beta_2}\right)\,. \tag{2.4}$$

In our numerics, we adjust Λ so that $V(\phi_\star) := V_\star = 0$ so that there is no leftover energy from the scalar field once inflation ends. We choose a sum of exponentials for later convenience: experience shows that power-law inflation arises when the inflaton potential is dominated by a single exponential [37]. We need to use a sum, in general, so that our potential still has a minimum (since a global minimum does not exist for a single exponential potential).

Varying the action with respect to ϕ, A_M, and $\mathcal{R}$, we get three sets of field equations for our action: the Klein-Gordon equation, Maxwell equations, and Einstein equations. Respectively, these are:

$$\Box\,\phi - V'(\phi) = \nabla_M F^{MN} = \mathcal{G}_{MN} + \kappa^2 T_{MN} = 0\,, \tag{2.5}$$

where $\mathcal{G}_{MN} = \mathcal{R}_{MN} - \frac{1}{2}\,\mathcal{R}\,g_{MN}$ is the metric's Einstein tensor and the stress-energy tensor, T_{MN}, is

$$T_{MN} = \partial_M\phi\,\partial_N\phi + F_{MP}F^{P}{}_{N} - g_{MN}L_{\text{mat}}\,. \tag{2.6}$$

For cosmological applications, we write down a metric consisting of four FRW dimensions, with flat spatial slices, and two extra dimensions modeled as a sphere:

$$\begin{aligned} \mathrm{d}\hat{s}^2 &= \hat{g}_{\mu\nu}\,\mathrm{d}x^\mu\mathrm{d}x^\nu + g_{mn}\,\mathrm{d}y^m\mathrm{d}y^n \\ &= -\mathrm{d}\hat{t}^2 + \hat{a}^2(\hat{t}\,)\,\delta_{ij}\,\mathrm{d}x^i\,\mathrm{d}x^j + b^2(\hat{t}\,)\gamma_{mn}(y)\,\mathrm{d}y^m\mathrm{d}y^n\,. \end{aligned} \tag{2.7}$$

Here, γ_{mn} is the usual metric for the unit two-sphere, and $\hat{a}$ and b are the scale factors for the three- and two-dimensional spatial slices, respectively, whose coordinates are denoted x^i and y^m. We assume the scalar field to be spatially homogeneous so that it may be written only as a function of time: $\phi = \phi(\hat{t}\,)$. Additionally, we assume the only nonzero components of the Maxwell field to be $F_{mn} = f\epsilon_{mn}$, where ϵ_{mn} is the Levi-Civita tensor built from the extra-dimensional metric, g_{mn}.

Armed with the above *ansätze*, the EOM for the scalar field from the Klein-Gordon equation in (2.5) is

$$\phi'' + \left(3\hat{H} + 2\mathcal{H}\right)\phi' + \frac{\partial V}{\partial \phi} = 0\,, \tag{2.8}$$

where $\hat{H} := \hat{a}'/\hat{a}$, $\mathcal{H} := b'/b$ and primes denote derivatives with respect to $\hat{t}$. The Maxwell equation and Bianchi identity[1] give us the following two restrictions on the extra-dimensional flux:

$$\partial_m f = 0 \qquad \text{and} \qquad (fb^2)' = 0\,, \tag{2.9}$$

while quantization of the extra-dimensional magnetic flux implies

$$\int_{S^2} F = 4\pi f b^2 = \frac{2\pi n}{e} \implies f = \frac{\mathfrak{f}}{b^2} \quad \text{where} \quad \mathfrak{f} := \frac{n}{2e}\,, \tag{2.10}$$

with n an integer and e the Maxwell field's coupling constant. Clearly (2.10) satisfies (2.9).

The stress-energy tensor for this metric *ansatz* is diagonal and we again write down the most general stress-energy tensor consistent with homogeneity and isotropy in analogy with (1.3), but generalized to include the extra dimensional pressure:

$$T_{\mu\nu} = \begin{pmatrix} \rho & 0 & 0 \\ 0 & p_{(3)}\, g_{ij} & 0 \\ 0 & 0 & p_{(2)}\, g_{mn} \end{pmatrix}, \tag{2.11}$$

with its components given by

$$\begin{aligned} \rho &= \frac{1}{2}\left[\left(\phi'\right)^2 + f^2\right] + V\,, \\ p_{(3)} &= \frac{1}{2}\left[\left(\phi'\right)^2 - f^2\right] - V\,, \\ p_{(2)} &= \frac{1}{2}\left[\left(\phi'\right)^2 + f^2\right] - V\,, \end{aligned} \tag{2.12}$$

[1] The Bianchi identity, as it relates to Maxwell's equations, gives us the curved-spacetime-equivalent of Faraday's Law and Gauss' Magnetism Law (e.g., $\nabla \times \vec{E} = -\partial\vec{B}/\partial t$ and $\nabla \times \vec{B} = 0$). It is usually written as $F_{[\mu\nu;\alpha]} = F_{\mu\nu;\alpha} + F_{\nu\alpha;\mu} + F_{\alpha\mu;\nu} = 0$. See Section A.4.1 for more details.

where ρ is the energy density and the 3D and 2D pressures are $p_{(3)}$ and $p_{(2)}$. So, the Einstein equations become

$$\begin{aligned}
3\left(\frac{\hat{a}'}{\hat{a}}\right)^2+\left(\frac{b'}{b}\right)^2+6\left(\frac{\hat{a}'b'}{\hat{a}b}\right)+\frac{1}{b^2}&=\kappa^2\left\{\frac{1}{2}\left[\left(\phi'\right)^2+\frac{\mathfrak{f}^2}{b^4}\right]+V\right\},\\
2\left(\frac{\hat{a}''}{\hat{a}}+\frac{b''}{b}\right)+\left(\frac{\hat{a}'}{\hat{a}}\right)^2+\left(\frac{b'}{b}\right)^2+&\\
4\left(\frac{\hat{a}'b'}{\hat{a}b}\right)+\frac{1}{b^2}&=\kappa^2\left\{\frac{1}{2}\left[-\left(\phi'\right)^2+\frac{\mathfrak{f}^2}{b^4}\right]+V\right\},\\
\frac{b''}{b}+3\left[\frac{\hat{a}''}{\hat{a}}+\left(\frac{\hat{a}'}{\hat{a}}\right)^2\right]+3\left(\frac{\hat{a}'b'}{\hat{a}b}\right)&=\kappa^2\left\{-\frac{1}{2}\left[\left(\phi'\right)^2+\frac{\mathfrak{f}^2}{b^4}\right]+V\right\}.
\end{aligned}\tag{2.13}$$

Because we are using the most general metric consisting of translational and rotational invariance of the three spatial dimensions (a defining property of the FRW metric) and SO(3) symmetry of the extra dimensions (a property of spherical metrics), any solution to (2.13) must also satisfy the other 6D field equations.

2.1.1 Domain of Validity

We take a quick diversion to discuss the domains of validity of our solutions. Since we seek classical solutions to these equations in later chapters, we must remain within the bounds permitted by semiclassical methods. This demands curvatures be small relative to the 6D Planck scale, which also requires correspondingly small stress energy:

$$\hat{H}^2,\,\mathcal{H}^2,\,\frac{1}{b^2}\ll\frac{1}{\kappa}\implies V_\star\ll\frac{1}{\kappa^3}\quad\text{and}\quad F_{mn}F^{mn}\sim\frac{\mathfrak{f}^2}{b^4}\ll\frac{1}{\kappa^3}\,.\tag{2.14}$$

2.2 A Four-Dimensional Perspective

It is useful to *truncate* the 6D action, i.e., to rewrite the above 6D field equations in terms of an equivalent 4D formulation by integrating out the extra dimensions explicitly. This is useful because it provides us with a set of 4D equations for which we have a much more intuitive understanding, given that we live in an apparent 4D world. In this section, we first dimensionally reduce the 6D action by truncating it onto the class of 4D fields that evolve during the cosmologies explored later. In

Section 2.2.1, we sketch this procedure but leave the "play-by-play" derivation for Appendix B. We then argue that this dimensional reduction is actually a *consistent truncation* [38] (while saving the explicit details for Appendix C), which means solutions to the field equations obtained by varying the dimensionally-reduced 4D action also exactly satisfy all of the 6D field equations (rather than just being a low-energy approximation as would be the case of an effective theory).

2.2.1 Dimensional Reduction

In this section, we reduce our 6D action to an equivalent 4D action. While we describe the procedure here, the process is completed in much more explicit detail in Appendix B.

We first derive the dimensionally-reduced 4D action. This requires separating the full 6D action into 4D and 2D components, and integrating over the extra two. Using the metric

$$\mathrm{d}\hat{s}^2 = \hat{g}_{\mu\nu}(x)\,\mathrm{d}x^\mu \mathrm{d}x^\nu + b^2(x)\,\gamma_{mn}(y)\,\mathrm{d}y^m \mathrm{d}y^n\,, \tag{2.15}$$

where $\phi = \phi(x)$, we separate our 6D action into the x and y variables.

Direct substitution of this *ansatz* into the 6D action and integration over the extra dimensions (i.e., performing the d^2y-integral) leaves

$$S = -\int \mathrm{d}^4x \left(4\pi b^2\right) \sqrt{-\hat{g}} \left[\frac{\hat{\mathcal{R}}}{2\kappa^2} - \frac{2}{b^2}\left(\partial b\right)^2 + \frac{1}{2}\left(\partial\phi\right)^2 - \frac{2}{b^2} + \frac{f^2}{2} + V(\phi)\right], \tag{2.16}$$

where $\sqrt{-\hat{g}}$ and $\hat{\mathcal{R}}$ are the volume density and Ricci scalar for the 4D metric, $\hat{g}_{\mu\nu}$, the notation $(\partial b)^2 = \partial^\mu b\,\partial_\mu b = \hat{g}^{\mu\nu}\,\partial_\mu b\,\partial_\nu b$, and contracted indices run only over the four dimensions with coordinates x^μ.

We can transform to the 4D Einstein frame (4DEF)—the frame in which no field multiplies the Ricci scalar, $\mathcal{R}$—by rescaling our metric as

$$g_{\mu\nu} = e^{\psi/M_p}\hat{g}_{\mu\nu}\,, \tag{2.17}$$

where

$$M_p^2 := \frac{4\pi b_\star^2}{\kappa^2} =: 4\pi b_\star^2 M_{(6)}^4 \tag{2.18}$$

is the 4D Planck mass,[2] ψ is the radion which comes from the field-redefinition required to bring the kinetic term for b into canonical form (i.e., the coefficient on the kinetic term is $1/2$ only and not multiplied by any fields):

$$b = b_\star \, e^{\psi/2M_p} \,, \tag{2.19}$$

and the constant $b_\star := b(\hat{t}_\star)$ is the present size of the extra dimensions. This, together with (2.19), implies

$$b(\hat{t}_\star) = b_\star e^{\psi(\hat{t}_\star)/2M_p} \implies 1 = e^{\psi(\hat{t}_\star)/2M_p} \implies \psi(\hat{t}_\star) := \psi_\star = 0 \,. \tag{2.20}$$

This condition ensures that the Planck mass at $t_\star$, the present time, is the same M_p that we currently measure.

Finally, ϕ's kinetic term needs to be put into canonical form; we do this by making the following field redefinition for the inflaton:

$$\kappa\phi = \frac{\varphi}{M_p} \,. \tag{2.21}$$

Putting it altogether, we finally arrive at the 4D action:

$$S = -\int \mathrm{d}^4x \sqrt{-g} \left[\frac{M_p^2}{2}\mathcal{R} + \frac{1}{2}\left(\partial\psi\right)^2 + \frac{1}{2}\left(\partial\varphi\right)^2 + W(\varphi,\psi) \right] , \tag{2.22}$$

where the scalar potential, W, is

$$W(\varphi,\psi) := 4\pi b_\star^2 \, U(\varphi) e^{-\psi/M_p} - \frac{M_p^2}{b_\star^2} e^{-2\psi/M_p} + \frac{2\pi\mathfrak{f}^2}{b_\star^2} e^{-3\psi/M_p}, \tag{2.23}$$

[2] Since we are working with in a fundamentally 6D theory, $M_{(6)}$ is our fundamental Planck constant. This means we need to define the 4D Planck mass, M_p, in terms of the 6D one. The usual 4D Planck mass will always scale in terms of the volume of the extra dimensions: $M_{(4)}^2(t) = V(t)M_{(d)}^{d-2}$, where V is the volume of the extra dimensions. In our case, this means $M_{(4)}$ scales as $M_{(4)}^2(t) = 4\pi b^2(t) M_{(6)}^4$. So, as the size of the extra dimensions changes, so too does the size of $M_{(4)}$. Thus, we choose $M_p := M_{(4)}(t_\star)$ à la (2.18) so that M_p is the value we currently measure it to be. For more information, see Sections 3.8 and 3.9 in [39].

where $U(\varphi) = V(\phi)$.[3] In order to facilitate later discussions, we divide W into three terms by writing $W = W^{(\varphi)} + W^{(c)} + W^{(f)}$, where

$$W^{(\varphi)} = 4\pi b_\star^2\, U(\varphi)\, e^{-\psi/M_p}\,, \qquad W^{(c)} = -\left(\frac{M_p^2}{b_\star^2}\right) e^{-2\psi/M_p}\,,$$
$$\text{and} \qquad W^{(f)} = \left(\frac{2\pi \mathfrak{f}^2}{b_\star^2}\right) e^{-3\psi/M_p}\,. \tag{2.24}$$

$W^{(\varphi)}$ is the term due to the inflaton potential, $W^{(c)}$ is the contribution from the curvature of the extra dimensions, and $W^{(f)}$ is the extra-dimensional flux contributions.

The field equations for this 4D system become, for a homogeneous, spatially flat FRW metric,

$$\mathrm{d}s^2 = g_{\mu\nu}\mathrm{d}x^\mu \mathrm{d}x^\nu = -\mathrm{d}t^2 + a^2(t)\,\delta_{ij}\mathrm{d}x^i\mathrm{d}x^j\,, \tag{2.25}$$

in 4DEF with isotropic—i.e., $\varphi = \varphi(t)$ and $\psi = \psi(t)$—fields:

$$\begin{aligned} \ddot{\varphi} + 3H\dot{\varphi} + \frac{\partial W}{\partial \varphi} &= 0\,, \\ \ddot{\psi} + 3H\dot{\psi} + \frac{\partial W}{\partial \psi} &= 0\,, \\ \frac{\dot{\varphi}^2}{2} + \frac{\dot{\psi}^2}{2} + W &= 3M_p^2 H^2\,, \end{aligned} \tag{2.26}$$

where $H := \dot{a}/a$ and over-dots refer to derivatives with respect to t.

One of the attractive features of this 4D model is that we can trust these equations in situations where an effective 4D description usually does not hold, namely, when the Hubble scale is greater than the Kaluza-Klein mass scale: $H > m_{\mathrm{KK}}$. Normally, when one works in an effective theory, analysis is restricted to this regime. However, our dimensional reduction is a *consistent truncation* [38], in that, as shown in Appendix C, (2.26) is completely equivalent to (2.13). Recall that the field equations in (2.13) are sufficient to solve all the 6D field equations due to the maximal symmetries of our 6D metric *ansatz*. This means that our 4D equations *exactly* reproduce the information encoded in the full 6D system.

[3] For an example, see Footnote 3 in Appendix B on page 83.

Chapter 3

The Numerics

Now that we have prepared our 6D system for battle by truncating it into 4D, we are ready to solve the equations numerically. A typical numerical evolution of the 4D system yields either a trajectory that does not inflate, or one which does not inflate for long enough. However, many of the numerical evolutions appear to follow power-law, or scaling, paths. We identify scaling periods as those where the fields tend to move in straight line trajectories on plots with logarithmic axes (colloquially referred to as "log-log" plots). Upon observing this repeated pattern, we are led to perform a systematic and comprehensive power-law analysis on the system, which are discussed in the next chapter.

The rest of this chapter presents representative plots of typical numerical evolutions of the 4D EOMs. We begin by discussing the physical bounds imposed on our system, which restrict that parameter space over which we can integrate the equations. This is followed by a discussion of *static solutions* to the 6D EOMs; we discuss the conditions under which a static solutions can be found and then present a representative example that excellently demonstrates the intuitive behaviour of the 4D potential. We then present other representative runs that ultimately lead us to pursue the systematic power-law analysis. While we only include the results here, Appendix E contains *Mathematica* worksheets in the raw as well as the parameter values used to generate the figures.

3.1 Physical Bounds on the 4D System

In Section 2.1.1, we discuss the domain of validity for semi-classical solutions. Here, we compute the numerical values of these limits by plugging in a few numbers. Our systems must always abide by the following restrictions:

- The extra dimensions are always sub-Planckian (i.e., the extra-dimensional radius, b, is always larger than the 6D Planck length). This imposes a limit on the initial radius size, b_0, and consequently, initial radion size, ψ_0:

$$b_0^2 \geq \frac{\kappa}{8\pi} \implies \frac{\psi_0}{M_p} \geq -\ln\left(4\sqrt{\pi} b_\star M_p\right), \tag{3.1}$$

  where we use (2.18) to translate from the 6D Planck mass to M_p.

- The radius of the extra dimensions is less 1 μm today (the current observational lower bound) [40]. This requires the present-day size of the extra dimensions, $b_\star$, to satisfy:

$$b_\star \lesssim \frac{6 \times 10^{28}}{\sqrt{8\pi} M_p}, \tag{3.2}$$

  since 1 μm $\approx \left(6 \times 10^{28}\right) L_p$.

- The 6D potential for ϕ has to be sub-Planckian. Therefore, the 4D inflaton potential, $U(\varphi)$ must satisfy

$$U(\varphi) \leq \frac{M_p^3}{8\pi^{3/2} b_\star^3}. \tag{3.3}$$

  We build a check into our *Mathematica* code that verifies that the potential never exceeds this value.

Using the maximum allowable $b_\star$ from (3.2) in (3.1) gives us a limit on ψ_0:

$$\frac{\psi_0}{M_p} \geq -\ln\left(6\sqrt{2} \times 10^{28}\right) \approx -66. \tag{3.4}$$

This turns out to be the strictest limit on our parameter space and so we ensure all numerical evolutions satisfy this limit.

3.2 Static Solutions

One of the key features of our 6D system is that it allows a simple stabilization of the radius of the two-sphere [41–43] using one of the earliest examples of flux stabilization (i.e., using extra-dimensional flux over the extra dimensions as a means to stabilize the extra-dimensional modulus) [29, 44]. Recent observations [40] have placed upper constraints on the size of extra dimensions: thus, stabilization is necessary to restrict our extra dimensions to live within these constraints. We briefly describe this solution here in order to identify the parameter range needed for stabilization to occur. It also provides a very intuitive means by which we can discuss the 4D potential W.

For the stabilized solution, we let $b = b_\star$ and $\phi = \phi_\star$, constants, such that $V(\phi)$ is minimized at the value $V_\star := V(\phi_\star)$ and $b_\star$ is value of the stabilized radius. We also take the 4D metric, $\hat{g}_{\mu\nu}$, to be maximally symmetric. For de Sitter and flat solutions, we know $\hat{H} = \hat{a}'/\hat{a}$ is also constant (and so $\hat{a}''/\hat{a} = \hat{H}^2$). Applying the above conditions to (2.13), we see that the first two equations become equivalent, leaving us with only two linearly independent equations. Subtracting the last equation from twice the first to eliminate $\hat{H}$, we are left with:

$$\frac{2}{b_\star^2} = \kappa^2\left[\frac{3\mathfrak{f}^2}{2b_\star^4} + V_\star\right] \qquad \text{and} \qquad 6\hat{H}^2 = \kappa^2\left[-\frac{\mathfrak{f}^2}{2b_\star^4} + V_\star\right]. \tag{3.5}$$

Four-dimensional de Sitter space occurs when $\hat{H} > 0$. Therefore, the second expression in (3.5) shows that de Sitter space occurs when $V_\star > \mathfrak{f}^2/2b_\star^4$. However, our solution is flat ($\hat{H} = 0$) if $V_\star = \mathfrak{f}^2/2b_\star^4$. On the other hand, we can use the first expression in (3.5) to solve for the size of the extra dimensions in terms of $\mathfrak{f}$ and $V_\star$, with solutions

$$b_\pm^2 = \frac{3}{2}\kappa^2\mathfrak{f}^2\left[1 \pm \sqrt{1 - \frac{3}{2}\kappa^4\mathfrak{f}^2 V_\star}\right]^{-1}. \tag{3.6}$$

Here, b_+ is a local minimum of the potential for b while b_- is a local maximum. The minimum and maximum merge into an inflection point when $\kappa^4\mathfrak{f}^2 V_\star = \frac{2}{3}$. However, no stationary solutions exist for our *ansatz* for finite b if $\kappa^4\mathfrak{f}^2 V_\star > \frac{2}{3}$. This shows us that a minimum exists for the radion only for specific values of $V_\star$, and hence, ϕ. Therefore, if we wish to have a stabilized radius, then we must ensure our initial conditions satisfy the above. Furthermore, even when the minimum exists another mechanism is almost always required to stabilize the radion. Otherwise its kinetic energy causes it to roll past the local maximum, which is generically very

shallow, and inflate indefinitely. We use the 4D potential, W, to demonstrate this behaviour for various values of $V_\star$ in Figure 3.1.

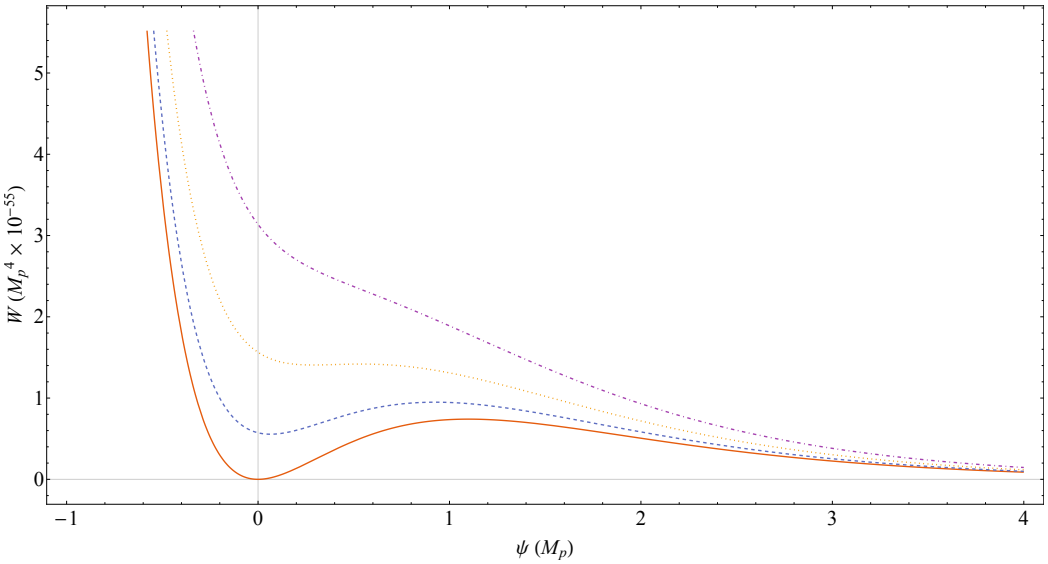

FIGURE 3.1: Plot of $W(\psi)$ vs ψ, both in 4D Planck units, for a few fixed values of φ. This is the 4D equivalent of the discussion in section 3.2. Notice that a minimum only exists for the radion for certain values of $U(\varphi)$ in accordance with (3.6). It is also important to highlight generically how shallow the well to trap ψ is, even when the minimum does exist, as explained in the main text.

3.2.1 General Stabilization of the Radius from a 4D Perspective

While the previous section uses the full 6D system to outline the conditions under which the radius can be stabilized, here we apply the above arguments to the 4D perspective; this yields conditions on the relative sizes of terms in the 4D potential, W.

Flux stabilizes the radion if the flux, inflaton potential, and extra-dimensional curvature stress-energies conspire at a certain point to have approximately the same magnitude, which we can see from the first equation in (3.5). Moreover, (3.6) gives us the explicit conditions under which a minimum for b exists. But given that the flux stress-energy scales as b^{-4}, while the curvature scales as b^{-2}, the flux would need to dominate over the curvature contributions at early times in order

for the two terms to converge at some future point (say, at a minimum for ψ) since it falls faster than the curvature term. This implies that at the beginning of, and during, inflation the flux stress-energy needs to dominate over the curvature's contributions to the stress-energy. In 4D, this means our inflationary solutions must exist in a regime where

$$\left|W^{(f)}\right| \gg \left|W^{(c)}\right| . \tag{3.7}$$

We ultimately find that one of our interesting scaling solutions exists in such a regime, whereas the second one does not.

3.3 A Static Solution: Cradle Inflation

Now that we are stocked with: 4D equations, flux stabilization, and numerical bounds, we are ready to embark on a quest of numerical evolution. The first solution we discover is *not* a scaling solution; we lovingly refer to it as *Cradle Inflation*, not because it should be trusted to hold a baby, but because it gently cradles the radion, ψ, as it approaches its global minimum, $\psi_\star = 0$.[1] Allow us to elaborate.

This solution is found by letting ψ start almost at rest and very close to the minimum of its potential. Note that we must ensure the initial value of our potential satisfies the condition imposed by (3.6) for a minimum to exist. In this scenario, the radion merely experiences damped oscillations about its local minimum, as shown in Figure 3.2.

Figure 3.2 also shows that ψ finds its minimum early on in the evolution. However, this does not mean that it is static thereafter. Because ψ's minimum depends on the value of φ, the value of the local minimum of ψ gets dragged down, cradling the radion on its way, as the inflaton continues to roll towards its own minimum. We might say φ is the field that rocks the cradle. Inflation continues until *both* fields arrive at their minima, at which point W goes to zero and inflation ends. This figure also provides an excellently explicit demonstration of the behaviour of W we see in Figure 3.1. There, we see W—and in particular, ψ's minimum—vary as a function of φ. In this scenario, we see that behaviour explicitly. Having a 4D potential about which we can make intuitive sense is one of the benefits of having dimensionally-reduced our 6D system to the 4D one.

[1] While the focus of this author was on the scaling solution analysis, this solution is discussed here both to demonstrate an example of a solution in which the radion is easily trapped, and since its behaviour is clearly justified by, and in agreement with, our intuitive understanding of W.

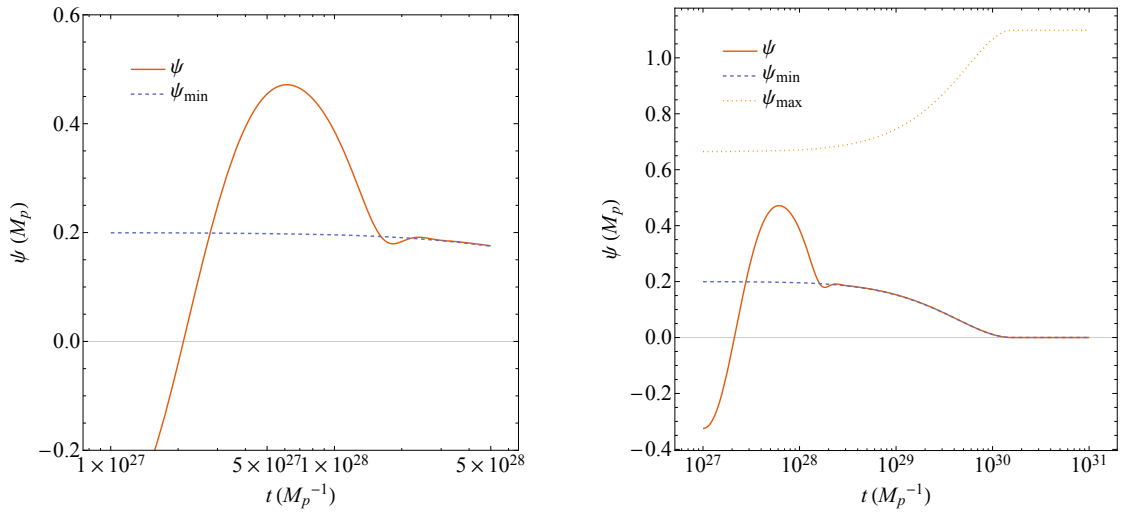

FIGURE 3.2: Behaviour of the radion in Cradle Inflation. $\psi_{\min}$ and $\psi_{\max}$ correspond to the $+$ and $-$ roots of (3.6), respectively. Behaviour at early times is enlarged in the left panel to show more clearly the oscillatory nature of ψ.

The evolution of φ is shown in the left panel of Figure 3.3. The 4D Hubble parameter during this roll is shown in the right panel of the same figure: Numeric H is the result of *Mathematica*'s integration of the 4D EOMs, while Semi-Analytic H is the solution to the second expression in (3.6) with our numerical functions substituted (hence, *semi*-analytic). The right panel in this figure also shows that $H < m_{KK}$ throughout the entire integration, which means that this scenario lives in the usual and well-studied effective 4D regime. This means we can perform the usual phenomenological analysis on it.

Because the rolling of φ is the driving factor behind the inflation and this scenario lives in the traditional 4D effective regime where $H < m_{KK}$, we can use a traditional slow-roll approach from Section 1.3.4 that predicts, for the scalar index, n_s, and tensor-to-scalar ratio, r,

$$n_s = 1 - 6\epsilon + 2\eta \qquad \text{and} \qquad r = 16\epsilon\,. \tag{3.8}$$

The observed limit $r \lesssim 0.07$ then creates an upper bound on $\epsilon \lesssim 0.1/16$. In the representative solution displayed in Figures 3.2–3.4, the slow-roll parameters ϵ and η approximately 60 e-foldings before inflation's end are $\epsilon \simeq 0.009$, and $\eta \simeq 0.016$,

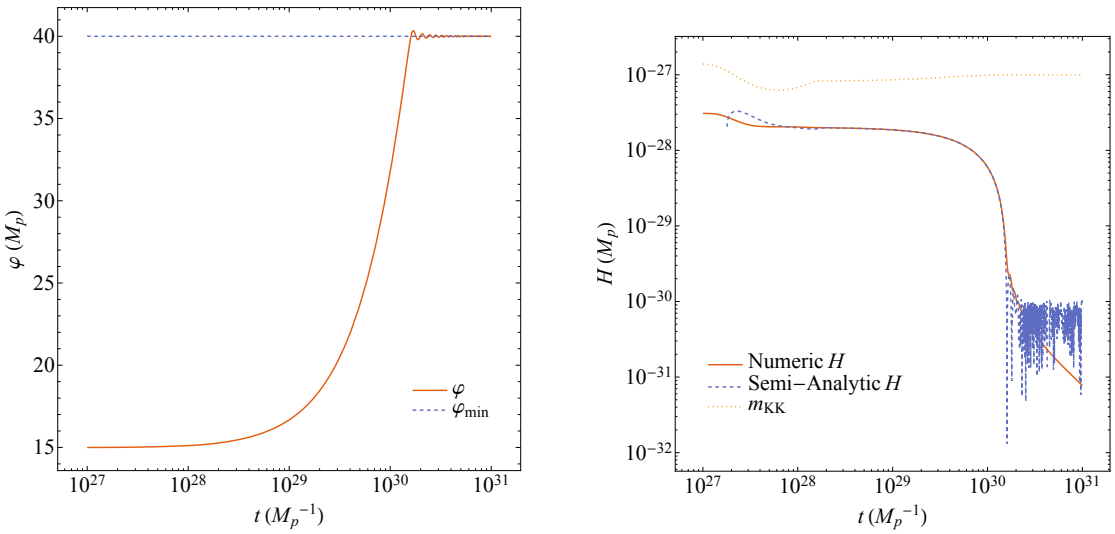

FIGURE 3.3: The inflaton and Hubble scale in Cradle Inflation. In the second plot, the semi-analytic curve is a plot of (3.6) converted to 4D quantities. The slow-roll inflationary regime occurs where the numeric and semi-analytic curves overlap. We also include m_{KK} in this plot to show that this scenario exists within the the standard effective 4D regime.

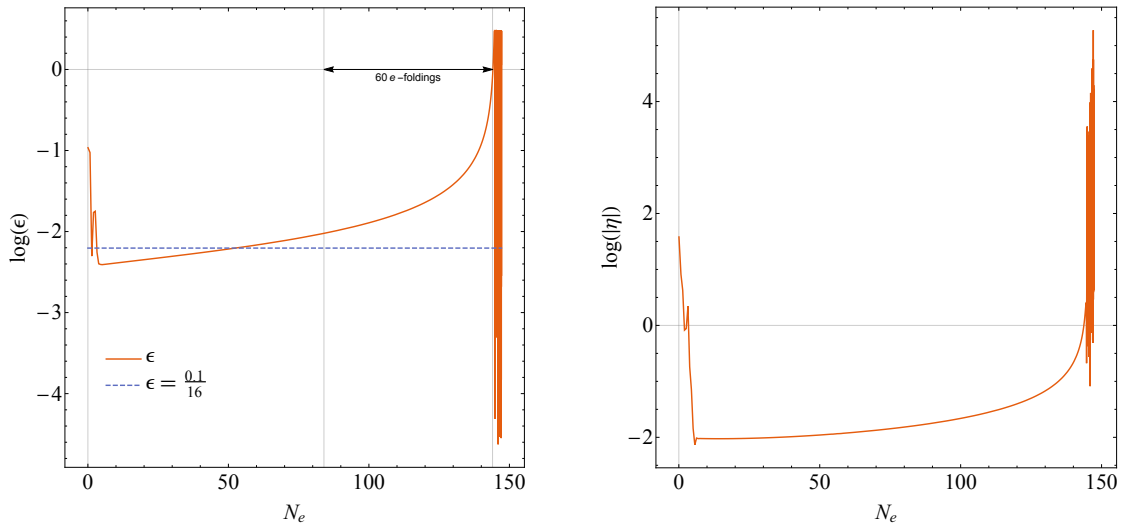

FIGURE 3.4: Slow-roll parameters ϵ and η during the inflationary regime for the Cradle scenario. They are plotted as a function of e-foldings, N_e. For convenience, we plot $\epsilon = 0.1/16$ since this is roughly the value observations demand 60 e-foldings prior to $\epsilon = 1$.

leading to the predictions $n_s \simeq 0.975$ and $r \simeq 0.15$. This value of r creeps beyond the observationally acceptable region of $r \lesssim 0.07$ [36] at horizon exit (when $\epsilon = 1$), and (with values taken from Figure 3.4) lies in the range $0.13 \lesssim r \lesssim 0.18$ if we stretch the limits on N_e slightly to $70 \gtrsim N_e \gtrsim 50$ e-foldings. One can imagine seeking better agreement if the post-inflationary physics allowed inflation to last for a longer time, or if the potential $V(\phi)$ is not chosen as the sum of exponentials as in (2.3) (which was chosen here more to study the scaling solutions described below).

For comparison's sake, we present two other evolutions in the same scenario that highlight some interesting behaviours. Figure 3.5 demonstrates an example where ψ starts too far from its minimum, or too fast (recall that we needed both of these conditions to begin in the cradle regime). Either way, the end result is the same: by the time the radion has rolled down the potential towards its minimum, it has acquired too much kinetic energy and rolls past its local maximum. This causes ψ to roll uninhibited and indefinitely, while the inflaton barely rolls at all since ψ has hogged all the energy.

The second additional evolution piques our interest in that it shows more explicitly the behaviour of Figure 3.1, confirming that we have a solid conceptual

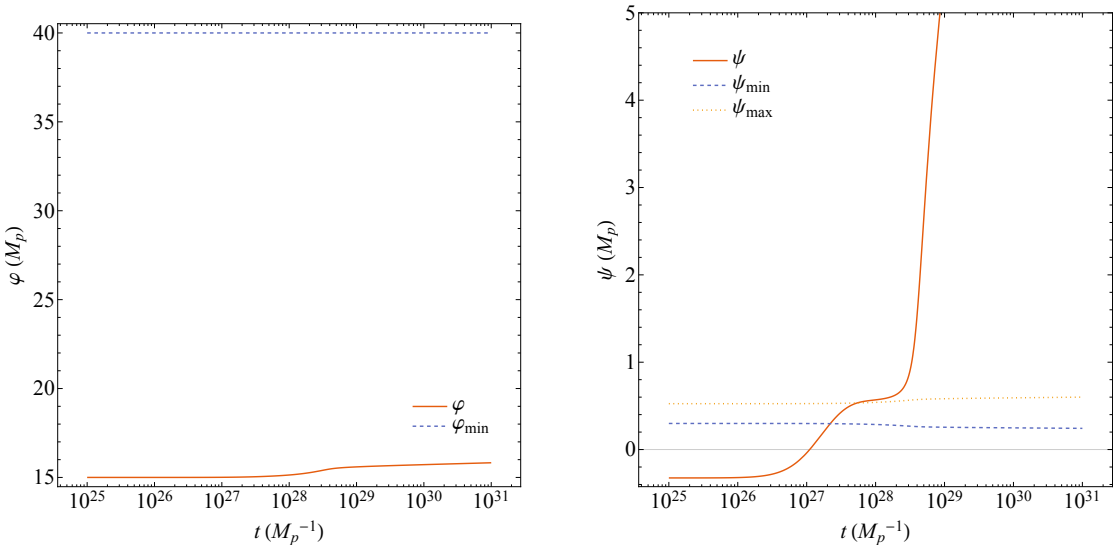

FIGURE 3.5: Plot of the inflaton (left) and radion (right) when ψ overshoots the shallow valley of its potential.

grasp of these solutions. Above, we claim that we must choose initial conditions such that the radion's minimum already exists. However, Figure 3.6 shows that this is not necessarily the case. We see that we only need to ensure that the minimum exists early enough in the radion's roll so that it may be cradled before it has rolled too far. The other interesting feature of these particular initial conditions is that we can "see" the evolution of W: initially, there is no minimum for ψ. As φ inflates, it drops W until the extrema spring fully-formed into existence.

3.4 General Integration: A Stab in the Dark

We close this chapter with a brief description of a representative same of general integrations performed. We highlight in particular the behaviour these solutions exhibit that leads us to perform a systematic, analytic search for scaling solutions to the 4D EOMs.

In Figure 3.7, we present the results of a typical *ad hoc* numerical run. Since the horizontal axes are all plotted logarithmically, the straight-line portions of the radion's trajectory (top right panel) smell suspiciously like power-law relationships.

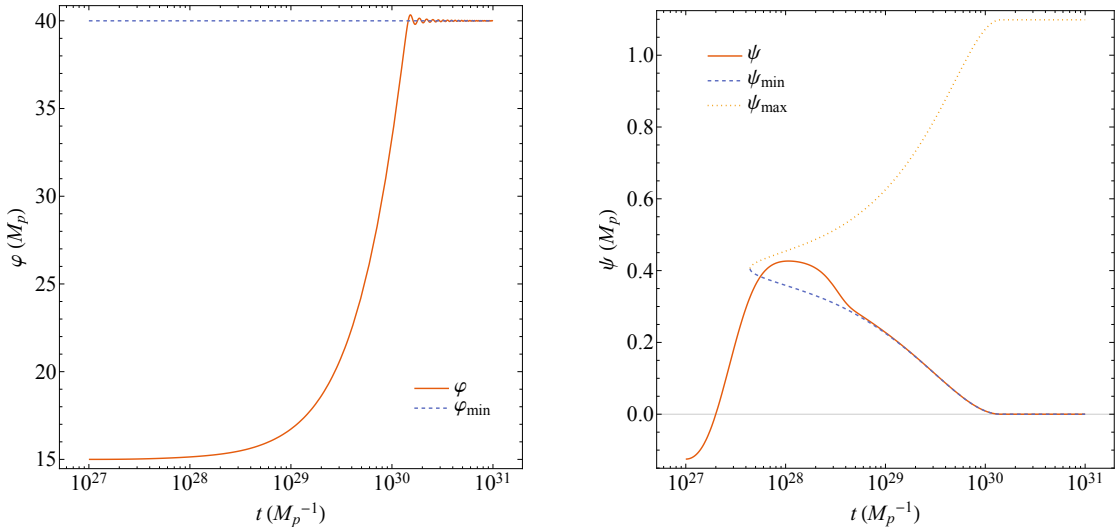

FIGURE 3.6: Plot of the inflaton (left) and radion (right) when ψ's minimum does not initially exist. We witness the twin births of the maximum and minimum from the inflection point early on the the evolution.

Additionally, the behaviour of ϵ (bottom left panel) is very typical: general integrations are attracted to particular values of ϵ, namely $\epsilon \simeq \frac{1}{2}, 3$. Constant values of ϵ are another indication of power-law inflation.

In order to better understand this behaviour and see if an analytic understanding of these numerical solutions allows us to achieve generic values of the inflationary parameters, we perform a comprehensive scaling solution search which we describe in the next chapter. Spoiler alert: the $\epsilon = \frac{1}{2}$ regime turns out to be interesting and is described in great detail in the next chapter, while the $\epsilon = 3$ scenario is described in Appendix D.

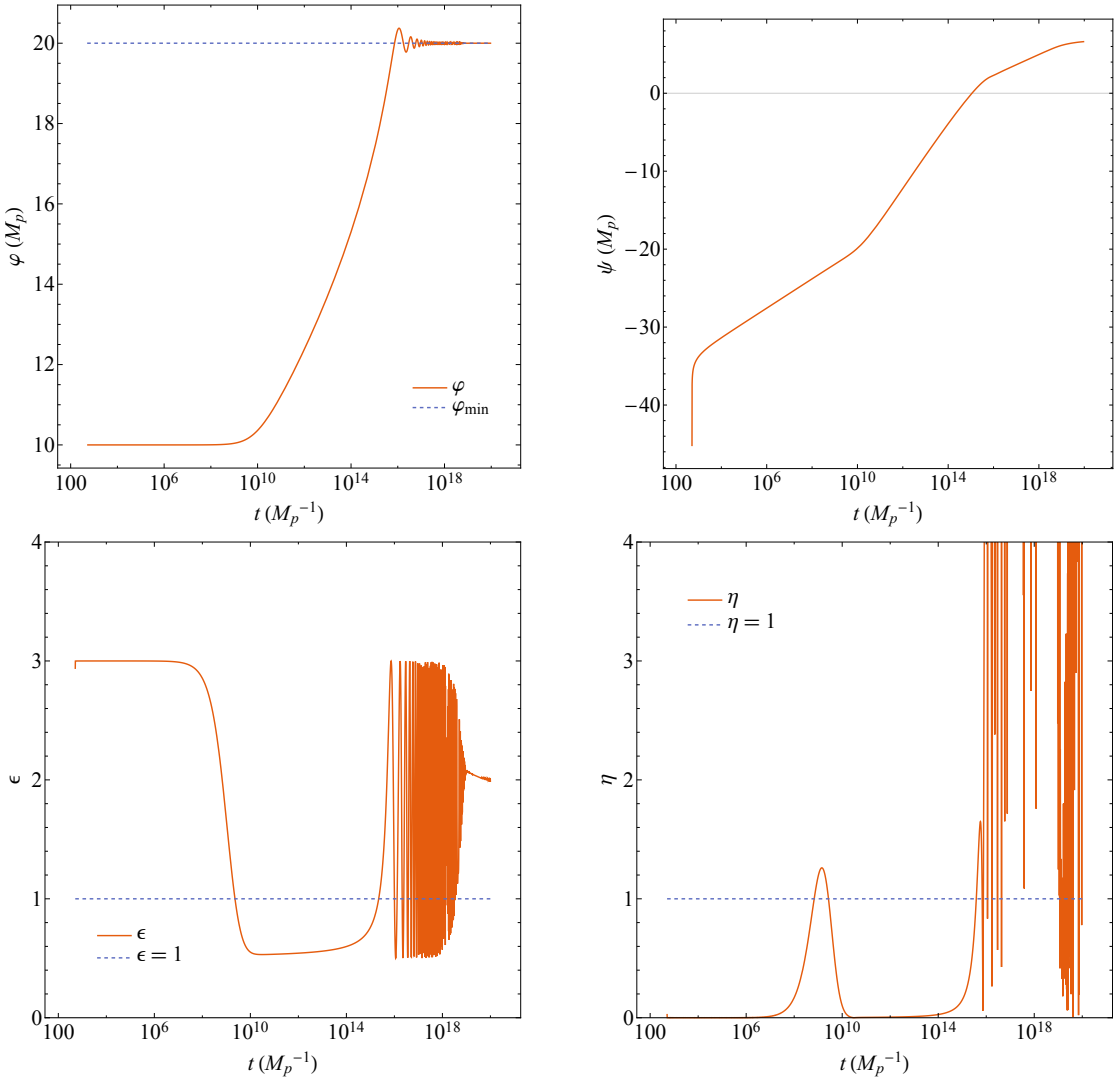

FIGURE 3.7: Plots (clockwise from top-left) of the inflaton, radion, η, and ϵ for a typical numeric evolution. Observe that the last three plots each demonstrate power-law behaviour in two different regimes: one in which $\epsilon \approx 3$, and the other $\epsilon \gtrsim 0.5$. In both regimes, power-law is revealed due to the straight-line trajectories in ψ, the constant behaviour of ϵ, and $\eta \approx 0$.

Chapter 4

The Power-Law Solutions

Having smelt scaling solutions sneaking around our numeric evolutions, we proceed to perform a comprehensive and systematic power-law analysis on our 4D EOMs. While we find many possible (and impossible) solutions in our analysis, we discuss the two interesting cases in detail here. A benefit of the power-law cases we describe here is that they can live in regimes where $H > m_{KK}$, an area of the sandbox which would normally be restricted; our consistent truncation grants us an all access pass and allows us to trust these solutions. We reserve Appendix D for the remaining cases. The parameters used to generate the figures in this chapter are detailed in Appendix E.

4.1 Scaling Solution Setup

This section outlines the power-law solutions we discover from the dimensionally-reduced 4D equations of motion. Once the general process is introduced, we highlight the two solutions of importance: a stable attractor solution and an unstable slow-roll solution. These are discussed in detail and we outline the benefits and drawbacks of each set of solutions. The stability of these two solutions is explicitly demonstrated in Appendix F.

Scaling solutions typically arise when the inflaton potential $U(\varphi)$ is dominated by a single exponential term [37]. In order to quantify and distinguish the various solutions, we take advantage of (2.24) which divides W, the total 4D potential, into three terms: $W^{(\varphi)}$, $W^{(c)}$, and $W^{(c)}$. These solutions can be classified according to the relative sizes of different terms in the total potential.

When seeking scaling solutions, we assume a single exponential dominates the inflaton potential, so we can approximate

$$U(\varphi) \simeq V_0\, e^{-\lambda\varphi/M_p}\,, \tag{4.1}$$

in the regime of interest. We then seek power-law scaling solutions to the 4D EOMs, (2.26), of the form

$$\begin{aligned} \frac{\varphi}{M_p} &= \frac{\varphi_0}{M_p} + p_1 \ln\left(\frac{t}{t_0}\right), \\ \frac{\psi}{M_p} &= \frac{\psi_0}{M_p} + p_2 \ln\left(\frac{t}{t_0}\right), \\ a &= a_0 \left(\frac{t}{t_0}\right)^{\alpha}, \end{aligned} \tag{4.2}$$

where φ_0, ψ_0, and a_0 are the initial values of the inflaton, radion, and scale factor respectively. From these *ansätze*, we also know

$$H = \frac{\alpha}{t} = H_0 \left(\frac{b_0}{b}\right)^{2/p_2}, \tag{4.3}$$

where $H_0 := \alpha/t_0$. To derive the second equality in (4.3), we solve our power-law assumption for ψ from (4.2) for t/t_0, and use (2.19) to write $t/t_0 = (b/b_0)^{2/p_2}$. The slow-roll parameters are then given by

$$\epsilon := -\frac{\dot{H}}{H^2} = \frac{1}{\alpha} \qquad \text{and so} \qquad \eta := \frac{\dot{\epsilon}}{H\epsilon} = 0\,. \tag{4.4}$$

Since inflation occurs when $\epsilon < 1$, these scaling solutions provide accelerated expansion when $\alpha > 1$. From (4.4), we now see explicitly how power-law inflation implies ϵ is constant, as seen in Figure gen:all.

One of the important behaviours we demand from our inflationary solutions is that they spend a sufficient time actually inflating. As described in Chapter 1, approximately 40–60 e-foldings of inflation are required to solve the Flatness and Horizon Problems, where N_e e-foldings means the scale factor a expanded by a factor of e^{N_e} [4]. Due to the form for H in (4.3), the scaling behaviour alone determines the amount of time the solution spends inflating. The number of e-foldings of inflation, as the fields inflate from t_0 to t_f, is given by

$$N_e := \int_{t_0}^{t_f} \mathrm{d}t\, H = \alpha \ln\left(\frac{t_f}{t_0}\right) = \frac{\alpha}{p_2}\left(\frac{\psi_f - \psi_0}{M_p}\right) = \frac{2\alpha}{p_2} \ln\left(\frac{b_f}{b_0}\right), \tag{4.5}$$

where the first equality uses (4.3), the second uses the power-law form of ψ from

(4.2) to replace t/t_0, and the last equality trades the canonical field ψ for the geometrical quantity b using (2.19). This provides a potentially novel connection between the number of e-foldings and the current size of the extra dimensions by providing an unexpected link between the two concepts. If α and p_2 are order unity and $b_f/b_0 \sim 10^{12}$ or 10^{16} during such a scaling regime,[1] then the above relation predicts our "usual" three spatial dimensions expand by about $N_e \approx 55$–70 e-foldings, which is close to the correct amount of inflation needed to solve the Horizon and Flatness Problems.

Substituting our power-law assumptions, (4.2), into our equations of motion, (2.26), we get:

$$\frac{p_1\,(3\alpha-1)}{t^2} = \lambda\frac{U_0}{M_p^2}\left(\frac{t}{t_0}\right)^{-(\lambda p_1+p_2)}, \tag{4.6}$$

$$\frac{2e^{-2\frac{\psi_0}{M_p}}}{b_\star^2}\left(\frac{t}{t_0}\right)^{-2p_2} + \frac{p_2(3\alpha-1)}{t^2} = \frac{U_0}{M_p^2}\left(\frac{t}{t_0}\right)^{-(\lambda p_1+p_2)} + \frac{6\pi\mathfrak{f}^2\,e^{-3\frac{\psi_0}{M_p}}}{b_\star^2 M_p^2}\left(\frac{t}{t_0}\right)^{-3p_2},$$

$$\frac{e^{-2\frac{\psi_0}{M_p}}}{b_\star^2}\left(\frac{t}{t_0}\right)^{-2p_2} + \frac{6\alpha^2-p_1^2-p_2^2}{2t^2} = \frac{U_0}{M_p^2}\left(\frac{t}{t_0}\right)^{-(\lambda p_1+p_2)} + \frac{2\pi\mathfrak{f}^2\,e^{-3\frac{\psi_0}{M_p}}}{b_\star^2 M_p^2}\left(\frac{t}{t_0}\right)^{-3p_2},$$

where $U_0 := 4\pi b_\star^2\,V_0\exp[-(\lambda\varphi_0+\psi_0)/M_p]$, a constant (and convenient shorthand). In deriving the above, we note the origins of the various terms in (4.6). By comparing with W in (2.23), we see:

- terms proportional to t^{-2p_2} are due to $W^{(c)}$,
- terms proportional to t^{-3p_2} and $\mathfrak{f}^2$ are due to $W^{(f)}$, and
- terms proportional to U_0 are due to $W^{(\varphi)}$.

The other terms (all proportional to t^{-2}) are due to the field terms and their derivatives.

In our analysis, (4.6) is the starting point. From here, we can derive solutions to the various powers p_1, p_2, and α by considering which terms dominate relative to each other. Depending on the various sizes of each of the terms mentioned above, (4.6) admits different classes of scaling solutions. We record and discuss

[1] Such ratios are possible if b runs from the Planck scale ($M_p \sim 10^{19}$ GeV) to the electroweak scale ($m_{\rm EW} \sim$ TeV), or from the electroweak scale to the micron scale ($m_{\rm micron} \sim$ eV).

the two interesting solutions discovered below and save the rest of the analysis for Appendix D.

4.2 Attractor Solution in 4D

The first solution we describe is an attractor (hence the title of this section). Other similar inflationary attractor solutions exist in the literature [37, 45–48]. We outline the benefits and drawbacks of this solution briefly before diving into the analytics.

The most attractive feature of this solution is its own attractive nature: when initial conditions are perturbed, nearby trajectories tend to converge towards this solution again at late times. This attractor behaviour is evident in our numerical solutions, which are often drawn towards this particular scaling solution even when starting from a wide range of initial conditions. We explicitly compute the stability of this solution in Appendix F, where the linearized equations are solved to show that perturbations converge like a calculable power of time. Once established, this solution tends to last until one of its underlying assumptions begins to fail; chief amongst these is the assumption that W is dominated by a particular exponential term. For instance, motion of the scalar field, ϕ, eventually finds its minimum at which point the inflaton potential is no longer dominated by a single exponential—which it cannot be if a minimum for the inflaton is to exist. So, without further ado, let us introduce the solution.

4.2.1 Analytics

This solution is obtained when $\left|W^{(\varphi)}\right| \gg \left|W^{(c)}\right|, \left|W^{(f)}\right|$. In this case, the power-law equations of motion, (4.6), reduce to

$$\begin{aligned}
\frac{p_1(3\alpha-1)}{t^2} &= \frac{\lambda U_0}{M_p^2}\left(\frac{t}{t_0}\right)^{-(\lambda p_1+p_2)}, \\
\frac{p_2(3\alpha-1)}{t^2} &= \frac{U_0}{M_p^2}\left(\frac{t}{t_0}\right)^{-(\lambda p_1+p_2)}, \\
\frac{6\alpha^2-p_1^2-p_2^2}{t^2} &= \frac{2U_0}{M_p^2}\left(\frac{t}{t_0}\right)^{-(\lambda p_1+p_2)}.
\end{aligned} \tag{4.7}$$

By equating exponents of time, we see that $\lambda p_1 + p_2 = 2$. Substituting this result back into the above, we are left with a system of equations that can be solved for the powers:

$$\alpha = \frac{2}{1+\lambda^2}\,, \qquad p_1 = \alpha\lambda\,, \qquad p_2 = \alpha\,; \tag{4.8}$$

and the relationship between the coefficients

$$t_0^2 = \frac{\left(5-\lambda^2\right)\alpha^2 M_p^2}{2U_0}\,, \tag{4.9}$$

which is the initial condition necessary to begin our integration in this solution.

Using (4.8) in (4.4) we are able to write

$$\epsilon = \frac{1}{\alpha} = \frac{1+\lambda^2}{2}\,, \tag{4.10}$$

while $\eta = 0$, as is always the case in power-law inflation. Clearly, ϵ has a lower bound $\epsilon \geq \frac{1}{2}$. Furthermore, since $\alpha = p_2$, the number of e-foldings according to (4.5) is

$$N_e = \frac{\psi_f - \psi_0}{M_p} = 2\ln\left(\frac{b_f}{b_0}\right)\,, \tag{4.11}$$

and so the power-dependence drops out, leaving N_e to depend solely on the ratio b_f/b_0.

4.2.2 Numerics

Using (4.2), we can write $\dot{\varphi}/M_p = p_1/t$ and $\dot{\psi}/M_p = p_2/t$. These velocities are useful in demonstrating that the analytical solution presented above provides a decent description of the numerical solutions. We can plot $p_1(t) = t\,\dot{\varphi}(t)/M_p$ and $p_2(t) = t\,\dot{\psi}(t)/M_p$ using our numerically integrated function for $\dot{\varphi}(t)$ and $\dot{\psi}(t)$, and compare this with the analytically calculated constants p_1 and p_2 from (4.8) above. Figure 4.1 shows, for a representative evolution, the regime of reasonable agreement between the analytics and the numerics. At later times in the plots, the agreement breaks down as our single-exponential approximation, (4.1), becomes less and less valid. This also provides a natural end to inflation, which is an attractive feature of this solution.

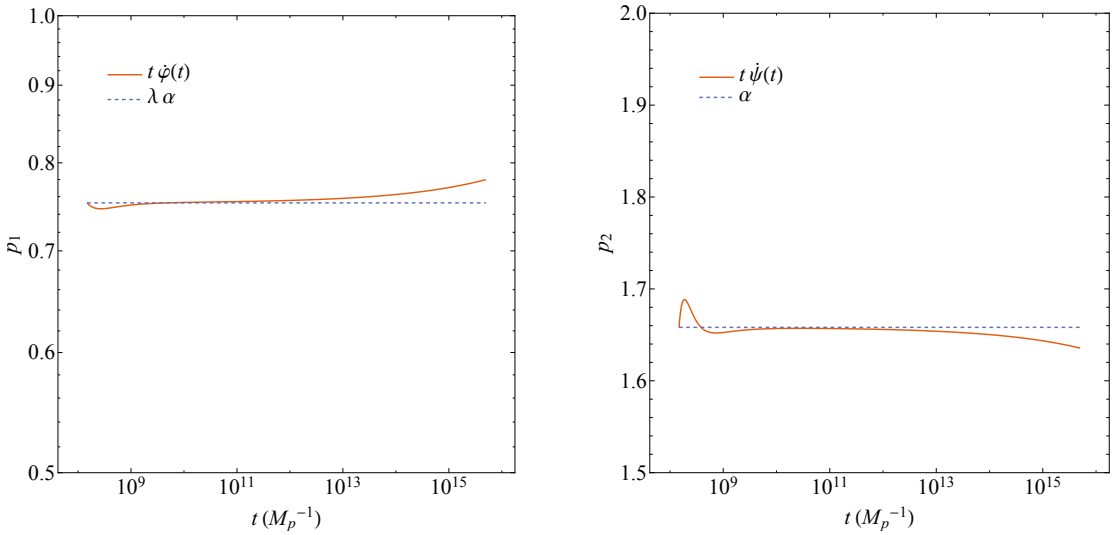

FIGURE 4.1: Plots of p_1 (left) and p_2 (right) vs t computed two ways. The first method is using the numerically-integrated $\dot{\varphi}$ and $\dot{\psi}$. These are compared with the analytical prediction from (4.8), which predicts $p_1 = \lambda\alpha$ and $p_2 = \alpha$. Reasonable agreement is seen between the numerics and analytics indicating we are arguably seeing the attractor scaling solution. Note that the agreement begins to break down as the approximation that $U(\varphi)$ is a single exponential begins to fail.

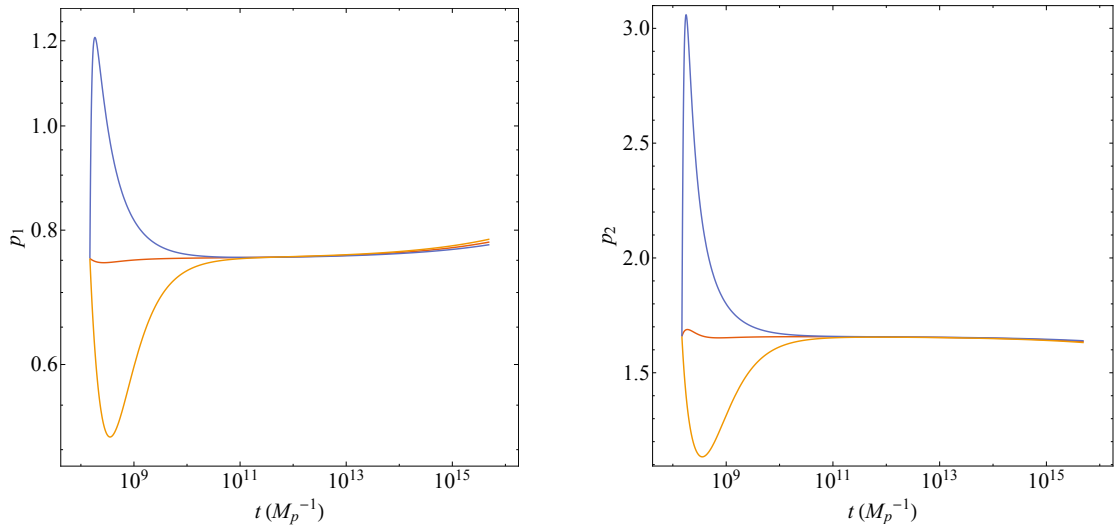

FIGURE 4.2: Plots of $p_1 = t\dot{\varphi}/M_p$ (left) and $p_2 = t\dot{\psi}/M_p$ (right) vs t for several similar initial conditions. Despite an assortment of initial conditions, each solution approaches roughly the same behaviour at late times demonstrating the attractor nature of this solution explicitly.

We can also use the field velocities to demonstrate this solution's attractor behaviour. In Figure 4.2, we plot p_1 and p_2 for a slew of different initial conditions and demonstrate explicitly that they all approach the same behaviour at late times. We are ignorant no longer to the behaviour noted in Section 3.4. In that section, we discuss the recurring behaviour of $\epsilon \simeq 0.5$, which can be seen about halfway through the representative plot in the lower left panel of Figure 3.7. The numerics consistently display this behaviour because the solution is an attractor for regimes in which $\left|W^{(\varphi)}\right| \gg \left|W^{(c)}\right|, \left|W^{(f)}\right|$.

Another feature that this solution enjoys is the fact that $H > m_{KK}$ for the entire evolution. This means it is a solution we would have been blind to had we opted to work in a 4D effective theory as is usually the case. However, because we consistently-truncated our 6D system onto the 4D realm, we can trust this solution regardless of the relationship between the Hubble- and KK-scales. This is demonstrated explicitly in Figure 4.3.

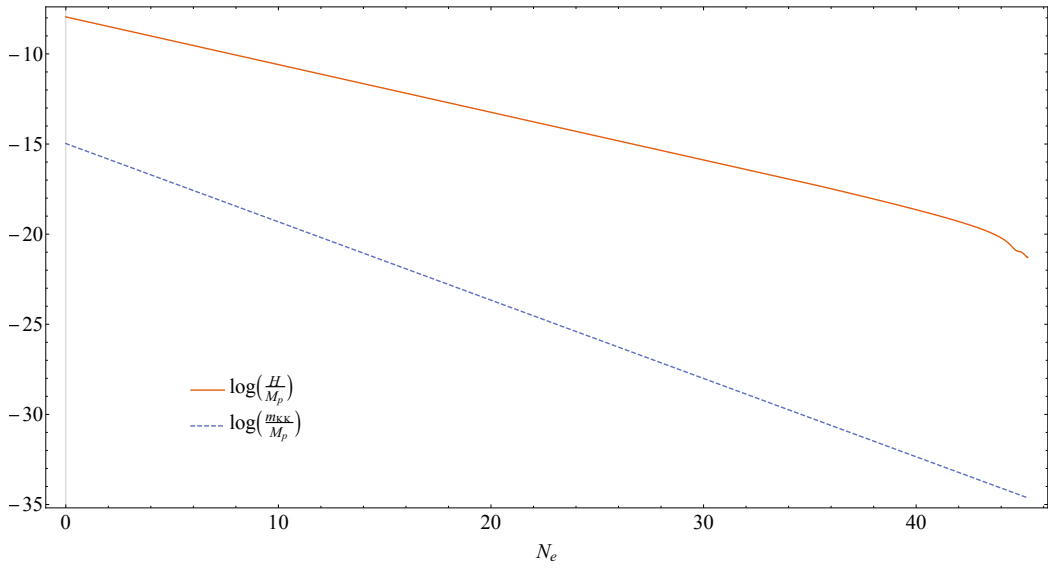

FIGURE 4.3: Plot of log H and log m_{KK} vs N_e. Notice that we live in an inflationary regime in which $H > m_{KK}$ for the whole evolution.

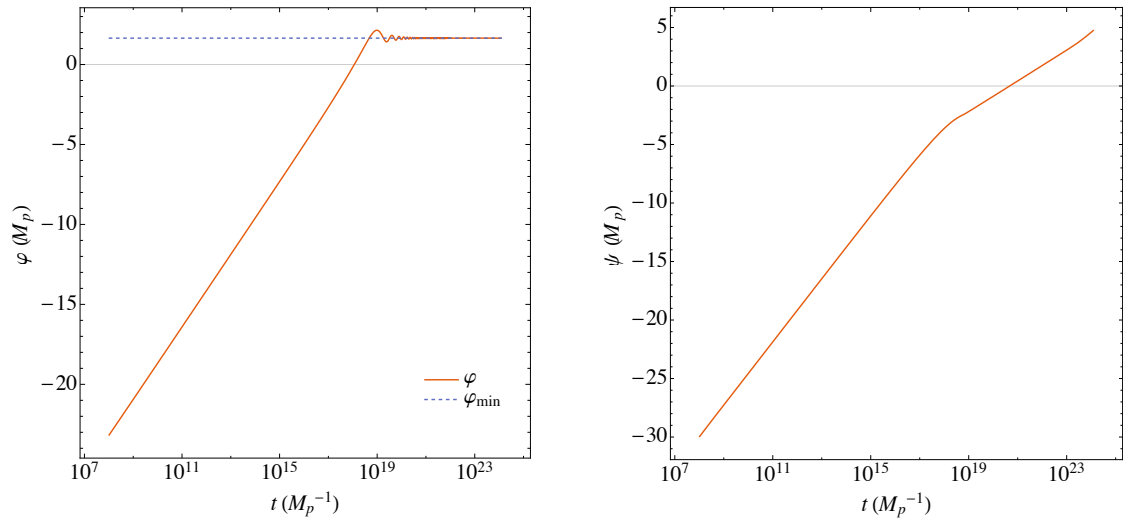

FIGURE 4.4: Plots of φ (left) and ψ (right) vs t without any additional means to trap ψ. Notice that the radion's minimum at $\psi = 0$ has no noticeable effect on its motion.

4.2.3 Radius Stabilization

In it useful at this point to recall the behaviour of W, whose shape is plotted in Figure 3.1. We can see from Figure 4.4 that φ and ψ are behaving exactly as we might expect them to. As the inflaton rolls towards its minimum, only one exponential is dominating its potential and so both the inflaton and radion roll as power-laws. However, we see ψ's behaviour change right as φ is approaching its minimum at about $t \sim 10^{19}$; here, our single-exponential approximation begins to break down as discussed in reference to Figure 4.1. As φ settles into its minimum, it brings W into a region where a minimum for ψ exists. To profit from modulus stabilization we desire inflationary solutions that conclude with ψ being trapped at its minimum. However, even if conditions are such that there exists a minimum into which ψ may settle, there is generically an overshoot problem: ψ comes in way too hot for a controlled landing. Typically, ψ acquires far too much kinetic energy to prevent it from climbing over the potential barrier and escaping towards infinity as shown in the late times of Figure 4.4's right panel. Indeed, care must be taken not to overshoot the local maximum (which is not very high) and this is what we see happen for all the choices of initial conditions we explored.

An alternative method [49, 50] of slowing down the radion was investigated during the course of the project (we introduced a bout of friction that the inflaton experiences, which removes sufficient kinetic energy from the system for ψ to not overshoot its minimum); however, this mechanism is not a focus of this author and hence any discussion is saved for [3].

4.2.4 Duration of Inflation

Even if the radion is trapped with some such mechanism, the resulting solution has one final drawback that is slightly more rigid. There is a strict upper bound on N_e. One might naïvely expect that, by substituting $\psi_0/M_p = -66$ from (3.4) and $\psi_f = 0$ into (4.11), we could easily have sufficient e-foldings. However, there exists a stricter limit on ψ_0 than the one imposed by (3.1). In this scenario, recall that power-law is achieved when $\left|W^{(\varphi)}\right| \gg \left|W^{(c)}\right|, \left|W^{(f)}\right|$. Moreover, since there exists flux to trap the radion, $\left|W^{(c)}\right| < \left|W^{(f)}\right|$, and hence the flux contributions will

be competing with $\left|W^{(\varphi)}\right|$ at early times. Explicitly,

$$\left|W^{(\varphi)}\right| \geq \left|W^{(f)}\right| \implies 4\pi b_\star^2 e^{-\psi/M_p} U(\varphi) \geq \frac{M_p^2\, e^{-3\psi/M_p}}{2b_\star^2}\,. \tag{4.12}$$

Therefore

$$\frac{\psi_0}{M_p} \geq -\frac{1}{2}\ln\left(\frac{8\pi b_\star^4\, U(\varphi)}{M_p^2}\right). \tag{4.13}$$

This limit is optimized when U and $b_\star$ are as large as they can be, whose values are given in (3.2) and (3.3), and so

$$\frac{\psi_0}{M_p} \geq -\frac{1}{2}\ln\left(\frac{b_\star M_p}{\sqrt{\pi}}\right) \simeq -\frac{1}{2}\ln\left(\frac{2\times 10^{28}}{\pi}\right) \approx -32\,. \tag{4.14}$$

So, by substituting (4.14) into (4.11)—with $\psi_f = \psi_\star = 0$, its present-day value, we find this solution provides, at most, $N_e \approx 32$ e-foldings of inflation.

4.3 Slow-Roll Solution

There is a second power-law solution that our numerical solutions exposed which differs from the attractor solution described in the previous section in several ways. The main two of these are: it can allow much smaller values of ϵ (hence why we refer to it as a *slow-roll* solution); and it is not an attractor, since the stability analysis of Appendix F reveals a single growing mode for perturbed trajectories. We see, in general, numerical solutions that start in the present scaling solution eventually cross over to other solutions, such as the attractor solution from the previous section.

4.3.1 Analytics

For this solution, we require the hierarchy amongst terms in W to be $\left|W^{(\varphi)}\right| \sim \left|W^{(c)}\right| \gg \left|W^{(f)}\right|$. In this case, the power-law equations of motion, (4.6), reduce to:

$$\begin{aligned}
\frac{p_1(3\alpha-1)}{t^2} &= \frac{\lambda U_0}{M_p^2}\left(\frac{t}{t_0}\right)^{-(\lambda p_1+p_2)}\,, \\
\frac{p_2(3\alpha-1)}{t^2} &= \frac{U_0}{M_p^2}\left(\frac{t}{t_0}\right)^{-(\lambda p_1+p_2)} - \frac{2}{b_\star^2}\,e^{-2\psi_0/M_p}\left(\frac{t}{t_0}\right)^{-2p_2}\,, \\
\frac{6\alpha^2-p_1^2-p_2^2}{t^2} &= \frac{2U_0}{M_p^2}\left(\frac{t}{t_0}\right)^{-(\lambda p_1+p_2)} - \frac{2}{b_\star^2}\,e^{-2\psi_0/M_p}\left(\frac{t}{t_0}\right)^{-2p_2}\,.
\end{aligned} \tag{4.15}$$

Again, by equating the exponents and coefficients of time, we can solve for the predicted powers

$$p_1 = \frac{1}{\lambda}\,, \qquad p_2 = 1\,, \qquad \text{and} \qquad \alpha = \frac{1+\lambda^2}{2\lambda^2}\,, \tag{4.16}$$

and for the relationships between our initial conditions

$$U_0 = \frac{2M_p^2}{(1-\lambda^2)\,b_\star^2}\,e^{-2\psi_0/M_p} \qquad \text{and} \qquad t_0^2 = \frac{\left(\lambda^2+3\right)M_p^2}{2\lambda^4 U_0}\,. \tag{4.17}$$

The expression for α in (4.16) implies the slow-roll parameters for this solution are

$$\epsilon = \frac{1}{\alpha} = \frac{2\lambda^2}{1+\lambda^2}\,, \qquad \text{and} \qquad \eta = 0\,, \tag{4.18}$$

which shows that ϵ can be made arbitrarily small merely by choosing λ to be sufficiently small.

Additionally, since $p_2 = 1$ in this case, the number of e-foldings given by (4.5) is

$$N_e = \frac{\psi_f - \psi_0}{\epsilon\, M_p} = \frac{2}{\epsilon}\,\ln\left(\frac{b_f}{b_0}\right), \tag{4.19}$$

which can be large for sufficiently small ϵ even if b_f/b_0 is not. Therefore, we have found a solution that has no restrictions on N_e or ϵ, and must also naturally end

due to its unstable nature.

4.3.2 Numerics

Our systematic power-law calculations revealed this unstable solution to which we otherwise would have been blind. Without being aware of this unstable solution, the chances of us choosing (4.17) as our initial conditions are minuscule. However, the veil is lifted from our eyes and we can see, clearly, that this solution exists. And, like a colonial power, we must take advantage of this land of milk and honey.

From the point of view of inflationary phenomenology, (4.18) is a huge advantage of this solution. We can choose ϵ to be as small as we like by choosing λ appropriately. In the example illustrated, we choose $\epsilon = 0.006$ (which corresponds to $\lambda \approx 0.055$) so that, if 4D calculations of fluctuations were to apply, we would expect $n_s \simeq 0.96$ and $r \simeq 0.096$ from (3.8). Our numerics agree with these predictions to within one part in 10^8 and one part in 10^5, for ϵ and η respectively.

We can again characterize this solution by the velocities of φ and ψ which are parametrized by $p_1(t) = t\,\dot{\varphi}(t)/M_p$ and $p_2(t) = t\,\dot{\psi}(t)/M_p$. Figure 4.5 shows a numerical evolution with the solution behaving exactly as our analytics predict. Initial conditions are chosen using (4.17) so that our numerics start in this scaling solution. We find the time spent in this solution is consistent with the machine precision with which *Mathematica* operates which in turn creates imprecise initial conditions. These deviations from (4.17) slowly grow with time until eventually they cause the system to leave the slow-roll regime. The right two panels in Figure 4.5 also show how the system tends towards the attractor solution (characterized by the values of p_1 and p_2) once it leaves the unstable slow-roll solution.

Unlike our previous scaling solution, this particular evolution lives in an area where $H < m_{KK}$. Figure 4.6 plots H and m_{KK} to demonstrate this explicitly. This plot further highlights the instability of this solution since we see two distinct regions in the figure. While this particular solution lives below the KK-scale, there is nothing that explicitly restricts these solutions to that realm.

4.3.3 Radius Stabilization

The instability of the scaling solution is arguably both a blessing and a curse. On one hand, it provides a simple, natural way to end inflation: any discrepancy between the initial conditions and the scaling solution will be amplified as the solution evolves without any of our power-law assumptions changing. This provides

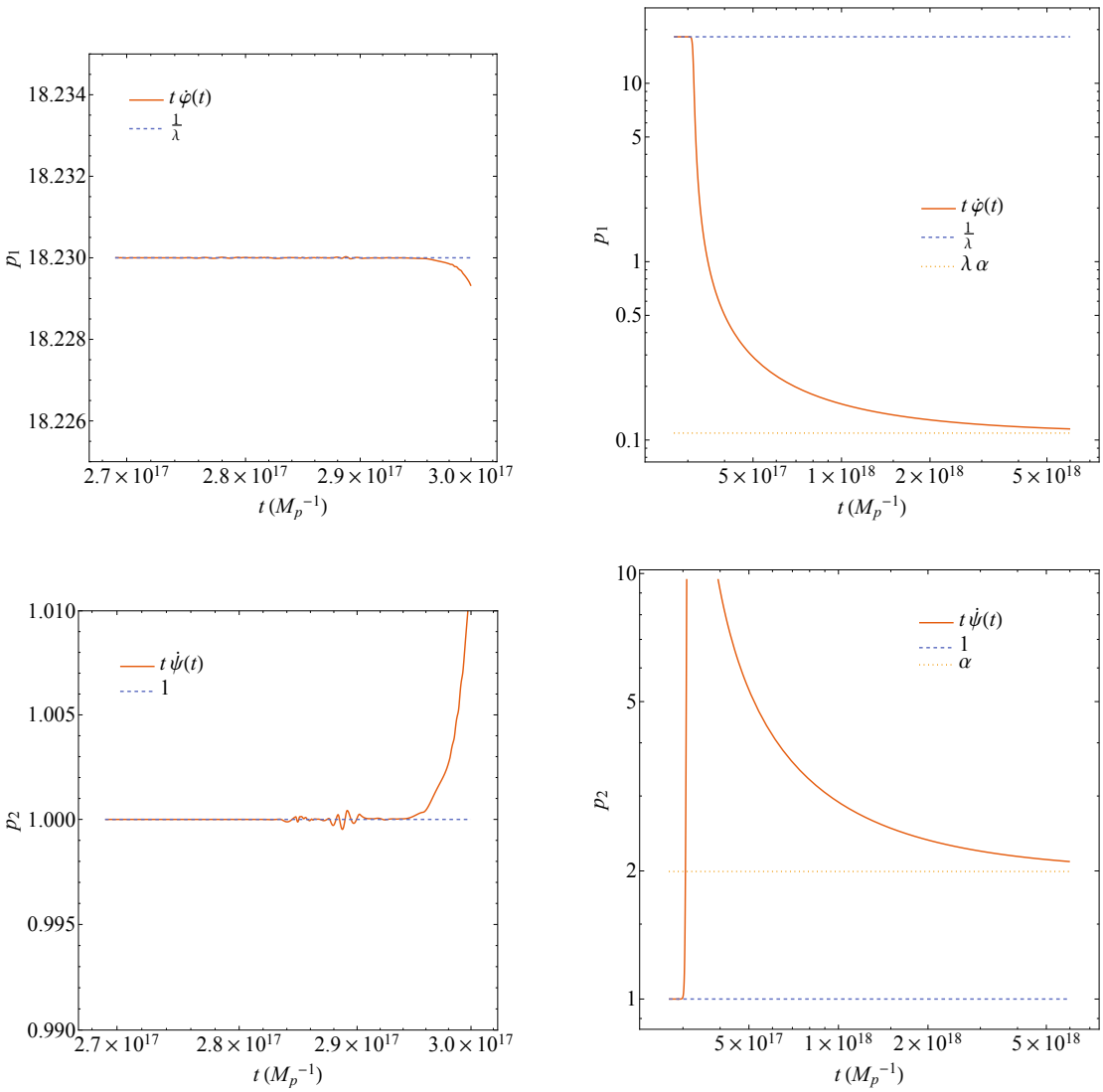

FIGURE 4.5: Plots of $p_1 = t\dot{\varphi}/M_p$ (top) and $p_2 = t\dot{\psi}/M_p$ (bottom) vs t for the slow-roll scaling solution. On the left is an enlarged view of the slow-roll regime which highlights the agreement of our numerical solutions with the analytical predictions of (4.16), repeated in the legend of convenience. On the right, we see the transition from the unstable to the stable attractor solution by comparing the numerically-determined p_i with the powers predicted in the attractor case from (4.8).

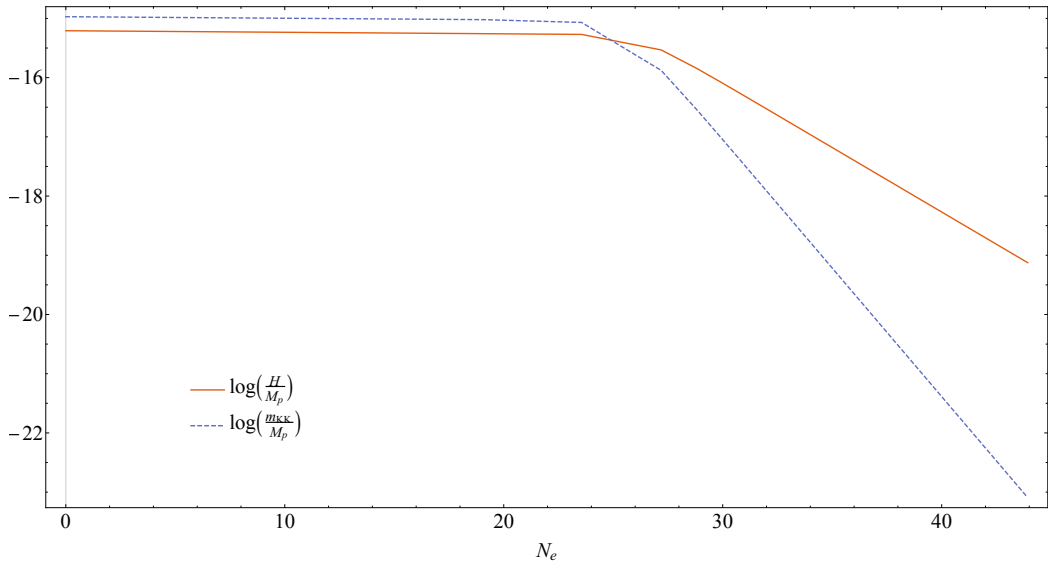

FIGURE 4.6: Plot of $\log H$ and $\log m_{\mathrm{KK}}$ in Planck units vs N_e. This plot also explicitly shows the transition from the unstable solution (in which $H < m_{KK}$) to the attractor solution. The straight lines on this log-log plot beautifully demonstrate the power-law behaviour.

a simple method by which we can generate as many e-foldings as is desirable, but at the cost of introducing specially chosen initial conditions.

On the other hand, describing inflation via this solution does not allow for simple trapping of the radion. This is because this solution's defining condition, $\left|W^{(\varphi)}\right| \sim \left|W^{(c)}\right| \gg \left|W^{(f)}\right|$, makes it impossible to end at a time when there is a flux-stabilized minimum for ψ. Recall from (3.7) that, for a minimum to exist, the flux contributions to the stress-energy during inflation must exceed those of the curvature's stress-energy. So we can see that if we want a minimum to exist for ψ it is impossible to achieve solely within solution. Consequently, the stabilization of the modulus in this class of solutions would require a different mechanism than the one studied here. However, this does not afford us too much concern: due to its unstable nature this solution can be tuned to pass into a regime in which stabilization can occur naturally, such as the attractor solution.

4.4 Summary of Power-law Inflationary Solutions

Let us briefly pause to recount both our goals and outcomes. Given the 6D model of Chapter 2, Chapter 3 recounts our attempts and desires to numerically integrate the EOMs. Upon noticing regimes in our plots indicative of power-law relationships, we pursue the power-law analysis described in this chapter. While we perform a systematic power-law search, the bulk of which is described in Appendix D, we only find two solutions that provide us with interesting inflationary results.

In addition to being an attractor, the first solution is interesting for a number of other reasons, chief amongst these, perhaps, is the fact that it lives where no effective theory has gone before, where $H > m_{KK}$. Moreover, it allows for inflation to naturally end. In any theory of inflation, we only want a brief period of inflation (for the 40–60 e-foldings or so) after which the universe's expansion is no longer accelerating. As both the inflaton and radion approach their minima our single-exponential approximation begins to lose its validity as the second exponential appears to form φ's minimum. This naturally drives our period of inflation to a halt when both fields arrive at their minima.

Two principle phenomenological drawbacks of this particular solution are its lower bound of $\epsilon \geq \frac{1}{2}$ and upper bound on the number of e-foldings of $N_e \lesssim 32$. In order to agree with the most recent constraints of $r \sim 0.1$, we require $\epsilon \sim 0.1/16 \approx 0.00625 \ll 0.5$: this precludes using it to describe primordial fluctuations using the standard mechanism of inflaton vacuum fluctuations. Furthermore, as described

in Chapter 1, a good theory of inflation requires about 40–60 e-foldings of inflation, yet this solution is restricted to $N_e \lesssim 30$. Additionally, we find that there exists a rather generic overshoot problem when we attempt to stabilize the radius of the extra dimensions.

The second solution of interest is not attractive to generic initial conditions, but we are not shallow and so can see the beauty that lies within. Perhaps the most attractive feature of this solution is that it restricts neither ϵ nor N_e, unlike the previously-described attractor case which had fairly strict bounds on both quantities. This allows us, via a particular choice of initial conditions and parameters, to find a small enough ϵ that can satisfy current observational bounds (hence why we call it a *slow-roll* solution), while allowing inflation to last for the desired ~ 60 e-foldings.

This solution's unstable nature provides a natural way of ending inflation—the point in time at which the solution is perturbed significantly so that it ultimately crosses over to another solution, like the attractor solution, say—but also necessarily requires finely-tuned initial conditions to land squarely in this solution.

Finally, this solution explicitly forbids a minimum for ψ, which means a realistic scenario described by this solution requires an alternative means for modulus stabilization beyond the simplest flux-stabilization mechanism employed in this project.

Conclusions

In this chapter, we summarize the project and re-cap the important points of the system described in the main body of the thesis.

We seek to find solutions that exist outside of a usual 4D effective theory's lamp-post. In order to do this, we dimensionally reduce a 6D inflationary model onto 4D by performing a consistent truncation, which means that our 4D equations all exactly solve the 6D field equations as well. After performing a general scan over a wide range of initial conditions in an attempt to numerically integrate the equations of motion for an inflaton and radion, we notice that a wide range of solutions demonstrated scaling behaviour. This ultimately leads us to search, analytically, for scaling solutions.

While the search is complete, general, and extensive, we ultimately find only two scaling solutions of particular interest. In addition to being an attractor, the first solution is interesting for another reason: it allows for inflation to naturally end. In any theory of inflation, we only want a brief period of inflation (for 40–60 e-foldings or so) after which the universe's expansion is no longer inflation-driven. As both the inflaton and radion approach their respective minima (i.e., as they roll down their potentials) our single-exponential approximation loses its validity as the second exponential appears to form φ's minimum. This naturally drives our period of inflation to a halt when both fields arrive at their minima. This is possible because the relative sizes of the various terms in the 4D potential allowed for the radion to be trapped by flux stabilization.

Two principle phenomenological drawbacks of this particular solution are its lower bound of $\epsilon \geq \frac{1}{2}$ and upper bound on the number of e-foldings of $N_e \lesssim 32$. In order to agree with the most recent constraints of $r \sim 0.1$, we require $\epsilon \sim 0.1/16 \approx 0.00625 \ll 0.5$: this precludes using it to describe primordial fluctuations using the standard mechanism of inflaton vacuum fluctuations. However, since it does not live in the usual 4D effective realm, other descriptions of primordial fluctuations could present a different expected value for ϵ. Furthermore, as we describe in Chapter 1, a good theory of inflation requires about 40–60 e-foldings of inflation, yet this solution was restricted to $N_e \lesssim 30$.

The second solution of interest is not attractive to generic initial conditions, but it restricts neither ϵ nor N_e, unlike the previously described attractor case which has fairly strict bounds on both quantities. This enables us, via a particular choice of initial conditions and parameters, to find a small enough ϵ that can satisfy current observational bounds and last long enough.

This solution's unstable nature also provides a natural way of ending inflation, but also necessarily requires finely-tuned initial conditions to begin in this solution.

Finally, this solution explicitly forbids W from having a minimum for ψ, which means a realistic scenario described by this solution requires an alternative means for modulus stabilization beyond the simplest flux-stabilization mechanism employed herein.

We strive to present *Goldilocks* models of inflation that are well-posed to answer UV-completion questions using extra dimensions. We perform this analysis outside of the usual neighbourhood of 4D effective theories (which restrict themselves to neighbourhoods were $H < m_{KK}$) by instead solving all the 6D field equations explicitly in an equivalent 4D setting, an important feature of our models. Additionally, we exploit a Maxwell field embedded solely in the extra dimensions as a mechanism for modulus stabilization to prevent it from growing indefinitely. The final interesting property of our analysis came as a revelation during the analysis itself, as opposed to a motivating, attractive feature. We find our power-law solutions give rise to an alluring relationship between the number of e-foldings of inflation, N_e and the size of the extra dimensions, b:

$$N_e = 2\left(\frac{\alpha}{p_2}\right)\ln\left(\frac{b_f}{b_0}\right),$$

an interesting relationship since it ties together the size of two seemingly-unrelated quantities. This also gives some tantalizing numerology in that if the extra dimensions were to expand from about the EW scale to the Planck scale, the universe would inflate approximately 60 e-foldings, if α and p_2 are $\mathcal{O}(1)$. This perhaps hints at a fundamental connection between the two parameters.

We ultimately present models that can be of use in the future study of extra-dimensional inflation due to the above four attractive properties these models enjoy: they exactly solve the general 6D field equations, they include flux stabilization, they are Goldilocks models, and they reveal an interesting numerological relationship between the inflation of the 4D universe and the size of the extra dimensions. Furthermore, due to the systematic scaling solution search performed by this author, we are able to classify two classes of power-law inflation. While the

attractor case has the potential to exploit the flux stabilization, the kinetic energy of the radion shut this down pretty quickly, whereas the slow-roll, unstable solution can not even allow the modulus to be stabilized by the extra-dimensional flux leaving additional slowing mechanisms to be desired or designed. However, the two Goldilocks scaling solutions described herein both exactly solve the 6D field equations and both have an interesting relationship between N_e and b. In these ways, our models have been presented as a new set of tools that your friendly neighbourhood cosmologist may add to his/her toolkit as he/she tinkers with the universe.

References

[1] PLANCK collaboration, P. A. R. Ade et al., *Planck 2013 results. I. Overview of products and scientific results*, *Astron. Astrophys.* **571** (2014) A1, [1303.5062].

[2] P. J. Mohr, D. B. Newell and B. N. Taylor, *CODATA Recommended Values of the Fundamental Physical Constants: 2014*, 1507.07956.

[3] C. P. Burgess, J. J. H. Enns, P. Hayman and S. P. Patil, *Goldilocks Models of Higher-Dimensional Inflation (including modulus stabilization)*, 1605.03297.

[4] A. H. Guth, *The Inflationary Universe: A Possible Solution to the Horizon and Flatness Problems*, *Phys. Rev.* **D23** (1981) 347–356.

[5] A. D. Linde, *A New Inflationary Universe Scenario: A Possible Solution of the Horizon, Flatness, Homogeneity, Isotropy and Primordial Monopole Problems*, *Phys. Lett.* **B108** (1982) 389–393.

[6] A. Albrecht and P. J. Steinhardt, *Cosmology for Grand Unified Theories with Radiatively Induced Symmetry Breaking*, *Phys. Rev. Lett.* **48** (1982) 1220–1223.

[7] M. Gasperini and G. Veneziano, *Pre - big bang in string cosmology*, *Astropart. Phys.* **1** (1993) 317–339, [hep-th/9211021].

[8] J. Khoury, B. A. Ovrut, P. J. Steinhardt and N. Turok, *The Ekpyrotic universe: Colliding branes and the origin of the hot big bang*, *Phys. Rev.* **D64** (2001) 123522, [hep-th/0103239].

[9] A. Ashtekar, A. Corichi and P. Singh, *Robustness of key features of loop quantum cosmology*, *Phys. Rev.* **D77** (2008) 024046, [0710.3565].

[10] E. I. Buchbinder, J. Khoury and B. A. Ovrut, *New Ekpyrotic cosmology*, *Phys. Rev.* **D76** (2007) 123503, [hep-th/0702154].

[11] D. A. Easson, I. Sawicki and A. Vikman, *G-Bounce*, *JCAP* **1111** (2011) 021, [1109.1047].

[12] C. Kounnas, H. Partouche and N. Toumbas, *S-brane to thermal non-singular string cosmology*, *Class. Quant. Grav.* **29** (2012) 095014, [1111.5816].

[13] R. H. Brandenberger, C. Kounnas, H. Partouche, S. P. Patil and N. Toumbas, *Cosmological Perturbations Across an S-brane*, *JCAP* **1403** (2014) 015, [1312.2524].

[14] R. H. Brandenberger, *Inflationary cosmology: Progress and problems*, in *IPM School on Cosmology 1999: Large Scale Structure Formation Tehran, Iran, January 23-February 4, 1999*, 1999. hep-ph/9910410.

[15] C. P. Burgess and L. McAllister, *Challenges for String Cosmology*, *Class. Quant. Grav.* **28** (2011) 204002, [1108.2660].

[16] A. Ijjas and P. J. Steinhardt, *Implications of Planck2015 for inflationary, ekpyrotic and anamorphic bouncing cosmologies*, *Class. Quant. Grav.* **33** (2016) 044001, [1512.09010].

[17] E. E. Flanagan, S. H. H. Tye and I. Wasserman, *Cosmological expansion in the Randall-Sundrum brane world scenario*, *Phys. Rev.* **D62** (2000) 044039, [hep-ph/9910498].

[18] L. Randall and R. Sundrum, *A Large mass hierarchy from a small extra dimension*, *Phys. Rev. Lett.* **83** (1999) 3370–3373, [hep-ph/9905221].

[19] J. M. Cline, *Cosmological expansion in the Randall-Sundrum warped compactification*, in *Proceedings, 3rd International Conference on Particle Physics and the Early Universe (COSMO 1999)*, pp. 472–479, 2000. hep-ph/0001285. DOI.

[20] H. B. Kim, *Cosmology of Randall-Sundrum models with an extra dimension stabilized by balancing bulk matter*, *Phys. Lett.* **B478** (2000) 285–293, [hep-th/0001209].

[21] J. Lesgourgues, S. Pastor, M. Peloso and L. Sorbo, *Cosmology of the Randall-Sundrum model after dilaton stabilization*, *Phys. Lett.* **B489** (2000) 411, [hep-ph/0004086].

[22] A. D. Linde, *Inflation and string cosmology*, *Prog. Theor. Phys. Suppl.* **163** (2006) 295–322, [hep-th/0503195].

[23] C. P. Burgess, *Lectures on Cosmic Inflation and its Potential Stringy Realizations*, *Class. Quant. Grav.* **24** (2007) S795, [0708.2865].

[24] D. Baumann and L. McAllister, *Advances in Inflation in String Theory*, *Ann. Rev. Nucl. Part. Sci.* **59** (2009) 67–94, [0901.0265].

[25] L. van Nierop and C. P. Burgess, *Sculpting the Extra Dimensions: Inflation from Codimension-2 Brane Back-reaction*, *JCAP* **1204** (2012) 037, [1108.2553].

[26] M. Cicoli and F. Quevedo, *String moduli inflation: An overview*, *Class. Quant. Grav.* **28** (2011) 204001, [1108.2659].

[27] C. P. Burgess, M. Cicoli and F. Quevedo, *String Inflation After Planck 2013*, *JCAP* **1311** (2013) 003, [1306.3512].

[28] E. Silverstein, *Inflation in string theory confronts data/Les modèles d'inflation en théorie des cordes face aux observations*, 1512.02089.

[29] S. B. Giddings, S. Kachru and J. Polchinski, *Hierarchies from fluxes in string compactifications*, *Phys. Rev.* **D66** (2002) 106006, [hep-th/0105097].

[30] M. Grana, *Flux compactifications in string theory: A Comprehensive review*, *Phys. Rept.* **423** (2006) 91–158, [hep-th/0509003].

[31] Wolfram Research, Inc., "Mathematica."

[32] S. Weinberg, *Gravitation and Cosmology*. John Wiley and Sons, New York, 1972.

[33] D. Baumann, *Inflation*, in *Physics of the large and the small, TASI 09, proceedings of the Theoretical Advanced Study Institute in Elementary Particle Physics, Boulder, Colorado, USA, 1-26 June 2009*, pp. 523–686, 2011. 0907.5424. DOI.

[34] S. Rahvar, *Cooling in the universe*, physics/0603087.

[35] W. Hu and M. J. White, *A CMB polarization primer*, *New Astron.* **2** (1997) 323, [astro-ph/9706147].

[36] BICEP2, KECK ARRAY collaboration, P. A. R. Ade et al., *Improved Constraints on Cosmology and Foregrounds from BICEP2 and Keck Array Cosmic Microwave Background Data with Inclusion of 95 GHz Band*, *Phys. Rev. Lett.* **116** (2016) 031302, [1510.09217].

[37] E. J. Copeland, A. R. Liddle and D. Wands, *Exponential potentials and cosmological scaling solutions*, *Phys. Rev.* **D57** (1998) 4686–4690, [gr-qc/9711068].

[38] M. Duff and C. Pope, *Consistent truncations in kaluza-klein theories*, *Nuclear Physics B* **255** (1985) 355 – 364.

[39] B. Zwiebach, *A first course in string theory*. Cambridge University Press, 2006.

[40] PLANCK collaboration, R. Adam et al., *Planck 2015 results. I. Overview of products and scientific results*, 1502.01582.

[41] A. Salam and E. Sezgin, *Chiral Compactification on Minkowski x S**2 of N=2 Einstein-Maxwell Supergravity in Six-Dimensions*, *Phys. Lett.* **B147** (1984) 47.

[42] Y. Aghababaie, C. P. Burgess, S. L. Parameswaran and F. Quevedo, *SUSY breaking and moduli stabilization from fluxes in gauged 6-D supergravity*, *JHEP* **03** (2003) 032, [hep-th/0212091].

[43] A. P. Braun, A. Hebecker and M. Trapletti, *Flux Stabilization in 6 Dimensions: D-terms and Loop Corrections*, *JHEP* **02** (2007) 015, [hep-th/0611102].

[44] K. Dasgupta, G. Rajesh and S. Sethi, *M theory, orientifolds and G - flux*, *JHEP* **08** (1999) 023, [hep-th/9908088].

[45] K.-i. Maeda, *Inflation as a Transient Attractor in R**2 Cosmology*, *Phys. Rev.* **D37** (1988) 858.

[46] V. Muller, H. J. Schmidt and A. A. Starobinsky, *Power law inflation as an attractor solution for inhomogeneous cosmological models*, *Class. Quant. Grav.* **7** (1990) 1163–1168.

[47] J. Garcia-Bellido and D. Wands, *General relativity as an attractor in scalar - tensor stochastic inflation*, *Phys. Rev.* **D52** (1995) 5636–5642, [gr-qc/9503049].

[48] P. G. Ferreira and M. Joyce, *Cosmology with a primordial scaling field*, *Phys. Rev.* **D58** (1998) 023503, [astro-ph/9711102].

[49] A. Albrecht, C. P. Burgess, F. Ravndal and C. Skordis, *Natural quintessence and large extra dimensions*, *Phys. Rev.* **D65** (2002) 123507, [astro-ph/0107573].

[50] J. P. Conlon, R. Kallosh, A. D. Linde and F. Quevedo, *Volume Modulus Inflation and the Gravitino Mass Problem*, *JCAP* **0809** (2008) 011, [0806.0809].

[51] R. M. Wald, *General Relativity*. 1984, 10.7208/chicago/9780226870373.001.0001.

[52] S. M. Carroll, *Spacetime and geometry: An introduction to general relativity*. 2004.

Master of Science—Jared J.H. Enns, McMaster University—Physics

Appendix A

Derivation of the 6D Field Equations

In this appendix, we derive the 6D field equations of Section 2.1 in much greater detail than in the main text. We start with the metric and then proceed to derive the results of the Maxwell equations and the Einstein equations used in the main text.

A.1 The Metrics

We start by quoting the 6D metric *ansatz*, (2.7) in the main text,

$$\mathrm{d}\hat{s}^2 = \hat{g}_{\mu\nu}(x)\mathrm{d}x^\mu \mathrm{d}x^\nu + b^2(\hat{t})\gamma_{mn}(y)\mathrm{d}y^m \mathrm{d}y^n \,, \tag{A.1}$$

where $\hat{g}_{\mu\nu}(x)$ is the usual FRW metric in flat spacetime,

$$\hat{g}_{\mu\nu}\mathrm{d}x^\mu \mathrm{d}x^\nu = -\mathrm{d}\hat{t}^2 + a^2(\hat{t})\delta_{ij}\mathrm{d}x^i \mathrm{d}x^j \,, \tag{A.2}$$

and $\gamma_{mn}(y)$ is the metric for a unit 2-sphere:[1]

$$\gamma_{mn}\mathrm{d}y^m \mathrm{d}y^n = \mathrm{d}\theta^2 + \sin^2\theta \mathrm{d}\chi^2 \,. \tag{A.3}$$

Altogether, then, the metric is

$$\mathrm{d}\hat{s}^2 = -\mathrm{d}\hat{t}^2 + \hat{a}^2(\hat{t})\delta_{ij}\mathrm{d}x^i \mathrm{d}x^j + b^2(\hat{t})\left(\mathrm{d}\theta^2 + \sin^2\theta \mathrm{d}\chi^2\right) . \tag{A.4}$$

[1] It is traditional to use ϕ for the second angular variable. We sacrifice conventionality for clarity by using χ, since we reserve ϕ for the inflaton field.

A.2 Christoffels and Ricci (Tensor and Scalar)

The non-zero Christoffels for (A.4) are:

$$\Gamma^0_{ij} = \hat{a}\hat{a}'\delta_{ij}, \quad \Gamma^0_{44} = bb', \quad \Gamma^0_{55} = \Gamma^0_{44}\sin^2\theta,$$
$$\Gamma^i_{0j} = \frac{\hat{a}'}{\hat{a}}\delta^i_j, \quad \Gamma^m_{0n} = \frac{b'}{b}\delta^m_n, \quad \Gamma^4_{55} = -\cos\theta\sin\theta, \quad \Gamma^5_{45} = \cot\theta\,. \tag{A.5}$$

where i, j run over the "usual" three spatial dimensions and m, n run over the two extra dimensions. Next, we use (A.5) to calculate the Ricci Tensor, which, in Weinberg conventions, is defined as:

$$\mathcal{R}_{MN} := \Gamma^A_{MA,N} - \Gamma^A_{MN,A} + \Gamma^A_{NB}\Gamma^B_{MA} - \Gamma^A_{AB}\Gamma^B_{MN}\,. \tag{A.6}$$

We write its components in the form $\mathcal{R}^M{}_N = g^{MA}\mathcal{R}_{AN}$:

$$\begin{aligned}
\mathcal{R}^0{}_0 &= -\left[3\frac{\hat{a}''}{\hat{a}} + 2\frac{b''}{b}\right], \\
\mathcal{R}^i{}_j &= -\delta^i_j\left[\frac{\hat{a}''}{\hat{a}} + 2\left(\frac{\hat{a}'}{\hat{a}}\right)^2 + 2\frac{\hat{a}'b'}{\hat{a}b}\right], \\
\mathcal{R}^m{}_n &= -\delta^m_n\left[\frac{b''}{b} + \left(\frac{b'}{b}\right)^2 + \frac{1}{b^2} + 3\frac{\hat{a}'b'}{\hat{a}b}\right].
\end{aligned} \tag{A.7}$$

The Ricci Scalar, computed from $\mathcal{R} = g^{MN}\mathcal{R}_{MN}$, is:

$$\begin{aligned}
\mathcal{R} &= -2\left[3\frac{\hat{a}''}{\hat{a}} + 3\left(\frac{\hat{a}'}{\hat{a}}\right)^2 + 6\frac{\hat{a}'b'}{\hat{a}b} + 2\frac{b''}{b} + \left(\frac{b}{2}\right)^2 + \frac{1}{b^2}\right] \\
&= -2\left[\frac{1}{b^2} + 3\left(2\hat{H}^2 + 2\hat{H}\mathcal{H} + \mathcal{H}^2 + \hat{H}'\right) + 2\mathcal{H}'\right],
\end{aligned} \tag{A.8}$$

where $\hat{H} := \hat{a}'/\hat{a}$ and $\mathcal{H} := b'/b$ as in the main text.

A.3 Einstein Tensor

The Einstein tensor is defined as:

$$\mathcal{G}_{MN} := \mathcal{R}_{MN} - \frac{1}{2}\mathcal{R}g_{MN}\,. \tag{A.9}$$

Using (A.4), (A.7), and (A.8), we calculate its components to be:

$$\begin{aligned}
\mathcal{G}^0{}_0 &= 3\left(\frac{a'}{a}\right)^2 + 6\frac{a'b'}{ab} + \left(\frac{b'}{b}\right)^2 + \frac{1}{b^2}\,,\\
\mathcal{G}^i{}_j &= \delta^i_j\left[2\frac{a''}{a} + \left(\frac{a'}{a}\right)^2 + 4\frac{a'b'}{ab} + 2\frac{b''}{b} + \left(\frac{b'}{b}\right)^2 + \frac{1}{b^2}\right],\\
\mathcal{G}^m{}_n &= \delta^m_n\left[3\frac{a''}{a} + \left(\frac{a'}{a}\right)^2 + 3\frac{a'b'}{ab} + \frac{b''}{b}\right],
\end{aligned} \tag{A.10}$$

or:

$$\begin{aligned}
\mathcal{G}^0{}_0 &= \frac{1}{b^2} + 3\hat{H}^2 + 6\hat{H}\mathcal{H} + \mathcal{H}^2\,,\\
\mathcal{G}^i{}_j &= \delta^i_j\left[\frac{1}{b^2} + 3\hat{H}^2 + 4\hat{H}\mathcal{H} + 3\mathcal{H}^2 + 2\hat{H}' + 2\mathcal{H}'\right],\\
\mathcal{G}^m{}_n &= \delta^m_n\left[6\hat{H}^2 + 3\hat{H}\mathcal{H} + \mathcal{H}^2 + 3\hat{H}' + \mathcal{H}'\right].
\end{aligned} \tag{A.11}$$

A.4 Stress-Energy Tensor

The stress-energy tensor is calculated in the usual way:

$$T_{AB} := 2\frac{\delta L_{\text{mat}}}{\delta g^{AB}} - g_{AB}L_{\text{mat}} \implies T^A{}_B = 2g^{AC}\frac{\delta L_{\text{mat}}}{\delta g^{CB}} - \delta^A_B L_{\text{mat}}\,, \tag{A.12}$$

where:

$$\begin{aligned}
L_{\text{mat}} &= \frac{1}{2}(\partial\phi)^2 + \frac{1}{4}F^2 + V(\phi)\\
&= \left(\frac{1}{2}g^{MN}\partial_M\phi\partial_N\phi + \frac{1}{4}g^{RT}g^{SU}F_{RS}F_{TU} + V(\phi)\right).
\end{aligned} \tag{A.13}$$

First, we compute the derivative:

$$\frac{\delta L_{\text{mat}}}{\delta g^{CB}} = \frac{1}{2}\partial_C\phi\partial_B\phi + \frac{1}{2}g^{SU}F_{CS}F_{BU} \implies 2\frac{\delta L_{\text{mat}}}{\delta g^{CB}} = \partial_C\phi\partial_B\phi + g^{SU}F_{CS}F_{BU}\,.$$

$$\therefore 2g^{AC}\frac{\delta L_{\text{mat}}}{\delta g^{CB}} = \partial^A\phi\partial_B\phi + g^{AC}g^{SU}F_{CS}F_{BU} = \partial^A\phi\partial_B\phi + F^{AU}F_{BU}\,. \tag{A.14}$$

Putting (A.14) and (A.13) into (A.12):

$$T^A{}_B = -\frac{1}{2}\delta^A_B(\partial\phi)^2 + \partial^A\phi\partial_B\phi - \delta^A_B V(\phi) - \frac{1}{4}\delta^A_B F^2 + F^{AC}F_{BC}\,. \tag{A.15}$$

Let us clean this up one term at a time. Since ϕ depends only on time, the ϕ-terms become:

$$-\frac{1}{2}\delta^A_B(\partial\phi)^2 + \partial^A\phi\partial_B\phi - \delta^A_B V(\phi) = \delta^A_B\left(\frac{(\phi')^2}{2} - V(\phi)\right) - \delta^A_0\delta^0_B\left(\phi'\right)^2\,. \tag{A.16}$$

where the prime indicates a derivative with respect to $\hat{t}$, as in the main text. As for the flux term, we work out each term separately, using $F_{mn} = f\epsilon_{mn}$, where ϵ_{mn} is the 2D Levi-Civita Tensor.[2] We use this to simplify the two terms:

$$F^2 = F^{mn}F_{mn} = g^{am}g^{bn}F_{ab}F_{mn} = f^2g^{am}g^{bn}\epsilon_{ab}\epsilon_{mn} = f^2\epsilon^{mn}\epsilon_{mn} = 2f^2\,, \tag{A.17}$$

and

$$F^{AC}F_{BC} = F^{ac}F_{bc} = f^2\epsilon^{ac}\epsilon_{bc} = f^2\delta^a_b = f^2\left(\delta^a_4\delta^4_b + \delta^a_5\delta^5_b\right). \tag{A.18}$$

Altogether, our stress-energy tensor becomes

$$T^A{}_B = \delta^A_B\left(\frac{(\phi')^2}{2} - V(\phi) - \frac{f^2}{2}\right) - \delta^A_0\delta^0_B\left(\phi'\right)^2 + f^2\left(\delta^A_4\delta^4_B + \delta^A_5\delta^5_B\right). \tag{A.19}$$

[2] The Levi-Civita *tensor* is composed of the Levi-Civita *symbol* (a tensor density of weight 1) multiplied by factors of the determinant (a density of weight -2) so that we end up constructing a tensor: $\epsilon_{mn} = \sqrt{|g|}\varepsilon_{mn}$, where ε_{mn} is the 2D Levi-Civita symbol. The inverse is $\epsilon^{mn} = (1/\sqrt{|g|})\varepsilon^{mn}$, so that $\epsilon^{mn}\epsilon_{mn} = \varepsilon^{mn}\varepsilon_{mn} = n! = 2$, in our 2D case.

We parametrize our stress-energy tensor as

$$T^{A}{}_{B} = \text{diag}\left(-\rho, p_{(3)}, p_{(3)}, p_{(3)}, p_{(2)}, p_{(2)}\right). \tag{A.20}$$

which yields (2.12) from the main text:

$$\begin{aligned} \rho &= \frac{1}{2}\left[\left(\phi'\right)^2 + f^2\right] + V(\phi)\,, \\ p_{(3)} &= \frac{1}{2}\left[\left(\phi'\right)^2 - f^2\right] - V(\phi)\,, \\ p_{(2)} &= \frac{1}{2}\left[\left(\phi'\right)^2 + f^2\right] - V(\phi)\,. \end{aligned} \tag{A.21}$$

A.4.1 Maxwell Equations & Flux Quantization

Above, and in the main text, we define the field strength tensor over the two extra dimensions as

$$F_{mn} = f\epsilon_{mn} = \sqrt{|g|} f \varepsilon_{mn} = \sqrt{\gamma}\begin{pmatrix} 0 & fb^2 \\ -fb^2 & 0 \end{pmatrix}, \tag{A.22}$$

where f is some generic function of any coordinates, and g is the determinant of the extra-dimensional metric, g_{mn}, since F_{mn} is only constructed from g_{mn}. Maxwell's equation is

$$\partial_M\left(\sqrt{-g}F^{MN}\right) = 0\,, \tag{A.23}$$

and the Bianchi identity (constituting the other half of Maxwell's equations in curved spacetime) is

$$\nabla_{[M}F_{AB]} = 0\,. \tag{A.24}$$

Since $F_{MN} = 0$ for $M, N = 0, 1, 2, 3$, we will only consider the extra-dimensional components of both (A.23) and (A.24). Then, cleaning up the left-hand side of

(A.23) :

$$\begin{aligned}\partial_m\left(\sqrt{-g}F^{mn}\right) &= \partial_m\left(b^2\sqrt{-\hat{g}(x)\gamma(y)}F^{mn}\right) = \partial_m\left(b^2(\hat{t})\sqrt{-\hat{g}(x)\gamma(y)}f\epsilon^{mn}\right)\\ &= \partial_m\left(fb^2(\hat{t})\sqrt{-\hat{g}(x)\gamma(y)}\left(\frac{\varepsilon^{mn}}{b^2(\hat{t})\sqrt{\gamma(y)}}\right)\right) \qquad \text{(A.25)}\\ &= \partial_m\left(f\sqrt{-\hat{g}(x)}\varepsilon^{mn}\right) = \sqrt{-\hat{g}(x)}\left(\partial_m f\right)\varepsilon^{mn}\,.\end{aligned}$$

Therefore, Maxwell gives us the condition

$$\partial_m f = 0\,, \qquad \text{(A.26)}$$

meaning that f is independent of the y^m coordinates.

Then, if we expand the LHS of (A.24), we get

$$\nabla_{[M}F_{AB]} = \nabla_M F_{AB} + \nabla_A F_{BM} + \nabla_B F_{MA} = \partial_M F_{AB} + \partial_A F_{BM} + \partial_B F_{MA}\,, \qquad \text{(A.27)}$$

where the second equality occurs due to the fact that all the Christoffel terms cancel out due to the symmetry of the Christoffels and the anti-symmetry of the field-strength tensors.

Let us now examine each of the components of one of the derivative terms in (A.27). We know that the regular 4D components of $F_{AB} = 0$, so we just look at the following components of $\partial_A F_{mn}$:

$$\partial_0 F_{mn} = \partial_{\hat{t}}\left(fb^2(\hat{t})\sqrt{\gamma(y)}\right)\varepsilon_{mn} = \sqrt{\gamma}\left(fb^2\right)'\varepsilon_{mn}\,, \qquad \text{and} \qquad \text{(A.28)}$$

$$\partial_i F_{mn} = \partial_i\left(fb^2(\hat{t})\sqrt{\gamma(y)}\right)\varepsilon_{mn} = b^2\sqrt{\gamma}\left(\partial_i f\right)\varepsilon_{mn}\,. \qquad \text{(A.29)}$$

These (and their permutations) are the only two non-zero terms in (A.27). Clearly, if one of M, A, or B is equal to 0–3, then only one of the three derivative terms will survive in (A.27) due to the fact that the flux exists only in the extra dimensions.

However, if one of the indices is 4, say, then the other two need to be 4 and 5. This would allow a component that looks like

$$\partial_4 F_{45} + \partial_4 F_{54} + \partial_5 F_{44} = \partial_4 F_{45} - \partial_4 F_{45} + 0 = 0\,, \qquad \text{(A.30)}$$

which vanishes. Generalizing this argment, it is easy see that the components of the Bianchi Identity that are wholly composed of extra-dimensional terms are all zero. Therefore, the only non-zero components of the LHS of (A.24) are (A.28) and (A.29). This leads to the two more conditions on f:

$$\partial_i f = 0, \qquad \left(f b^2\right)' = 0\,. \tag{A.31}$$

These imply f is independent of our 3D spatial coordinates (x^i), and that the quantity fb^2 is a constant, as described in the main text.

We compute that constant using flux quantization (i.e., we demand that the extra-dimensional field be quantized):

$$\int_{S^2} F = 4\pi f b^2 = \frac{2\pi n}{e} \implies f b^2 = \mathfrak{f}, \quad \text{where } \mathfrak{f} := \frac{n}{2e} \tag{A.32}$$

with e the Maxwell coupling, and $n \in \mathbb{Z}$. Clearly, (A.32) satisfies both (A.26) and (A.31).

A.5 Einstein Equations in 6D

Einstein's equations—without a cosmological constant—are

$$\mathcal{G}^A{}_B = -\kappa^2 T^A{}_B \tag{A.33}$$

where $\mathcal{G}_{AB}$ is the Einstein tensor as defined in (A.9) and $T^A{}_B$ is the total stress-energy tensor outlined in Section A.4. We then just need to use (A.10) and (A.20) in (A.33) in order to read off Einstein's equations:

$$\begin{aligned}
3\left(\frac{\hat{a}'}{\hat{a}}\right)^2 + \left(\frac{b'}{b}\right)^2 + 6\left(\frac{\hat{a}'b'}{\hat{a}b}\right) + \frac{1}{b^2} &= \kappa^2\left\{\frac{1}{2}\left[\left(\phi'\right)^2 + \frac{\mathfrak{f}^2}{b^4}\right] + V\right\}, \\
2\left(\frac{\hat{a}''}{\hat{a}} + \frac{b''}{b}\right) + \left(\frac{\hat{a}'}{\hat{a}}\right)^2 + \left(\frac{b'}{b}\right)^2 + 4\left(\frac{\hat{a}'b'}{\hat{a}b}\right) + \frac{1}{b^2} &= \kappa^2\left\{\frac{1}{2}\left[-\left(\phi'\right)^2 + \frac{\mathfrak{f}^2}{b^4}\right] + V\right\}, \\
\frac{b''}{b} + 3\left[\frac{\hat{a}''}{\hat{a}} + \left(\frac{\hat{a}'}{\hat{a}}\right)^2\right] + 3\left(\frac{\hat{a}'b'}{\hat{a}b}\right) &= \kappa^2\left\{-\frac{1}{2}\left[\left(\phi'\right)^2 + \frac{\mathfrak{f}^2}{b^4}\right] + V\right\},
\end{aligned}$$

which are exactly (2.13) in the main text.

Master of Science—Jared J.H. Enns, McMaster University—Physics

Appendix B

Integrating Out the Extra Dimensions

In this appendix, we work through the dimensional reduction of Section 2.2.1 in much more explicit detail.

We start with (2.1), our action in 6D:[1]

$$S = -\int \mathrm{d}^6X\sqrt{-g_{(6)}}\left(\frac{\mathcal{R}_{(6)}}{2\kappa^2} + L_{\text{mat}}\right), \tag{B.1}$$

with matter content given by (2.2):

$$L_{\text{mat}} = \frac{1}{4}F_{MN}F^{MN} + \frac{1}{2}\,\partial_M\phi\,\partial^M\phi + V(\phi)\,. \tag{B.2}$$

We need to break everything up into 4D and 2D quantities. We start with the 6D Ricci Scalar. Given the metric (2.7), we can write:

$$\mathcal{R}_{(6)} = \hat{\mathcal{R}}_{(4)} + \frac{\mathcal{R}_{(2)}}{b^2} + 4\left(\frac{\hat{\Box}b}{b}\right) + 2\left(\frac{\hat{\partial}b}{b}\right)^2, \tag{B.3}$$

where $\mathcal{R}_{(2)}$ is the curvature of the 2-sphere[2] (i.e., the Ricci scalar of our 2D metric, γ_{mn}) and all contractions are only over 4D indices. We also have:

$$\sqrt{-G} = \sqrt{-\hat{g}\cdot b^4\cdot\gamma} = b^2\sqrt{-\hat{g}}\sqrt{\gamma}\,, \quad \text{and} \quad \mathrm{d}^6X = \mathrm{d}^4x\,\mathrm{d}^2y\,. \tag{B.4}$$

[1] Note that we have tweaked some of the notation in this appendix relative to the main text. We trade this slight inconsistency for clarity.

[2] Recall that we are using Weinberg conventions [32], where $\mathcal{R}_{(2)} = -2$.

We begin by substituting (B.3) and (B.4) into our action. This yields:

$$S = -\int \left(\mathrm{d}^4x\,\mathrm{d}^2y\right)\left(b^2\sqrt{-\hat{g}}\sqrt{\gamma}\right)\left\{\frac{1}{2\kappa^2}\left[\hat{\mathcal{R}}_{(4)} - \frac{2}{b^2} + 4\frac{\hat{\Box}b}{b} + 2\left(\frac{\hat{\partial}b}{b}\right)^2\right] + L_{\text{mat}}\right\}.$$

We perform the y-integral first. Only γ, the determinant of the extra dimensional metric, depends on y^m, so: $\int \mathrm{d}^2y\,\sqrt{\gamma} = 4\pi$. Then, we are left with:

$$S = -\int \mathrm{d}^4x\sqrt{-\hat{g}}\left\{\frac{4\pi}{2\kappa^2}\left[b^2\hat{\mathcal{R}}_{(4)} - 2 + 4b\hat{\Box}b + 2\left(\hat{\partial}b\right)^2\right] + 4\pi b^2 L_{\text{mat}}\right\}. \tag{B.5}$$

Now, under the integral, we can simplify the derivative terms. In general, we have

$$\begin{aligned}\int \mathrm{d}^4x\,\sqrt{-g}\,b\Box b &= \int \mathrm{d}^4x\,\sqrt{-g}\,b\left(g^{\mu\nu}\nabla_\mu\nabla_\nu b\right)\\ &= -\int \mathrm{d}^4x\,\sqrt{-g}\,g^{\mu\nu}\nabla_\mu b\nabla_\nu b\\ &= -\int \mathrm{d}^4x\,\sqrt{-g}\,(\partial b)^2\,,\end{aligned} \tag{B.6}$$

where, in going from the first line to the second line, we integrate by parts and ignore the surface terms that do not contribute to the action. We also need to note a few properties of covariant derivatives to account for the movement of our derivatives. The first is that the covariant derivatives of the metric and functions of the metric—like g, its determinant—are zero. Secondly, since b is a scalar function, $\nabla_A b = \partial_A b$. So, (B.6) tells us that, under the integral, $b\Box b = -(\partial b)^2$. Using this in (B.5), we get:

$$S = -\int \mathrm{d}^4x\sqrt{-\hat{g}}\left\{\frac{4\pi}{2\kappa^2}\left[b^2\hat{\mathcal{R}}_{(4)} - 2 - 2\left(\hat{\partial}b\right)^2\right] + 4\pi b^2 L_{\text{mat}}\right\}. \tag{B.7}$$

Next, we perform a coordinate transformation in order to work in the 4D Einstein frame (4DEF)—i.e., the frame in which no field multiplies the Ricci scalar. We define:

$$g_{\mu\nu} := e^{\psi/M_p}\hat{g}_{\mu\nu}\,, \tag{B.8}$$

$$b := b_\star e^{\psi/(2M_p)}\,. \tag{B.9}$$

Trivially, (B.8) implies:

$$g^{\mu\nu} = e^{-\psi/M_p}\hat{g}^{\mu\nu}\,. \tag{B.10}$$

Now we need to write all the quantities in (B.7) in terms of the 4DEF redefinitions. We start with $\hat{\mathcal{R}}_{(4)}$: given a re-scaling of the form (B.8), any standard GR textbook [32, 51, 52] tells us,

$$\begin{aligned}\hat{\mathcal{R}}_{(4)} &= e^{\psi/M_p} g^{\mu\nu}\left[\mathcal{R}_{\mu\nu} - 6\nabla_\mu\nabla_\nu\left(\frac{\psi}{2M_p}\right) + 6\,\nabla_\mu\left(\frac{\psi}{2M_p}\right)\nabla_\nu\left(\frac{\psi}{2M_p}\right)\right] \\ &= e^{\psi/M_p} g^{\mu\nu}\left[\mathcal{R}_{\mu\nu} - \frac{3}{M_p}\nabla_\mu\nabla_\nu\,\psi + \frac{3}{2M_p^2}\,\nabla_\mu\psi\,\nabla_\nu\psi\right] \\ &= e^{\psi/M_p}\left[\mathcal{R}_{(4)} - \frac{3}{M_p}\Box\psi + \frac{3}{2M_p^2}\,(\partial\psi)^2\right]\,.\end{aligned} \tag{B.11}$$

Next, we tackle the determinant: directly from (B.8), we have

$$\sqrt{-g} = \sqrt{-\left(e^{\psi/M_p}\right)^4\hat{g}} = e^{2\psi/M_p}\sqrt{-\hat{g}} \implies \sqrt{-\hat{g}} = e^{-2\psi/M_p}\sqrt{-g}\,. \tag{B.12}$$

Then, we can get the following relation directly from (B.9):

$$\left(\hat{\partial}b\right)^2 = \hat{g}^{\mu\nu}\partial_\mu b\,\partial_\nu b = \left(e^{\psi/M_p}g^{\mu\nu}\right)\left(\frac{b_\star}{2M_p}e^{\psi/(2M_p)}\partial_\mu\psi\right)\left(\frac{b_\star}{2M_p}e^{\psi/(2M_p)}\partial_\nu\psi\right).$$

$$\therefore \left(\hat{\partial}b\right)^2 = \frac{b_\star^2\,e^{2\psi/M_p}}{4M_p^2}\,(\partial\psi)^2\,, \tag{B.13}$$

where we use (B.10) in the first line of (B.13). It is now prudent to recall our definition of the Planck mass from (2.18):

$$\frac{4\pi}{\kappa^2} = \frac{M_p^2}{b_\star^2}\,. \tag{B.14}$$

Thus, subbing (B.9) and (B.11)–(B.14) all into (B.7), we get:

$$S = -\int \mathrm{d}^4x \left(e^{-2\psi/M_p}\sqrt{-g}\right)\left\{\frac{M_p^2}{2b_\star^2}\left[\left(b_\star^2 e^{\psi/M_p}\right)e^{\psi/M_p}\left(\mathcal{R}_{(4)} - \frac{3}{M_p}\Box\psi + \frac{3}{2M_p^2}\left(\partial\psi\right)^2\right) - 2 - 2\frac{b_\star^2}{4M_p^2}e^{2\psi/M_p}\left(\partial\psi\right)^2\right] + 4\pi\left(b_\star^2 e^{\psi/M_p}\right)L_{\mathrm{mat}}\right\} \tag{B.15}$$

Clearly, (B.15) could use some clean-up. First, we note that, $\Box\psi$ is only equal to surface terms, so we can drop it wholly from the action. Then, after some basic algebra, we get

$$S = -\int \mathrm{d}^4x\sqrt{-g}\left\{\frac{M_p^2}{2}\mathcal{R}_{(4)} + \frac{1}{2}\left(\partial\psi\right)^2 - \frac{M_p^2}{b_\star^2}e^{-2\psi/M_p} + 4\pi b_\star^2 e^{-\psi/M_p}L_{\mathrm{mat}}\right\} \tag{B.16}$$

Finally, we need to take care of the matter Lagrangian. Using (B.2) and our previous substitutions

$$\begin{aligned} 4\pi b_\star^2 e^{-\psi/M_p}L_{\mathrm{mat}} &= 4\pi b_\star^2 e^{-\psi/M_p}\left[\frac{1}{2}\left(\hat{\partial}\phi\right)^2 + \frac{\mathfrak{f}^2}{2b^4} + V(\phi)\right] \\ &= 4\pi b_\star^2 e^{-\psi/M_p}\left[\frac{1}{2}\left(\partial\phi\right)^2 e^{\psi/M_p} + \frac{\mathfrak{f}^2}{2b_\star^4}e^{-2\psi/M_p} + V(\phi)\right] \\ &= \frac{1}{2}\left(\partial\varphi\right)^2 + \frac{2\pi\mathfrak{f}^2}{b_\star^2}e^{-3\psi/M_p} + 4\pi b_\star^2 e^{-\psi/M_p}U(\varphi)\,, \end{aligned} \tag{B.17}$$

in which we define the canonical normalization of ϕ:

$$\varphi := \sqrt{4\pi}b_\star\,\phi\,, \tag{B.18}$$

and $U(\varphi)$ is defined such that $V(\phi) = U(\varphi)$.[3] Using (B.17), the action in (B.16) now arrives in its final form as presented in the main text.

$$S = -\int \mathrm{d}^4x\sqrt{-g}\left\{\frac{M_p^2}{2}\mathcal{R}_{(4)} + \frac{1}{2}\left(\partial\psi\right)^2 + \frac{1}{2}(\partial\varphi)^2 + W(\varphi,\psi)\right\} \tag{B.19}$$

where,

$$W(\varphi,\psi) := 4\pi b_\star^2 e^{-\psi/M_p}U(\varphi) - \frac{M_p^2}{b_\star^2}e^{-2\psi/M_p} + \frac{2\pi\mathfrak{f}^2}{b_\star^2}e^{-3\psi/M_p}. \tag{B.20}$$

[3] As an example: if we had $V = V_0 e^{\kappa\phi}$, then $V(\phi) = V_0 e^{\kappa\phi} = V_0 e^{\kappa\varphi/(\sqrt{4\pi}b_\star)} = V_0 e^{\varphi/M_p} = U(\varphi)$.

Appendix C

Consistency of the Truncation

Here, we demonstrate that the 4D equations of motion for homogeneous fields are fully equivalent to the nontrivial 6D equations of motion. This establishes consistency of the truncation because we have already checked that solving these 6D equations suffices to ensure a solution of the full 6D field equations, because the truncations required to obtain our *ansatz* are consistent with the equations of motion.

We first note that the changes of variables, which can be computed by comparing our two conformally-related metrics,

$$a = \hat{a}\, e^{\psi/2M_p} \qquad \text{and} \qquad t' = \frac{\mathrm{d}t}{\mathrm{d}\hat{t}} = e^{\psi/2M_p} \tag{C.1}$$

ensure

$$H = \frac{\dot{a}}{a} = \left(\hat{H} + \frac{\psi'}{2M_p}\right) e^{-\psi/2M_p}\,, \tag{C.2}$$

while the definition $b := b_\star\, e^{\psi/2M_p}$ provides

$$\mathcal{H} = \frac{b'}{b} = \frac{\psi'}{2M_p} \qquad \text{and} \qquad \frac{b''}{b} = \frac{\psi''}{2M_p} + \mathcal{H}^2\,. \tag{C.3}$$

We write out the transformations between the 4D and 6D variables for convenience. Using $\varphi = \sqrt{4\pi}\, b_\star\, \phi$ and the definition of $W(\psi, \varphi)$ from (2.23) gives the

transformations for the inflaton variables:

$$\dot{\varphi} = \sqrt{4\pi} b_\star \frac{\mathrm{d}\phi}{\mathrm{d}t} = \sqrt{4\pi} b_\star \left(\frac{\mathrm{d}\phi}{\mathrm{d}\hat{t}}\right)\left(\frac{\mathrm{d}\hat{t}}{\mathrm{d}t}\right) = \sqrt{4\pi} b_\star \phi' e^{-\psi/2M_p}\,, \tag{C.4}$$

$$\ddot{\varphi} = \sqrt{4\pi} b_\star \left(e^{-\psi/2M_p}\frac{\mathrm{d}}{\mathrm{d}\hat{t}}\right)\left(\phi' e^{-\psi/2M_p}\right) = \sqrt{4\pi} b_\star \left(\phi'' - \frac{\psi'}{2M_p}\phi'\right) e^{-\psi/M_p}\,,$$

$$\frac{\partial W}{\partial \varphi} = 4\pi b_\star^2 e^{-\psi/M_p}\frac{\partial U}{\partial \varphi} = \sqrt{4\pi} b_\star \frac{\partial V}{\partial \phi} e^{-\psi/M_p}\,.$$

In similar fashion, the radion variables transform as:

$$\begin{aligned}
\dot{\psi} &= \psi' e^{-\psi/2M_p}\,,\\
\ddot{\psi} &= \left(\psi'' - \frac{(\psi')^2}{2M_p}\right) e^{-\psi/M_p}\,,\\
\frac{\partial W}{\partial \psi} &= -\frac{4\pi b_\star^2}{M_p} V(\phi) + \frac{2M_p^2}{b_\star^2} e^{-2\psi/M_p} - \frac{6\pi \mathfrak{f}^2}{b_\star^2 M_p} e^{-2\psi/M_p}\,.
\end{aligned} \tag{C.5}$$

Substituting (C.2), (C.4), and (C.5) into (2.26) gives:

$$\begin{aligned}
\phi'' - \frac{\psi'}{2M_p}\phi' + 3\left(\frac{\psi'}{2M_p} + \hat{H}\right)\phi' + \frac{\partial V}{\partial \phi} = 0\,,\\
\psi'' - \frac{(\psi')^2}{2M_p} + 3\left(\frac{\psi'}{2M_p} + \hat{H}\right)\psi' - \frac{4\pi b_\star^2}{M_p} V(\phi) + \frac{2M_p}{b_\star^2} e^{-\psi/M_p} - \frac{6\pi \mathfrak{f}^2}{b_\star^2 M_p} e^{-2\psi/M_p} = 0\,,\\
4\pi b_\star^2 \frac{(\phi')^2}{2} + \frac{(\psi')^2}{2} + 4\pi b_\star^2 V(\phi) - \frac{M_p^2}{b_\star^2} e^{-\psi/M_p}\\
+ \frac{2\pi \mathfrak{f}^2}{b_\star^2} e^{-2\psi/M_p} = 3M_p^2\left(\frac{\psi'}{2M_p} + \hat{H}\right)^2.
\end{aligned} \tag{C.6}$$

Using (C.3) and a bit of algebra to clean up (C.6) leaves:

$$\phi'' + \left(3\hat{H} + 2\mathcal{H}\right)\phi' + \frac{\partial V}{\partial \phi} = 0\,, \tag{C.7}$$

$$\frac{b''}{b} + 3\hat{H}\mathcal{H} + \mathcal{H}^2 = \frac{4\pi b_\star^2}{M_p^2}\left(\frac{1}{2}V(\phi) + \frac{3}{4}\frac{\mathfrak{f}^2}{b^4}\right) - \frac{1}{b^2}\,, \tag{C.8}$$

and

$$\frac{4\pi b_\star^2}{M_p^2}\left\{\frac{1}{2}\left[(\phi')^2+\frac{\mathfrak{f}^2}{b^4}\right]+V(\phi)\right\}-\frac{1}{b^2}=3\hat{H}^2+6\hat{H}\mathcal{H}+\mathcal{H}^2\,. \tag{C.9}$$

Clearly, (C.7) is equivalent to the 6D inflaton equation of motion, (2.8). Recalling that $\kappa^2=4\pi b_\star^2/M_p^2$ shows that (C.9) is equivalent to the 6D Friedmann equation—the first line in (2.13). Finally, we observe that (C.8) is equivalent to a linear combination of the Einstein equations (2.13). Solutions to the 4D equations therefore satisfy the homogeneous 6D equations and so (because the truncation is consistent) also exactly solve the full system of 6D classical field equations.

Appendix D

Systematic Power-Law Analysis

In this appendix, we outline the comprehensive classes of solutions in both 6D and 4D. These are sorted into two categories: superfluous solutions that are mathematically possible but not physically relevant because they do not present any interesting solution; and inconsistent solutions, those which cannot be admitted mathematically. We start with the equivalent 6D solutions to the two interesting cases from Chapter 4 and then move on to the additional cases in 6D, then 4D. These solutions are presented primarily for the sake of completion—and since they represent a portion of work performed by this author—and less exposition is present here than in the main text. Discussion is usually limited to why a particular solution was "important" enough to be relegated to this appendix.

Moreover, it should be true, that, if our truncation from Section 2.2.1 is indeed a consistent truncation (which we verified in Appendix C), the scaling solutions in 4D and 6D should be equivalent. We conclude this appendix by demonstrating this explicitly by finding transformations between the 6D and 4D powers and showing that a direct substitution of these quantities into the 6D power-law equations of motion reproduces the 4D equations. Again, while this does not fit naturally into the main story, it is presented here since it was a particular focus of this author, and because it provides an additional analytic check on our equations.

D.1 Power-law Solutions in 6D

We begin by performing a completely analogous analysis (say that three times fast) to Chapter 4. We start with the general 6D setup and then proceed to derive the equivalent 6D attractor and unstable solutions using the same criteria as in the main text: by comparing the relative sizes of various potential contributions.

In general, power-law solutions typically arise when the inflaton potential is dominated by a single exponential. We find various classes of solutions depending

on the relative sizes of various terms in the field equations: the inflaton's potential, $V(\phi)$, the extra-dimensional curvature, $1/b^2$, and the contribution due to the extra-dimensional flux, $\mathfrak{f}^2/b^4$. We proceed in complete analogy to Section 4.1. Since we perform all our numerical evolution in 4D in the main text, these solutions are listed for reference's sake and little discussion is allowed them.

When seeking analytic scaling solutions, we assume only one of the exponentials of the 6D potential (2.3) dominates, so we can approximate

$$V(\phi) \simeq V_0\, e^{-\lambda\kappa\phi}\,, \tag{D.1}$$

in the regime of interest. We then seek power-law scaling solutions of the form

$$\begin{aligned} \hat{a} &= \hat{a}_0 \left(\frac{\hat{t}}{\hat{t}_0}\right)^{\hat{\alpha}}, \\ b &= b_0 \left(\frac{\hat{t}}{\hat{t}_0}\right)^{\beta}, \\ \phi &= \phi_0 + \frac{p}{\kappa} \ln\left(\frac{\hat{t}}{\hat{t}_0}\right), \end{aligned} \tag{D.2}$$

from which we also know

$$\hat{H} := \frac{\hat{a}'}{\hat{a}} = \frac{\hat{\alpha}}{\hat{t}} \tag{D.3}$$

These scaling solutions provide accelerated expansion when $\alpha > 1$ and (as is always true for power-law solutions) the slow-roll parameters are given by

$$\hat{\epsilon} := -\frac{\hat{H}'}{\hat{H}^2} = \frac{1}{\hat{\alpha}} \qquad \text{and so} \qquad \hat{\eta} := \frac{\hat{\epsilon}'}{\hat{H}\hat{\epsilon}} = 0\,. \tag{D.4}$$

We now proceed to derive the power-law equations of motion in 6D. We start by deriving general equations by merely applying our power-law assumptions (D.2) to the 6D EFEs (2.13). In order to write the equations in a form that more easily yields solutions, we take the following linear combinations of (2.13) to eliminate the $\dot{\phi}$-terms and leave isolated $\ddot{a}$ and $\ddot{b}$ equations:

$$\frac{(2.13.1) - (2.13.2) + 2\,(2.13.3)}{4} \quad \text{and} \quad \frac{(2.13.1) + 3\,(2.13.2) - 2\,(2.13.3)}{4}\,, \tag{D.5}$$

where $(2.13.i)$ refers to the i^{th} equation in (2.13). This results in

$$\begin{aligned}
\frac{a''}{a} + 2\left(\frac{a'}{a}\right)^2 + 2\left(\frac{a'b'}{ab}\right) &= \frac{\kappa^2}{2}\left(V - \frac{\mathfrak{f}}{2b^4}\right), \\
\frac{b''}{b} + 2\left(\frac{b'}{b}\right)^2 + 3\left(\frac{a'b'}{ab}\right) + \frac{1}{b^2} &= \frac{\kappa^2}{2}\left(V + \frac{3\mathfrak{f}}{2b^4}\right).
\end{aligned} \tag{D.6}$$

Applying power-law assumptions to the scalar equation of motion as well, we arrive at the following four equations:

$$\begin{aligned}
\frac{1}{b_0^2}\left(\frac{\hat{t}}{\hat{t}_0}\right)^{-2\beta} - \frac{\kappa^2\mathfrak{f}^2}{2b_0^4}\left(\frac{\hat{t}}{\hat{t}_0}\right)^{-4\beta} + \frac{3\hat{\alpha}^2 + 6\hat{\alpha}\beta + \beta^2 - \frac{1}{2}p^2}{\hat{t}^2} &= \kappa^2\hat{U}_0\left(\frac{\hat{t}}{\hat{t}_0}\right)^{-p\lambda}, \\
\frac{\kappa^2\mathfrak{f}^2}{2b_0^4}\left(\frac{\hat{t}}{\hat{t}_0}\right)^{-4\beta} + \frac{2\hat{\alpha}(3\hat{\alpha} + 2\beta - 1)}{\hat{t}^2} &= \kappa^2\hat{U}_0\left(\frac{\hat{t}}{\hat{t}_0}\right)^{-p\lambda}, \\
\frac{2}{b_0^2}\left(\frac{\hat{t}}{\hat{t}_0}\right)^{-2\beta} - \frac{3\kappa^2\mathfrak{f}^2}{2b_0^4}\left(\frac{\hat{t}}{\hat{t}_0}\right)^{-4\beta} + \frac{2\beta(3\hat{\alpha} + 2\beta - 1)}{t^2} &= \kappa^2\hat{U}_0\left(\frac{\hat{t}}{\hat{t}_0}\right)^{-p\lambda}, \\
\frac{\frac{p}{\lambda}(3\hat{\alpha} + 2\beta - 1)}{t^2} &= \kappa^2\hat{U}_0\left(\frac{\hat{t}}{\hat{t}_0}\right)^{-p\lambda},
\end{aligned} \tag{D.7}$$

where $\hat{U}_0 := V_0 e^{-\lambda\kappa\phi_0}$. We note, for later convenience, the origins of some of the terms in (D.7):

- extra-dimensional curvature terms are those proportional to $1/b_0^2$,
- flux terms are proportional to $\mathfrak{f}^2/b_0^4$, and
- terms due to the scalar potential, $V(\phi)$ are proportional to $\hat{U}_0$.

The rest of the discussion in this section is devoted to analyzing (D.7) and deriving various classes of solutions, which we now show. Depending on the relative sizes of various terms in the power-law forms of the field equations, (D.7) admits different classes of solutions.

D.1.1 Attractor Solution in 6D

This solution is obtained when both the curvature and flux contributions to (D.7) are negligible, as in the 4D case. Then, the field equations reduce to

$$\begin{aligned}
\frac{3\hat{\alpha}^2 + 6\hat{\alpha}\beta + \beta^2 - \frac{1}{2}p^2}{\hat{t}^2} &= \kappa^2 \hat{U}_0 \left(\frac{\hat{t}}{\hat{t}_0}\right)^{-p\lambda}, \\
\frac{2\hat{\alpha}(3\hat{\alpha} + 2\beta - 1)}{\hat{t}^2} &= \kappa^2 \hat{U}_0 \left(\frac{\hat{t}}{\hat{t}_0}\right)^{-p\lambda}, \\
\frac{2\beta(3\hat{\alpha} + 2\beta - 1)}{t^2} &= \kappa^2 \hat{U}_0 \left(\frac{\hat{t}}{\hat{t}_0}\right)^{-p\lambda}, \\
\frac{\frac{p}{\lambda}(3\hat{\alpha} + 2\beta - 1)}{t^2} &= \kappa^2 \hat{U}_0 \left(\frac{\hat{t}}{\hat{t}_0}\right)^{-p\lambda}.
\end{aligned} \tag{D.8}$$

Equating exponents of time and the overall coefficients of those powers, we find that $p\lambda = 2$. Using this result in (D.8), we get:

$$\begin{aligned}
3\hat{\alpha}^2 + 6\hat{\alpha}\beta + \beta^2 - \frac{2}{\lambda^2} &= \kappa^2 \hat{U}_0 \hat{t}_0^2, \\
2\hat{\alpha}(3\hat{\alpha} + 2\beta - 1) &= \kappa^2 \hat{U}_0 \hat{t}_0^2, \\
2\hat{\beta}(3\hat{\alpha} + 2\beta - 1) &= \kappa^2 \hat{U}_0 \hat{t}_0^2, \\
\frac{2}{\lambda^2}(3\hat{\alpha} + 2\beta - 1) &= \kappa^2 \hat{U}_0 \hat{t}_0^2.
\end{aligned} \tag{D.9}$$

We proceed to solve the above for the remaining powers

$$\hat{\alpha} = \beta = \frac{1}{\lambda^2}, \tag{D.10}$$

and a relationship between the coefficients,

$$t_0^2 = \frac{2\left(5 - \lambda^2\right)\hat{\alpha}^2}{\kappa^2 \hat{U}_0}. \tag{D.11}$$

We only end up with three solutions from the four equations in (D.9) since only three of the equations are linearly independent.

D.1.2 Slow-roll Scaling Solution in 6D

This solution is obtained when only the flux contributions are neglected. With that assumption in mind, the field equations become:

$$\begin{aligned}
\frac{1}{b_0^2}\left(\frac{\hat{t}}{\hat{t}_0}\right)^{-2\beta} + \frac{3\hat{\alpha}^2 + 6\hat{\alpha}\beta + \beta^2 - \frac{1}{2}p^2}{\hat{t}^2} &= \kappa^2\hat{U}_0\left(\frac{\hat{t}}{\hat{t}_0}\right)^{-p\lambda}, \\
\frac{2\hat{\alpha}(3\hat{\alpha} + 2\beta - 1)}{\hat{t}^2} &= \kappa^2\hat{U}_0\left(\frac{\hat{t}}{\hat{t}_0}\right)^{-p\lambda}, \\
\frac{2}{b_0^2}\left(\frac{\hat{t}}{\hat{t}_0}\right)^{-2\beta} + \frac{2\beta(3\hat{\alpha} + 2\beta - 1)}{t^2} &= \kappa^2\hat{U}_0\left(\frac{\hat{t}}{\hat{t}_0}\right)^{-p\lambda}, \\
\frac{\frac{p}{\lambda}(3\hat{\alpha} + 2\beta - 1)}{t^2} &= \kappa^2\hat{U}_0\left(\frac{\hat{t}}{\hat{t}_0}\right)^{-p\lambda}.
\end{aligned} \tag{D.12}$$

Again, equating the exponents and coefficients of time leads to the following two predictions for the powers

$$p\lambda = 2, \qquad \text{and} \qquad \beta = 1\,, \tag{D.13}$$

which renders the equations of motion as

$$\begin{aligned}
\frac{\hat{t}_0^2}{b_0^2} + 3\hat{\alpha}^2 + 6\hat{\alpha} + 1 - \frac{2}{\lambda^2} &= \kappa^2\hat{U}_0\hat{t}_0^2\,, \\
2\hat{\alpha}(3\hat{\alpha} + 1) &= \kappa^2\hat{U}_0\hat{t}_0^2\,, \\
2\frac{\hat{t}_0^2}{b_0^2} + 2(3\hat{\alpha} + 1) &= \kappa^2\hat{U}_0\hat{t}_0^2\,, \\
\frac{2}{\lambda^2}(3\hat{\alpha} + 1) &= \kappa^2\hat{U}_0\hat{t}_0^2\,.
\end{aligned} \tag{D.14}$$

We now have a system of equations to solve for the remaining power,

$$\hat{\alpha} = \frac{1}{\lambda^2}\,, \tag{D.15}$$

and the coefficients:

$$\hat{U}_0 = \frac{2}{(1-\lambda^2)\, b_0^2 \kappa^2}\,, \qquad \text{and} \qquad \hat{t}_0^2 = \frac{b_0^2\left(3-2\lambda^2-\lambda^4\right)}{\lambda^4}\,. \tag{D.16}$$

Again, we only have three solutions since the system contains one redundant equation. Note that both equations in (D.16) require that $|\lambda| < 1$ in order for $\hat{t}_0$ to be real and $\hat{U}_0$ to be positive, both of which are required for inflation to occur, a feature we saw in the 4D case as well.

D.1.3 Superfluous Solutions in 6D

Here we present superfluous solutions we found in our 6D power-law analysis of our system. We classify them as superfluous due to the fact that they present no interesting inflationary dynamics. Most often, they result in solutions where the 4D inflationary parameter $\epsilon > 1$, which implies that they are non-inflating solutions.

From (D.7), we note that both the curvature and flux terms cannot be relevant simultaneously if we are to see power-law solutions. So, we know we will always have to have at least one of those terms negligible.

In general, we find that our numerics tend towards scaling solutions when the flux term is very small. Therefore, we analyze analytically all possible cases where the flux term would be relevant and find that none of them could produce 4D inflation. Our first superfluous solution demonstrates this explicitly.

In this case, both the flux term and potential terms are large compared to the curvature contributions (recall that flux and curvature cannot simultaneously be relevant). In this form, (D.7) becomes:

$$\begin{aligned}
-\frac{\kappa^2 \mathfrak{f}^2}{2b_0^4}\left(\frac{\hat{t}}{\hat{t}_0}\right)^{-4\beta} + \frac{3\hat{\alpha}^2+6\hat{\alpha}\beta+\beta^2-\frac{1}{2}p^2}{\hat{t}^2} &= \kappa^2\hat{U}_0\left(\frac{\hat{t}}{\hat{t}_0}\right)^{-p\lambda}\,,\\
\frac{\kappa^2 \mathfrak{f}^2}{2b_0^4}\left(\frac{\hat{t}}{\hat{t}_0}\right)^{-4\beta} + \frac{2\hat{\alpha}(3\hat{\alpha}+2\beta-1)}{\hat{t}^2} &= \kappa^2\hat{U}_0\left(\frac{\hat{t}}{\hat{t}_0}\right)^{-p\lambda}\,,\\
-\frac{3\kappa^2 \mathfrak{f}^2}{2b_0^4}\left(\frac{\hat{t}}{\hat{t}_0}\right)^{-4\beta} + \frac{2\beta(3\hat{\alpha}+2\beta-1)}{t^2} &= \kappa^2\hat{U}_0\left(\frac{\hat{t}}{\hat{t}_0}\right)^{-p\lambda}\,,\\
\frac{\frac{p}{\lambda}(3\hat{\alpha}+2\beta-1)}{t^2} &= \kappa^2\hat{U}_0\left(\frac{\hat{t}}{\hat{t}_0}\right)^{-p\lambda}\,.
\end{aligned} \tag{D.17}$$

Here, we read off that $\beta = \frac{1}{2}$ and $p = \frac{2}{\lambda}$. Plugging these in and simplifying, we get the following system:

$$\begin{aligned} 3\hat{\alpha}\left(\hat{\alpha}+1\right) + \frac{1}{4} - \frac{2}{\lambda^2} &= \kappa^2 \hat{t}_0^2 \left(\hat{U}_0 + \frac{\mathfrak{f}^2}{2b_0^4}\right), \\ 6\hat{\alpha}^2 &= \kappa^2 \hat{t}_0^2 \left(\hat{U}_0 - \frac{\mathfrak{f}^2}{2b_0^4}\right), \\ 3\hat{\alpha} &= \kappa^2 \hat{t}_0^2 \left(\hat{U}_0 + \frac{3\mathfrak{f}^2}{2b_0^4}\right), \\ 6\hat{\alpha} &= \lambda^2 \kappa^2 \hat{U}_0 \hat{t}_0^2 . \end{aligned} \tag{D.18}$$

These equations can be solved for the remaining power,

$$\hat{\alpha} = \frac{8-\lambda^2}{6\lambda^2} \tag{D.19}$$

and relations between the coefficients,

$$\frac{\mathfrak{f}^2}{b_0^4} = \left(\frac{\lambda^2-2}{3}\right)\hat{U}_0 , \qquad \text{and} \qquad \hat{t}_0^2 = \frac{6\hat{\alpha}}{\hat{U}_0 \kappa^2 \lambda^2} . \tag{D.20}$$

At first glance, this solution does not immediately appear to have anything wrong with it at all. However, because the flux terms scale as b^{-4}, and the curvature terms scale as b^{-2}, any solution that starts off in this form will eventually leave it. Thus, since flux falls quicker than the curvature term, we choose to drop it in our power-law analysis.

The second superfluous case we consider is the case where the flux, curvature, and potential terms are all negligible. In this case, (D.7) reduces to only two linearly independent equations:

$$\begin{aligned} \hat{\alpha}\left(3\hat{\alpha}+2\beta-1\right) = \beta\left(3\hat{\alpha}+2\beta-1\right) = p\left(3\hat{\alpha}+2\beta-1\right) = 0 , \qquad \text{and} \\ 3\hat{\alpha}^2 + 6\hat{\alpha}\beta + \beta^2 = \frac{p^2}{2} , \end{aligned} \tag{D.21}$$

which we can only solve for two of $\hat{\alpha}$, β, or p in the non-trivial case. For later convenience, we shall record the solutions to (D.21) as

$$\hat{\alpha} = \frac{1}{3}(1 - 2\beta)\,, \qquad \text{with} \qquad p^2 = \frac{2}{3}(-5\beta^2 + 2\beta + 1)\,. \tag{D.22}$$

D.1.4 Inconsistent Solutions in 6D

We now highlight the solutions that, after analyzing their equations, yield mathematically inconsistent solutions rendering them completely and utterly useless.

The first of these we examine is a solution where the flux and potential terms are negligible. Under these assumptions, our power-law equations look like:

$$\begin{aligned} \frac{p^2 - 6\hat{\alpha}^2 - 12\hat{\alpha} - 2}{2} &= \frac{\hat{t}_0^2}{b_0^2}\,, \\ \hat{\alpha}\,(3\hat{\alpha} + 1) &= 0\,, \\ -\,(3\hat{\alpha} + 1) &= \frac{\hat{t}_0^2}{b_0^2}\,, \\ p\,(3\hat{\alpha} + 1) &= 0\,, \end{aligned} \tag{D.23}$$

after reading off $\beta = 1$ by comparing the powers of $\hat{t}$. We have two "solutions" to the above system. From the second equation, we have $\hat{\alpha} = 0, -\frac{1}{3}$. If $\hat{\alpha} = 0$, this forces $p = 0$ and $\hat{t}_0^2/b_0^2 = -1$ in the next two equations which is unacceptable on both physical and mathematical grounds; the second requires $t_0 = 0$, and $p^2 = -\frac{4}{3}$, which can also be discarded on mathematical grounds, since we require our powers to be real. So, this system of equations is clearly inconsistent.

Another inconsistent situation we investigate involves neglecting the flux contributions and terms due to the field-derivatives (i.e., the terms proportional to $1/\hat{t}^2$. This solution might arise if the other terms were all falling slower than $\hat{t}^{-2}$). They provide solutions which are either inconsistent, or violate our scaling solution assumptions. The simplest, the case, in which the flux and $1/\hat{t}^2$ are negligible, is noticeably inconsistent. Clearly, these solutions do not actually exist physically and so are not worth pursuing.

D.2 Supplemental 4D Power-Law Analysis

We now repeat the exercise of Section D.1, but in 4D. The two interesting cases that this analysis revealed are discussed in great detail in the main text of the thesis. These solutions either do not admit $\epsilon < 1$ (and so are classified as superfluous), or they are not physically possible due to inconsistencies, or imaginary—or negative in the case of U_0—solutions to the coefficients. They are therefore given cursory treatments here. Again, we note that (4.6) does not allow both $W^{(c)}$ and $W^{(f)}$ to be relevant simultaneously (unless $p_2 = 0$, in which case the radion is not inflating at all).

D.2.1 Superfluous 4D Scaling Solutions

In our first 4D superfluous case, both $\left|W^{(f)}\right|$ and $W^{(\varphi)}$ are large compared to the contributions due to $W^{(c)}$. We use this case to demonstrate the fact that flux terms must always be neglected to find any solution of interest. With these assumptions, (4.6) becomes:

$$\begin{aligned}
\frac{p_1\,(3\alpha-1)}{t^2} &= \lambda\frac{U_0}{M_p^2}\left(\frac{t}{t_0}\right)^{-(\lambda p_1+p_2)}\,, \\
-\frac{6\pi\mathfrak{f}^2\,e^{-3\frac{\psi_0}{M_p}}}{b_\star^2 M_p^2}\left(\frac{t}{t_0}\right)^{-3p_2} + \frac{p_2(3\alpha-1)}{t^2} &= \frac{U_0}{M_p^2}\left(\frac{t}{t_0}\right)^{-(\lambda p_1+p_2)}\,, \\
-\frac{2\pi\mathfrak{f}^2\,e^{-3\frac{\psi_0}{M_p}}}{b_\star^2 M_p^2}\left(\frac{t}{t_0}\right)^{-3p_2} + \frac{6\alpha^2-p_1^2-p_2^2}{2t^2} &= \frac{U_0}{M_p^2}\left(\frac{t}{t_0}\right)^{-(\lambda p_1+p_2)}\,.
\end{aligned} \tag{D.24}$$

Here, we read off that $p_2 = 2/3$ and $\lambda p_1 + p_2 = 2$ which implies $p_1 = 4/(3\lambda)$. Plugging these in and simplifying, we get the following system of equations:

$$\begin{aligned} \frac{4\,(3\alpha-1)}{3\lambda^2} &= \frac{U_0 t_0^2}{M_p^2}\,, \\ \frac{2\,(3\alpha-1)}{3} &= \frac{t_0^2}{M_p^2}\left(U_0 + \frac{6\pi \mathfrak{f}^2\, e^{-3\frac{\psi_0}{M_p}}}{b_\star^2}\right)\,, \\ \frac{\lambda^2\left(27\alpha^2-2\right)-8}{9\lambda^2} &= \frac{t_0^2}{M_p^2}\left(U_0 + \frac{2\pi \mathfrak{f}^2\, e^{-3\frac{\psi_0}{M_p}}}{b_\star^2}\right)\,. \end{aligned} \tag{D.25}$$

These equations can be solved for the remaining power,

$$\alpha = \frac{8+2\lambda^2}{9\lambda^2} \tag{D.26}$$

and relations between the coefficients,

$$\frac{\mathfrak{f}^2}{b_\star^2} = \frac{U_0\left(\lambda^2-2\right)e^{3\frac{\psi_0}{M_p}}}{12\pi}\,, \qquad \text{and} \qquad \hat{t}_0^2 = \frac{4\left(8-\lambda^2\right)M_p^2}{9U_0\lambda^4}\,. \tag{D.27}$$

For the exact same reason as in the previous section, we choose to not pursue this line of solution-space. Because $W^{(f)}$ falls faster than $W^{(c)}$, any solution that starts in a regime with $\left|W^{(f)}\right| > \left|W^{(c)}\right|$ (like the one just discussed) will eventually switch over to a solution with $\left|W^{(c)}\right| > \left|W^{(f)}\right|$. Thus, all our analytic pursuits from hereon out will neglect $W^{(f)}$.

The second superfluous case we consider is the case where $W^{(f)}$, $W^{(c)}$, and $W^{(\varphi)}$ are all negligible. In this case, (4.6) reduces to the simple system:

$$p_1\,(3\alpha-1) = p_2\,(3\alpha-1) = 6\alpha^2 - p_1^2 - p_2^2 = 0\,. \tag{D.28}$$

In this case, we can only solve for two of the three powers since (D.28) contains one redundant equation. We choose α and p_1, which are

$$\alpha = \frac{1}{3} \qquad \text{and} \qquad p_1 = \pm\sqrt{\frac{2}{3} - p_2^2}\,. \tag{D.29}$$

In this case, it is clear why this solution is not desirable: this solution only admits $\epsilon = 1/\alpha = 3 > 1$, which does not allow for any inflation. When performing our initial parameter search numerically, we find many solutions that appeared to be stuck at $\epsilon = 3$. (This is shown in the early behaviour of ϵ as plotted in the lower left panel in Figure 3.7.) This provides us with an intuition and the ability to explain the behaviour of our numeric evolutions and force them to bow to our analytic command.[1]

D.2.2 Inconsistent 4D Results

While the above can exist physically (and some we even see numerically), the situations we test in this section can not exist.

The first case we examine is a solution wherein $W^{(f)}$ and $W^{(\varphi)}$ are negligible and $W^{(c)}$ is the only significant term from W—i.e., $\left|W^{(c)}\right| \gg \left|W^{(f)}\right|, \left|W^{(\varphi)}\right|$. Under these assumptions, our power-law equations look like:

$$\begin{aligned} \frac{p_1\,(3\alpha - 1)}{t^2} &= 0\,, \\ \frac{2e^{-2\frac{\psi_0}{M_p}}}{b_\star^2}\left(\frac{t}{t_0}\right)^{-2p_2} + \frac{p_2(3\alpha - 1)}{t^2} &= 0\,, \\ \frac{e^{-2\frac{\psi_0}{M_p}}}{b_\star^2}\left(\frac{t}{t_0}\right)^{-2p_2} + \frac{6\alpha^2 - p_1^2 - p_2^2}{2t^2} &= 0\,, \end{aligned} \tag{D.30}$$

[1] While a stability calculation was never performed on this solution, one might infer from this behaviour that it behaves as an attractor since a wide range of general initial conditions often pick out this solution.

from which we can read off $p_2 = 1$. This reduces the system even further to:

$$\begin{aligned} p_1\,(3\alpha - 1) &= 0\,, \\ 3\alpha - 1 &= -\frac{2t_0^2}{b_\star^2} e^{-2\frac{\psi_0}{M_p}}\,, \\ 6\alpha^2 - p_1^2 - 1 &= -\frac{2t_0^2}{b_\star^2} e^{-2\frac{\psi_0}{M_p}}\,. \end{aligned} \tag{D.31}$$

In this case, we only have trivial (e.g., $p_1 = 0$, a case which has the inflaton not really living up to its name) or imaginary solutions possible for our remaining powers and coefficients. So, we see that this amounts to an unphysical scenario not worth pursuing in our investigation.

As in the 6D case, other potential scenarios we investigate—and ultimately reject—involve neglecting $W^{(f)}$ and terms due to the field-derivatives, which are the terms proportional to $1/t^2$ in (4.6). This solution might arise if the other terms all fall slower than t^{-2}. They provide solutions which are either inconsistent or demand negative potentials or imaginary times.

D.3 Equality of the 4D and 6D Scaling Solutions

It should be true, that, if our 4D equations of motion are exactly equivalent to the 6D EOMs, our scaling solutions should be equivalent as well. This provides a useful,but superfluous,[2]) check on our dimensional reduction.

We start by finding a transformation that relates $\hat{t}$ and t using (4.2), our power-law *ansatz* for ψ, and (C.1):

$$\mathrm{d}\hat{t} = e^{-\psi/2M_p}\,\mathrm{d}t = e^{-\psi_0/2M_p}\left(\frac{t}{t_0}\right)^{-p_2/2}\mathrm{d}t\,. \tag{D.32}$$

Integrating both sides of the above equation, we find

$$\frac{\hat{t}}{\hat{t}_0} = \left(\frac{t}{t_0}\right)^{1-p_2/2} \implies \frac{t}{t_0} = \left(\frac{\hat{t}}{\hat{t}_0}\right)^{2/(2-p_2)}, \quad \text{with} \quad \hat{t}_0 := \frac{2\,e^{-\psi_0/2M_p}}{2-p_2}\,t_0\,. \tag{D.33}$$

[2]While it adds nothing additional to the overall story, it is included here since it is a component of the comprehensive power-law analysis that forms a significant portion of this author's work—hence its inclusion in an appendix.

Now we are in a position to find the relationships between the scaling powers in 6D ($\hat{\alpha},\ \beta,\ p$) and 4D ($\alpha,\ p_1,\ p_2$).

We begin with the first of (C.1):

$$\hat{a} = a\, e^{-\psi/2M_p} = \left[a_0 \left(\frac{t}{t_0}\right)^{\alpha}\right]\left[e^{-\psi_0/2M_p}\left(\frac{t}{t_0}\right)^{-p_2/2}\right] = \hat{\alpha}_0 \left(\frac{t}{t_0}\right)^{\alpha - p_2/2}, \quad \text{(D.34)}$$

where we use our power-law forms for ψ and a across the second equality, and defined $\hat{a}_0 := a_0\, e^{-\psi_0/2M_p}$ across the last. Finally, using (D.33), we can write

$$\hat{a} = \hat{\alpha}_0 \left(\frac{\hat{t}}{\hat{t}_0}\right)^{(2\alpha - p_2)/(2-p_2)}, \quad \text{(D.35)}$$

from which we can read off

$$\hat{\alpha} = \frac{2\alpha - p_2}{2 - p_2}\,. \quad \text{(D.36)}$$

Following a similar procedure we can solve for β in terms of the 4D powers. We start with the relationship between ψ and b, and substitute the power-law form for b. This amounts to

$$\begin{aligned}\frac{\psi}{M_p} &= 2\ln\left(\frac{b}{b_\star}\right) = 2\ln\left[\frac{b_0}{b_\star}\left(\frac{\hat{t}}{\hat{t}_0}\right)^{\beta}\right] = 2\ln\left(\frac{b_0}{b_\star}\right) + 2\beta\ln\left(\frac{\hat{t}}{\hat{t}_0}\right) \\ &= \frac{\psi_0}{M_p} + \beta\,(2-p_2)\ln\left(\frac{t}{t_0}\right), \quad \text{where} \quad \frac{\psi_0}{2M_p} := \ln\left(\frac{b_0}{b_\star}\right). \end{aligned} \quad \text{(D.37)}$$

Comparing (D.37) to our power-law form of ψ, we can read off

$$\beta(2-p_2) = p_2 \implies \beta = \frac{p_2}{2-p_2}\,. \quad \text{(D.38)}$$

Finally, we solve for p as a function of the 4D scaling powers. We start from the canonical normalization of φ (2.19) and substitute in the 4D power-law form of φ:

$$\phi = \frac{\varphi}{\kappa M_p} = \frac{\varphi_0}{\kappa M_p} + \frac{p_1}{\kappa}\ln\left(\frac{t}{t_0}\right) = \phi_0 + \frac{p_1}{\kappa}\left(\frac{2}{2-p_2}\right)\ln\left(\frac{\hat{t}}{\hat{t}_0}\right), \quad \text{(D.39)}$$

where we use (D.33) again to change from t to $\hat{t}$ and define $\kappa\phi_0 := \varphi_0/M_p$. Comparing (D.39) to the last line in (D.2), we can read off the last relationship

$$\frac{p}{\kappa} = \frac{p_1}{\kappa}\left(\frac{2}{2-p_2}\right) \implies p = \frac{2p_1}{2-p_2}\,. \tag{D.40}$$

Applying these transformations on any set of 6D power-law equations reduces it to the equivalent set in 4D. We demonstrate this here explicitly for only one case, but note that this same procedure applies to any and all of our power-law solutions. Substituting (D.36), (D.38), and (D.40) into (D.21) we get

$$\frac{p_1\,(6\alpha-2)}{(2-p_2)^2} = \frac{p_2\,(6\alpha-2)}{(2-p_2)^2} = 0 = 12\alpha^2 - 2p_1^2 - 2p_2^2 \tag{D.41}$$

which, for $p_2 \neq 2$, is exactly twice (D.28), showing the equivalence explicitly.

Appendix E

Mathematica Files

In this appendix, we attach representative samples of the raw *Mathematica* files we use to perform the numerical calculations. Note that outputs have been omitted for readability of the code. The three files attached are each specific to a particular case, presented in the order they are discussed in the text. The files all look very similar, since they are basically iterations of the same process with different initial conditions, which we discuss below.

E.1 Initial Conditions

All numerical integrations utilize the same initial setup:

- A potential of the form (2.3):

$$U(\varphi) = V_0 \left(e^{-\beta_1 \phi / M_p} - e^{-\beta_2 \phi / M_p} \right) + \Lambda \,, \tag{E.1}$$

  where the β_i and V_0 are dials we choose and Λ is set so $U(\varphi_\star) = 0$, where $\varphi_\star$ is the value of φ that minimizes $U(\varphi)$. Note that in some cases, it is more convenient numerically to define the β_i in terms of their ratio and $\varphi_\star$:

$$X = \frac{\beta_1}{\beta_2} \qquad \text{and} \qquad \varphi_\star = \frac{1}{\beta_1 - \beta_2} \ln\left(\frac{\beta_1}{\beta_2}\right) , \tag{E.2}$$

  and so the β_i are often be presented in the form:

$$\beta_1 = \frac{X}{(X-1)\varphi_\star} \ln X \,, \qquad \beta_2 = \frac{1}{(X-1)\varphi_\star} \ln X \,. \tag{E.3}$$

- A total potential of the form (2.23):

$$W(\varphi,\psi) := 4\pi b_\star^2\, U(\varphi) e^{-\psi/M_p} - \frac{M_p^2}{b_\star^2} e^{-2\psi/M_p} + \frac{2\pi\mathfrak{f}^2}{b_\star^2} e^{-3\psi/M_p}\,, \tag{E.4}$$

  where $b_\star$ is another dial we choose. It is usually chosen to be $\mathcal{O}(10^{27})$ or $\mathcal{O}(10^{28})$ so as to be close to its maximum value as given by (3.2).

- The equations of motion given by (2.26) which require the following initial values: φ_0, $\dot\varphi_0$, ψ_0, $\dot\psi_0$ and a range (t_0, t_f) over which to integrate.

We now outline the specific numerical values of the above initial conditions required to produce all the figures in the main text of the thesis. All numerical values are given in units of M_p and recorded to the same degree of precision with which they are entered in *Mathematica*.

E.1.1 Cradle Inflation

For this case, Figures 3.2–3.4 are all generated by the same dials:

$$b_\star = 10^{27}, \quad \beta_1 = \frac{11}{40}\ln(1.1)\,, \quad \beta_2 = \frac{1}{4}\ln(1.1)\,, \quad V_0 = 10^{-108}\,; \tag{E.5}$$

and the same initial conditions:

$$(t_0, t_f) = \left(10^{27}, 10^{31}\right), \quad \varphi_0 = 15, \quad \psi_0 = -0.325, \quad \dot\varphi_0 = \dot\psi_0 = 0\,. \tag{E.6}$$

Figure 3.1 plots $W(\varphi,\psi)$ for $\varphi = \varphi_\star + \{0, 25, 50, 100\}$, where $\varphi_\star = 40$ from (2.4) and (E.5).

To demonstrate the rolling of ψ as in Figure 3.5, we choose $\psi_0 = -0.5$, so that the radion starts too high up its potential and rolls right on through. The same behavior can also be demonstrated by increasing $\dot\psi_0$.

To show the birth of the local extrema in the radion potential as in Figure 3.6, we see from (3.6) that the extrema depend on the value of the inflaton potential. So, we adjust $V_0 = 1.268 \times 10^{-108}$ (and then bump the radion up to $\psi_0 = -0.1$ so it does not roll over the local maximum) for this figure.

E.1.2 General Case

Section 3.4 describes a general integration and plots it in Figure 3.7. To generate these plots, the particular input values are:

$$b_\star = 10^{27}, \quad \beta_1 = \frac{11}{20}\ln(1.1), \quad \beta_2 = \frac{1}{2}\ln(1.1), \quad V_0 = 10^{-81}, \tag{E.7}$$

and

$$\begin{aligned}(t_0, t_f) = \left(507.635, 10^{20}\right), \quad \varphi_0 = 10, \quad \psi_0 = -50, \\ \dot{\varphi}_0 = 0.104, \quad \dot{\psi}_0 = 1.99\,.\end{aligned} \tag{E.8}$$

E.1.3 Power-law Solutions

In the power-law cases, we approximate our inflaton potential as being dominated by a single potential, as in (4.1), the role of which is played by the first term in (E.1). So, we see that λ is performed by β_1 in our numerics during the scaling regime.

As discussed in the main body of the text, the initial values for many of the parameters are determined by the scaling analysis. In both cases, we choose $b_\star = 10^{28}$ and note $\lambda = \beta_1$.

E.1.3.1 Attractor Case

In this case, Figures 4.1–4.4 are all generated using the following choices:

$$b_\star = 10^{28}, \quad \beta_1 = \lambda = \frac{7}{30}\ln 7, \quad \beta_2 = \frac{1}{30}\ln 7, \quad \varphi_0 = -18.6, \quad \psi_0 = -30\,. \tag{E.9}$$

According to the relationship in (4.9), we are free to choose either V_0 or t_0. We choose $V_0 = (8\pi^{3/2} b_\star^3)^{-1}$, the maximum value allowed by (3.3). The rest of the initial conditions are dependent on the above based on the analytic derivations in the text:

$$t_0^2 = \frac{\left(5 - \lambda^2\right)\alpha^2}{2U_0}, \quad \dot{\varphi}_0 = \frac{p_1}{t_0}, \quad \dot{\psi}_0 = \frac{p_2}{t_0}, \quad t_f = t_0\, e^{-\psi_0/p_2}\,, \tag{E.10}$$

where the powers p_i and α are given by (4.8) and depend on λ. The value for t_f is computed from solving the second equation in (4.2) for $t = t_f$, which occurs at

$\psi(t_f) = \psi_\star = 0$. To generate the other two trajectories in Figure 4.2 we add and subtract 1 from each of ψ_0 and φ_0.

E.1.3.2 Unstable Case

To depict the unstable case, Figures 4.1–4.4 are all produced by choosing:

$$\begin{aligned} b_\star = 10^{28}, \quad \beta_1 = \lambda = \frac{1}{18.23}, \quad \beta_2 = \frac{1}{36.16}, \\ t_f = 100 t_0, \quad \varphi_0 = -30, \quad \psi_0 = -30\,. \end{aligned} \tag{E.11}$$

In this case, (4.17) chooses both V_0 and t_0 on our behalf. These, along with the rest of the initial conditions, are dependent on the above based on the analytic derivations in the main text:

$$U_0 = \frac{2e^{-2\psi_0}}{(1-\lambda^2)b_\star^2}, \quad t_0^2 = \frac{(\lambda^2+3)}{2\lambda^4 U_0}, \quad \dot{\varphi}_0 = \frac{p_1}{t_0}, \quad \dot{\psi}_0 = \frac{p_2}{t_0}, \tag{E.12}$$

where the powers p_i are given by (4.16) and depend on λ.

E.2 Raw Files

We conclude this appendix with the raw, annotated *Mathematica* files, which span the next pages.

Cradle.nb

This file numerically integrates the equations of motion—and plots the results—for the Cradle solution.

Definitions

Here we have the definitions of our potentials, their derivatives, and some constants within them:

In[1]:=
```
V[ϕ_] := V0 * (Exp[-ϕ / A] - Exp[-ϕ / B] - Exp[-ϕmin / A] + Exp[-ϕmin / B])
Vtot[ϕ_, ψ_] := 4 * π * bmin^2 * Exp[-ψ] (V[ϕ] + Λ) +
  1 / bmin^2 * Exp[-2 * ψ] (1 / 2 * Exp[-ψ] - 1)

Vϕ[ϕ_] := (D[V[x], x]) /. x → ϕ
Vtotϕ[ϕ_, ψ_] := (D[Vtot[x, ψ], x]) /. x → ϕ
Vtotψ[ϕ_, ψ_] := (D[Vtot[ϕ, x], x]) /. x → ψ

H[t_] := Sqrt[1 / 3 (ϕ'[t]^2 / 2 + ψ'[t]^2 / 2 + Vtot[ϕ[t], ψ[t]])]
ϵ[t_] :=
 3 - 6 * Vtot[ϕ[t], ψ[t]] / (2 Vtot[ϕ[t], ψ[t]] + ϕ'[t]^2 + ψ'[t]^2)
η[t_] :=
 2 ((ϕ'[t] * ϕ''[t] + ψ'[t] * ψ''[t]) / (ϕ'[t]^2 + ψ'[t]^2) / H[t] + ϵ[t])

Λ := 1 / (8 * π * bmin^4)
A := ϕmin * (X - 1) / (X * Log[X])
B := ϕmin * (X - 1) / Log[X]
```

In[12]:=
```
ψmin[t_] := Log[3] - Log[2 + Sqrt[1 - 24 * bmin^4 * π * V[ϕ[t]]]]
ψstar[t_] := Log[3] - Log[2 - Sqrt[1 - 24 * bmin^4 * π * V[ϕ[t]]]]
```

Useful Quantities

Here, we define some of the quantities that may be useful to compute:

In[14]:=
```
(*b term*)
b[t_] := bmin * Exp[ψ[t] / 2]

(*Total Cosmological Constant*)
CC := V0 * (-Exp[-ϕmin / A] + Exp[-ϕmin / B]) + Λ

(*Scaling lambda: λ*)
λ := 1 / A

(*Flux-Term*)
FF[t_] := 1 / bmin^2 * Exp[-2 * ψ[t]] (1 / 2 * Exp[-ψ[t]])

(*Initial Radius*)
b0 := bmin * Exp[ψ0 / 2]

(*4D Kaluza-Klein Scale*)(*where m_KK=b_min/b^2*)
KK[t_] := bmin / b[t]^2
```

Dials

These are the dials we are free to tune in our models. We have defined the A and B parameters ($\beta_1$and β_2 in the main text) in our potential in terms of X and ϕ_{min}, as above, for numerical convenience.

In[34]:=
```
bmin := 10^27
ϕmin := 40
X := 11 / 10
V0 := 10^(-108)
```

Initial Conditions

Here, we define our initial conditions.

In[24]:=
```
t0 := 10^27
tmax := 10^31

ϕ0 := 15(*15*)
ϕdot0 := 0

ψ0 := -0.325
ψdot0 := 0
```

This line merely reads off a convenient chart that *Mathematica* exports containing all our numerical parameters.

```
In[41]:= parameters = Multicolumn[{
           HoldForm[b_min] == N[bmin],
           HoldForm[ϕ_min] == ϕmin,
           HoldForm[X] == X,
           HoldForm[V_0] == N[V0],
           ,
           HoldForm[t_0] == N[t0],
           HoldForm[t_max] == N[tmax],
           ,
           HoldForm[ϕ_0] == N[ϕ0],
           HoldForm[ϕ̇_0] == N[ϕdot0],
           HoldForm[ψ_0] == N[ψ0],
           HoldForm[ψ̇_0] == N[ψdot0],

           HoldForm[b_0] == b0,
           HoldForm[A] == A,
           HoldForm[B] == B,
           HoldForm[λ] == λ
         }, {4, Automatic}]
       1 / A // FullSimplify
       1 / B
```

Physical Checks

Here we install an internal check that our numerics satisfy physical limits:

(1) Extra Dimensions (now) $\geq 1\ \mu$m

(2) Extra dimensions (start) sub-Plackian

(3) $V(\phi) + \Lambda$ needs to be sub-Planckian

If any one of these conditions fail, the computation stops.

```
In[44]:= (*1*)If[bmin ≤ 6 * 10^28 / Sqrt[8 * π], "bmin ≤ 1μm ✓" , Quit[]]
       (*2*)If[ψ0 ≥ Log[1 / (4 * Sqrt[π] * bmin)],
        "b initial is sub-Planckian ✓" , Quit[]]
       (*3*)Plot[{V[ϕ] + Λ, 1 / (8 * π^(3 / 2) * bmin^3)},
        {ϕ, ϕ0, ϕmin}, PlotLabel → Text[Style[Planck Scale, Orange]] >
          Text[Style[Potential, Blue]], PlotStyle → {Blue, Orange}]
```

Differential Equations

In[47]:=
```
bgsols = NDSolve[{ϕ''[t] + 3 * H[t] * ϕ'[t] + Vtotϕ[ϕ[t], ψ[t]] == 0,
    ψ''[t] + 3 * H[t] * ψ'[t] + Vtotψ[ϕ[t], ψ[t]] == 0, H[t] == n'[t],
    ϕ[t0] == ϕ0, ϕ'[t0] == ϕdot0, ψ[t0] == ψ0, ψ'[t0] == ψdot0,
    n[t0] == 0}, {ϕ, ψ, n}, {t, t0, tmax}, MaxSteps → Infinity]
```

Important Numeric Calculations

Here, we compute the intial and final values of N and ϵ during inflation.

In[48]:=
```
FindRoot[(ϵ[t] /. bgsols[[1]]) == 1, {t, 10^30}]
nend = (*(n[t]/.bgsols/.%)[[1]]*)144
nstart = 144 - 60
n50 = nend - 50
n70 = nend - 70
t50 = t /. FindRoot[(n[t] /. bgsols[[1]]) == n50, {t, 10^30}]
t60 = t /. FindRoot[(n[t] /. bgsols[[1]]) == (nend - 60), {t, 10^30}]
t70 = t /. FindRoot[(n[t] /. bgsols[[1]]) == n70, {t, 7 * 10^29}]
ϵ50 = ϵ[t50] /. bgsols[[1]]
ϵ60 = ϵ[t60] /. bgsols[[1]]
ϵ70 = ϵ[t70] /. bgsols[[1]]


η50 = η[t50] /. bgsols[[1]]
η60 = η[t60] /. bgsols[[1]]
η70 = η[t70] /. bgsols[[1]]
```

In[62]:=
```
16 * ϵ50
16 * ϵ60
16 * ϵ70
1 - 6 * ϵ60 + 2 η60
```

Plots

Here we generate the plots.

In[66]:=
```
fontsize := Large
opts2 := {AxesStyle → fontsize, AspectRatio → 1,
  ImageSize → Large, FrameStyle → fontsize,
  PlotTheme → "Scientific"(*, RotateLabel→False*)}
```

```
LS[x_] := Style[x, fontsize]

ϕplot =
 (*ParametricPlot[{{n[t],ϕ[t]}/.bgsols,{n[t], ϕmin}/.bgsols},
  {t, t0, tmax}, PlotStyle→{{}, Dashed},
  PlotRange→Full, AxesLabel→{HoldForm[N], ϕ},
  PlotLegends→{LS[ϕ], LS[ϕmin]}, Evaluate[opts2]]*)
 LogLinearPlot[{{ϕ[t]} /. bgsols, ϕmin}, {t, t0, tmax},
  PlotStyle → {{}, Dashed}, PlotRange → Full,
  FrameLabel → {HoldForm[t "(Mp^-1)"], "φ (Mp)"}, PlotLegends →
   Placed[{LS[φ], LS[φmin]}, {0.85, 0.15}], Evaluate[opts2]]
ψplot = (*ParametricPlot[{{n[t],ψ[t]}/.bgsols,
   {n[t],ψmin[t]}/.bgsols, {n[t],ψstar[t]}/.bgsols},
  {t,t0, tmax},PlotStyle→{{}, Dashed, Dotted},
  PlotRange→Full, AxesLabel→{HoldForm[N], ψ},
  PlotLegends→{LS[ψ],LS[ψmin], LS[ψmax]} ,Evaluate[opts2]]*)
 LogLinearPlot[{ψ[t] /. bgsols, ψmin[t] /. bgsols,
   ψstar[t] /. bgsols}, {t, t0, tmax},
  PlotStyle → {{}, Dashed, Dotted}, PlotRange → Full,
  FrameLabel → {HoldForm[t "(Mp^-1)"], "ψ (Mp)"},
  PlotLegends → Placed[{LS[ψ], LS[ψmin], LS[ψmax]}, {0.2, 0.85}] ,
  AspectRatio → 1, Evaluate[opts2]]
ψplotclose = (*ParametricPlot[{{n[t],ψ[t]}/.bgsols,
   {n[t],ψmin[t]}/.bgsols, {n[t],ψstar[t]}/.bgsols},
  {t,t0, tmax},PlotStyle→{{}, Dashed, Dotted},
  PlotRange→Full, AxesLabel→{HoldForm[N], ψ},
  PlotLegends→{LS[ψ],LS[ψmin], LS[ψmax]} ,Evaluate[opts2]]*)
 LogLinearPlot[{ψ[t] /. bgsols, ψmin[t] /. bgsols},
  {t, t0, 5 * 10^(28)}, PlotStyle → {{}, Dashed, Dotted},
  PlotRange → {-0.2, 0.6},
  FrameLabel → {HoldForm[t "(Mp^-1)"], "ψ (Mp)"},
  PlotLegends → Placed[{LS[ψ], LS[ψmin], LS[ψmax]}, {0.2, 0.85}] ,
  AspectRatio → 1, Evaluate[opts2]]
Hplot = (*ParametricPlot[{{n[t],Log[H[t]]}/.bgsols,
   {n[t],Log10[KK[t]]}/.bgsols}, {t, t0, tmax},
  PlotStyle→{{}, Dashed},PlotRange→Full,
  AxesLabel→{HoldForm[N], Log[{H, 1/b}]}, PlotLegends→
```

```
    {LS[H], LS["Kaluza-Klein Scale"]}, Evaluate[opts2]]*)
 LogLogPlot[{H[t] /. bgsols, bmin * Exp[-ψ[t] / 2] *
       Sqrt[4 * π * (V[ϕ[t]] + Λ * (1 - Exp[-2 ψ[t]])) / 6] +
      Exp[-ψ[t] / 2] * ψ'[t] / 2 /. bgsols, KK[t] /. bgsols},
  {t, t0, tmax}, PlotStyle → {{}, Dashed, Dotted},
  PlotRange → Full,
  FrameLabel → {HoldForm[t "(M_p^-1)"], H "(M_p)"},
  PlotLegends → Placed[
    {LS[HoldForm["Numeric" H]], LS[HoldForm["Semi-Analytic" H]] ,
     LS[m_KK(*"4D Kaluza-Klein Scale"*)]},
    {0.3, 0.2}], Evaluate[opts2]]
ϵplot = ParametricPlot[{{n[t], Log10[ϵ[t]]} /. bgsols,
   {n[t], Log10[0.1 / 16]} /. bgsols(*,
   {n[t], Log10[ϵstart]}/.bgsols*)}, {t, t0, tmax},
  PlotStyle → {{}, Dashed, Dotted}, PlotRange → Full,
  FrameLabel → {HoldForm[N_e], Log[ϵ]},
  PlotLegends → Placed[{LS[HoldForm[ϵ]], LS[ϵ == HoldForm[0.1 / 16]]
     (*, LS[ê==N[ϵstart]]*)}, {0.2, 0.2}],
  GridLines → {{0, nstart, nend}, {0}}, Evaluate[opts2], Epilog →
   {Text[Style[60 e "-foldings", Medium], {(nstart + nend) / 2, -0.1}],
    {Arrowheads[{-.02, .02}], Arrow[{{nstart, 0}, {nend, 0}}]}}]
ηplot = ParametricPlot[{n[t], Log10[Abs[η[t]]]} /. bgsols,
  {t, t0, tmax}, PlotRange → Full,
  FrameLabel → {HoldForm[N_e], Log[HoldForm[Abs[η]]]},
  (*PlotLegends→Placed[{LS[Abs[η̂]]},After],*)Evaluate[opts2]]
nplot = (*ParametricPlot[{{n[t],ϕ[t]}/.bgsols,
   {n[t], ϕmin}/.bgsols}, {t, t0, tmax}, PlotStyle→{{}, Dashed},
  PlotRange→Full, AxesLabel→{HoldForm[N], ϕ},
  PlotLegends→{LS[ϕ], LS[ϕ_min]}, Evaluate[opts2]]*)
 LogLinearPlot[{{n[t]} /. bgsols}, {t, t0, tmax},
  PlotStyle → {{}, Dashed}, PlotRange → Full,
  FrameLabel → {HoldForm[t], N_e}, Evaluate[opts2]]

ψpotplot = Plot[Evaluate[{Vtot[ϕmin, ψ], Vtot[ϕmin + 25, ψ],
     Vtot[ϕmin + 50, ψ], Vtot[ϕmin + 100, ψ]} * 10^55],
  {ψ, -1, 4}, FrameLabel → {"ψ (M_p)", HoldForm[W "(M_p^4 × 10^-55)"]},
  PlotStyle → {{}, Dashed, Dotted, DotDashed},
```

```
  AspectRatio → 1 / 2, ImageSize → 1200, Evaluate[opts2]]

LogLogPlot[
 {FF[t] /. bgsols, (4 * π * bmin^2 * Exp[-ψ[t]] (V[ϕ[t]] + Λ)) /. bgsols,
  1 / b[t]^2 /. bgsols, ϕ'[t]^2 / 2 /. bgsols}, {t, t0, tmax},
 PlotLegends → {"Flux Term", "V-term", "Curv. Term"}]
```

Finally, we export the figures.

```
folder = FileNameJoin[{"..", "..", "Figures", "Plots", "Cradle"}];
 Export[
  FileNameJoin[{NotebookDirectory[], folder, "phi.pdf"}], ϕplot]
 Export[FileNameJoin[{NotebookDirectory[], folder, "psi.pdf"}],
  ψplot]
 Export[FileNameJoin[{NotebookDirectory[], folder, "psi_zoom.pdf"}],
  ψplotclose] *)
Export[FileNameJoin[{NotebookDirectory[], folder, "H.pdf"}], Hplot]
Export[
 FileNameJoin[{NotebookDirectory[], folder, "epsilon.pdf"}], ϵplot]
Export[FileNameJoin[{NotebookDirectory[], folder, "eta.pdf"}],
 ηplot]
Export[FileNameJoin[
  {NotebookDirectory[], folder, "parameters.pdf"}], parameters]
Export[FileNameJoin[{NotebookDirectory[], folder, "psi_pot.pdf"}],
 ψpotplot]
```

Attractor.nb

This file numerically evaluates the Attractor case and generates all the plots associated therewith.

Definitions

Here we have the definitions of our potentials, their derivatives, and some constants within them:

In[1]:=
```
VM[Q_, ϕ_] :=
 Q * (Exp[-ϕ / A] - Exp[-ϕ / B + κ ] - Exp[-ϕmin / A] + Exp[-ϕmin / B + κ])
V[ϕ_] :=
 V0 (Exp[-ϕ / A] - Exp[-ϕ / B + κ] - Exp[-ϕmin / A] + Exp[-ϕmin / B + κ])
Vtot[ϕ_, ψ_] := 4 * π * bmin^2 * Exp[-ψ] (V[ϕ] + Λ) +
   1 / bmin^2 * Exp[-2 * ψ] (1 / 2 * Exp[-ψ] - 1)

Vϕ[ϕ_] := (D[V[x], x]) /. x → ϕ
Vtotϕ[ϕ_, ψ_] := (D[Vtot[x, ψ], x]) /. x → ϕ
Vtotψ[ϕ_, ψ_] := (D[Vtot[ϕ, x], x]) /. x → ψ

H[t_] :=
 Sqrt[1 / 3 (ϕ'[t]^2 / 2 + ψ'[t]^2 / 2 + Vtot[ϕ[t], ψ[t]](*+ρ[t]*))]
ϵ[t_] := (ϕ'[t]^2 / 2 + ψ'[t]^2 / 2(*+(2/3)*ρ[t]*)) / H[t]^2;
η[t_] := (ϕ''[t] * ϕ'[t] + ψ''[t] * ψ'[t](*+2/3*ρ'[t]*)) /
    (H[t]^3 * ϵ[t]) + 2 * ϵ[t]

Γϕ[ϕ_] := Θϕ * Exp[-(ϕ - ϕdiss)^2 / σ^2]
Γψ[ϕ_] := Θψ * Exp[-(ϕ - ϕdiss)^2 / σ^2]
(*Q[t_]:=Γϕ[ϕ[t]]/(3*H[t])*)

Λ := 1 / (8 * π * bmin^4)
A := (ϕmin - ϕp) * (X - 1) / (X * (Log[X]))
B := (ϕmin - ϕp) * (X - 1) / (Log[X])
κ := ϕp * (1 / B - 1 / A)
```

In[16]:=
```
ψmin[t_] := Log[3] - Log[2 + Sqrt[1 - 24 * bmin^4 * π * V[ϕ[t]]]]
ψstar[t_] := Log[3] - Log[2 - Sqrt[1 - 24 * bmin^4 * π * V[ϕ[t]]]]
```

Useful Quantities

Here, we define some of the quantities that may be useful to compute:

In[18]:=
```
(*b term*)
b[t_] := bmin * Exp[ψ[t] / 2]

(*Total Cosmological Constant*)
CC := V0 * (-Exp[-ϕmin / A] + Exp[-ϕmin / B]) + Λ

(*Scaling lambda: λ*)
λ := 1 / A

(*(*Total Flux*)
flux[t_]:=(1/Sqrt[4*π])(1/bmin^2)*Exp[-ψ[t]]
*)
(*Flux-Term*)
FF[t_] := 1 / bmin^2 * Exp[-2 * ψ[t]] (1 / 2 * Exp[-ψ[t]])

(*Initial Radius*)
b0 := bmin * Exp[ψ0 / 2]

(*Kaluza-Klein Scale*)
KK[t_] := bmin / b[t]^2
```

Dials

These are the dials we are free to tune in our models. We have defined the A and B ($\beta_1$and β_2 in the main text) parameters in our potential in terms of X and $\phi_{\min}$, as above, for numerical convenience.

In[24]:=
```
bmin := 10^28.
ϕmin := 5
ϕp := 0
X := 7
ϕdiss := ϕmin - 4(*0.9*)
Θϕ := 0(*5*10^(-20)*)(*10^(-15)*)
Θψ := 0.
σ := 3

(*ψ0>*)
N[ Log[1 / (4 * Sqrt[π] * bmin)]]
```

Initial Conditions

Here, we define our initial conditions.

In[33]:=
```
V0 := V0sc

t0 := t0sc
tmax := tmaxsc * 10^5

ϕ0 := ϕ0sc
ϕdot0 := ϕdot0sc

b0 := bmin * Exp[ψ0 / 2](*0.2*bmin*)
ψ0 := ψ0sc
ψdot0 := ψdot0sc

ρ0 := 0

parameters = Multicolumn[{
    HoldForm[b_min] == N[bmin],
    HoldForm[ϕ_min] == ϕmin,
    HoldForm[X] == X,
    HoldForm[V_0] == N[V0],

    HoldForm[ϕ_diss] == N[ϕdiss],
    HoldForm[Θ_ϕ] == N[Θϕ],
    HoldForm[Θ_ψ] == N[Θψ],
```

```
    HoldForm[σ] == N[σ],

    HoldForm[t0] == N[t0],
    HoldForm[tmax] == N[tmax],
    HoldForm[b0] == N[b0],
    HoldForm[ρ0] == N[ρ0],

    HoldForm[ϕ0] == N[ϕ0],
    HoldForm[ϕdot0] == N[ϕdot0],
    HoldForm[ψ0] == N[ψ0],
    HoldForm[ψdot0] == N[ψdot0],
    HoldForm[A] == N[A],
    HoldForm[B] == N[B],
    HoldForm[κ] == N[κ]
  }, {4, Automatic}]
1 / A
1 / B
V0
```

Scaling Solutions:

Here we encode the intial conditions revealed by our scaling solution so that our numerics begin in the attractor solution. Note that we can choose one of V_0 or t_0. We choose V_0 to be its largest allowed value.

In[46]:=
```
ψ0sc = (*-0.5*Log[bmin]*)-30.
ϕ0sc = λ * ψ0sc - 5(*ϕmin+λ*ψ0sc*)

α = 2 / (1 + λ^2)
p1 = 2 * λ / (1 + λ^2)
p2 = 2 - λ * p1

V0sc = VTEMP /.
  Solve[VM[VTEMP, ϕ0sc] + Λ == 1 / (8 * π^(3 / 2) * bmin^3), VTEMP][[1]]
(*(5-λ^2)/(2*π*bmin^2*t0^2*(1+λ^2)^2)*Exp[λ*ϕ0sc+ψ0sc]*)

t0sc = Sqrt[
  (5 - λ^2) / (2 * π * bmin^2 * V0sc * (1 + λ^2)^2) * Exp[λ * ϕ0sc + ψ0sc]]
tmaxsc = t0sc * Exp[-ψ0sc / α]

ϕdot0sc = p1 / t0sc
ψdot0sc = p2 / t0sc
```

Physical Checks

Here we install an internal check that our numerics satisfy physical limits:
(1) Extra Dimensions (now) ≥ 1 μm
(2) Extra dimensions (start) sub-Plackian
(3) $V(\phi)$ + Λ needs to be sub-Planckian

If any one of these conditions fail, the computation stops.

```
(*1*)If[bmin ≤ 6 * 10^28 / Sqrt[8 * π], "bmin ≤ 1μm ✓" , Quit[]]
(*2*)If[ψ0 ≥ Log[1 / (4 * Sqrt[π] * bmin)],
 "b initial is sub-Planckian ✓" , Quit[]]
(*3*)(*If[V[ϕ]+Λ≤1/(8*π^(3/2)*bmin^3),
 "V(ϕ) is sub-Planckian ✓" , Quit[]]*)
(*3*)Plot[{V[ϕ] + Λ, 1 / (8 * π^(3 / 2) * bmin^3)},
 {ϕ, ϕ0, ϕmin}, PlotLabel → Text[Style[Planck Scale, Orange]] >
   Text[Style[Potential, Blue]], PlotStyle → {Blue, Orange}]
```

Differential Equations

Here, we numerically solve the EOMs for the above initial conditions.

```
(*Power Law, mKK, and Attractor*)
ϕ0 := ϕ0sc
ψ0 := ψ0sc
Θϕ := 0
bgsols1 = NDSolve[{
    ϕ''[t] + 3 * H[t] * ϕ'[t] + Vtotϕ[ϕ[t], ψ[t]] == -Γϕ[ϕ[t]] * ϕ'[t],
    ψ''[t] + 3 * H[t] * ψ'[t] + Vtotψ[ϕ[t], ψ[t]] == -Γψ[ϕ[t]] * ψ'[t],
    ρ'[t] == 0,
    H[t] == n'[t],
    ϕ[t0] == ϕ0, ϕ'[t0] == ϕdot0, ψ[t0] == ψ0,
    ψ'[t0] == ψdot0, ρ[t0] == ρ0, n[t0] == 0}, {ϕ, ψ, ρ, n},
  {t, t0, tmax}, MaxSteps → Infinity]
ψ0 := -31
ϕ0 := ϕ0sc - 1
bgsols2 = NDSolve[{
    ϕ''[t] + 3 * H[t] * ϕ'[t] + Vtotϕ[ϕ[t], ψ[t]] == -Γϕ[ϕ[t]] * ϕ'[t],
    ψ''[t] + 3 * H[t] * ψ'[t] + Vtotψ[ϕ[t], ψ[t]] == -Γψ[ϕ[t]] * ψ'[t],
    ρ'[t] + 4 * H[t] * ρ[t] == Γϕ[ϕ[t]] * ϕ'[t]^2 + Γψ[ϕ[t]] * ψ'[t]^2,
    H[t] == n'[t],
    ϕ[t0] == ϕ0, ϕ'[t0] == ϕdot0, ψ[t0] == ψ0,
    ψ'[t0] == ψdot0, ρ[t0] == ρ0, n[t0] == 0}, {ϕ, ψ, ρ, n},
  {t, t0, tmax}, MaxSteps → Infinity]
ψ0 := -29
ϕ0 := ϕ0sc + 1
bgsols3 = NDSolve[{
    ϕ''[t] + 3 * H[t] * ϕ'[t] + Vtotϕ[ϕ[t], ψ[t]] == -Γϕ[ϕ[t]] * ϕ'[t],
    ψ''[t] + 3 * H[t] * ψ'[t] + Vtotψ[ϕ[t], ψ[t]] == -Γψ[ϕ[t]] * ψ'[t],
    ρ'[t] + 4 * H[t] * ρ[t] == Γϕ[ϕ[t]] * ϕ'[t]^2 + Γψ[ϕ[t]] * ψ'[t]^2,
    H[t] == n'[t],
    ϕ[t0] == ϕ0, ϕ'[t0] == ϕdot0, ψ[t0] == ψ0,
    ψ'[t0] == ψdot0, ρ[t0] == ρ0, n[t0] == 0}, {ϕ, ψ, ρ, n},
  {t, t0, tmax}, MaxSteps → Infinity]
In[69]:= λ // N
1 / α // N
```

Plots

Here we generate the plots.

In[71]:=
```
fontsize := Large
opts2 := {AxesStyle → fontsize, AspectRatio → 1,
  ImageSize → Large, FrameStyle → fontsize,
  PlotTheme → "Scientific"(*, RotateLabel→False*)}
LS[x_] := Style[x, fontsize]
(*
ϕplotTot=
 LogLinearPlot[{{ϕ[t]}/.bgsols1, {ϕ[t]}/.bgsols2,{ϕ[t]}/.bgsols3},
    {t, t0, tmax}, PlotStyle→{{}, Dashed},
    PlotRange→Full, AxesLabel→{HoldForm[t], ϕ},
    PlotLegends→{LS[ϕ], LS[ϕmin]}, Evaluate[opts2]]
ψplotTot=LogLinearPlot[{ψ[t]/.bgsols1,ψ[t]/.bgsols2,ψ[t]/.bgsols3},
     {t,t0, tmax},PlotStyle→{{}, Dashed, Dotted},
     PlotRange→Full, AxesLabel→{HoldForm[t], ψ},
     PlotLegends→{LS[ψ]} ,Evaluate[opts2]]
    VTermplot=LogLogPlot[{FF[t]/.bgsols1,
      (4*π*bmin^2*Exp[-ψ[t]](V[ϕ[t]]+Λ))/.bgsols1,
      (* 1/b[t]^2/.bgsols,*) 1/bmin^2*Exp[-2*ψ[t]]/.bgsols1},
     {t, t0, tmax}, PlotLegends→{"Flux Term",
       "V-term", "Curv. Term"}, Evaluate[opts2]]
    LogLogPlot[{V0(Exp[-ϕ[t]/A])/.bgsols1,V0*Exp[-ϕ[t]/B]/.bgsols1,
      V0*(Exp[-ϕmin/A]+Exp[-ϕmin/B])}, {t, t0, tmax},
     PlotRange→Full, PlotLegends→{a,bb,c}]*)
(*The following plots are for the paper.*)
p1plot = LogLogPlot[{ϕ'[t] * t /. bgsols1, λ * α},
  {t, t0, 5 * 10^15}, PlotRange → {0.5, 1},
  FrameLabel → {HoldForm[t "(Mp^-1)"], p1}, PlotStyle → {{}, Dashed},
  PlotLegends → Placed[{LS[ϕ̇[t] t], LS[HoldForm[λ α]]}, {0.2, 0.85}],
  Evaluate[opts2]]
p2plot = LogLogPlot[{ψ'[t] * t /. bgsols1, α},
  {t, t0, 5 * 10^15}, PlotRange → {1.5, 2},
  FrameLabel → {HoldForm[t "(Mp^-1)"], p2}, PlotStyle → {{}, Dashed},
  PlotLegends → Placed[{LS[ψ̇[t] t], LS[HoldForm[α]]}, {0.2, 0.85}],
  Evaluate[opts2]]
```

```
Hplot = ParametricPlot[{{n[t], Log10[H[t]]} /. bgsols1,
    {n[t], Log10[KK[t]]} /. bgsols1}, {t, t0, tmax},
  PlotStyle → {{}, Dashed}, PlotRange → Full,
  FrameLabel → {HoldForm[Ne]}, PlotLegends →
   Placed[{LS[Log[H / Mp]], LS[HoldForm[Log[mKK / Mp]]]}, {0.2, 0.2}],
  AspectRatio → 1 / 2, ImageSize → 1200, Evaluate[opts2]]
p1plotTot = LogLogPlot[{ϕ'[t] * t /. bgsols1, ϕ'[t] * t /. bgsols2,
    ϕ'[t] * t /. bgsols3(*, λ*α*)}, {t, t0, 5 * 10^15},
  PlotRange → Full, FrameLabel → {HoldForm[t "(Mp^-1)"], p1},
  PlotStyle → {{}, {}, {}, Dashed}, (*PlotLegends→
   Placed[{LS[" "],LS["Numerics"],LS[" "], LS["Analytics"]},
    {0.8, 0.85}],*)Evaluate[opts2]]
p2plotTot = LogLinearPlot[{ψ'[t] * t /. bgsols1, ψ'[t] * t /. bgsols2,
    ψ'[t] * t /. bgsols3(*,α*)}, {t, t0, 5 * 10^15},
  PlotRange → Full, FrameLabel → {HoldForm[t "(Mp^-1)"], p2},
  PlotStyle → {{}, {}, {}, Dashed}, (*PlotLegends→
   Placed[{LS[" "],LS["Numerics"],LS[" "], LS["Analytics"]},
    {0.8, 0.85}],*)Evaluate[opts2]]
```

Finally, we export the figures.

```
In[79]:= folder = FileNameJoin[
    {"..", "..", "Figures", "Plots", "Attractor_Max_E_Folds"}];
Export[FileNameJoin[{NotebookDirectory[], folder, "p1.pdf"}],
 p1plot]
Export[FileNameJoin[{NotebookDirectory[], folder, "p2.pdf"}],
 p2plot]
Export[FileNameJoin[{NotebookDirectory[], folder, "H.pdf"}], Hplot]
Export[FileNameJoin[
  {NotebookDirectory[], folder, "p1tot.pdf"}], p1plotTot]
Export[FileNameJoin[{NotebookDirectory[], folder, "p2tot.pdf"}],
 p2plotTot]
```

Below, we have some obsolete code that we retain for the sake of reference.

In[85]:=
```
(* folder=FileNameJoin[{"..", "Plots", "Attractor_Max_E_Folds"}];
Export[FileNameJoin[
  {NotebookDirectory[],folder,"phi_fric.pdf"}], ϕplotFric]
Export[FileNameJoin[{NotebookDirectory[],folder,"psi_fric.pdf"}],
 ψplotFric]
Export[FileNameJoin[{NotebookDirectory[],folder,"rho.pdf"}],
 ρplotFric]
Export[FileNameJoin[{NotebookDirectory[],folder,"phi.pdf"}],
 ϕplotTot]
Export[FileNameJoin[{NotebookDirectory[],folder,"psi.pdf"}],
 ψplotTot]*)
```

In[86]:=
```
(**)
```

In[87]:=
```
(*ϕplot=
 (*ParametricPlot[{{n[t],ϕ[t]}/.bgsols,{n[t], ϕmin}/.bgsols},
  {t, t0, tmax}, PlotStyle→{{}, Dashed},
  PlotRange→Full, AxesLabel→{HoldForm[N], ϕ},
  PlotLegends→{LS[ϕ], LS[ϕmin]}, Evaluate[opts2]]*)
 LogLinearPlot[{{ϕ[t]}/.bgsols, ϕmin}, {t, t0, tmax}, PlotStyle→
     {{}, Dashed},PlotRange→Full, AxesLabel→{HoldForm[t], ϕ},
    PlotLegends→{LS[ϕ], LS[ϕmin]}, Evaluate[opts2]]
   ψplot=(*ParametricPlot[{{n[t],ψ[t]}/.bgsols,
    {n[t],ψmin[t]}/.bgsols, {n[t],ψstar[t]}/.bgsols},
   {t,t0, tmax},PlotStyle→{{}, Dashed, Dotted},
   PlotRange→Full, AxesLabel→{HoldForm[N], ψ},
   PlotLegends→{LS[ψ],LS[ψmin], LS[ψmax]} ,Evaluate[opts2]]*)
  LogLinearPlot[{ψ[t]/.bgsols}, {t,t0, tmax},
    PlotStyle→{{}, Dashed, Dotted},PlotRange→Full, AxesLabel→
     {HoldForm[t], ψ},PlotLegends→{LS[ψ]} ,Evaluate[opts2]]
   Hplot=ParametricPlot[{{n[t],Log10[H[t]]}/.bgsols,
      {n[t],Log10[KK[t]]}/.bgsols}, {t, t0, tmax},
     PlotStyle→{{}, Dashed},PlotRange→Full,
     AxesLabel→{HoldForm[N], {Log[H], Log[mKK]}},
     PlotLegends→Placed[{LS[H], LS["Kaluza-Klein Scale"]}, After],
     Evaluate[opts2]]
   (*Plot[{H[t]/.bgsols,KK[t]/.bgsols}, {t, t0, tmax},
    PlotStyle→{{}, Dashed},PlotRange→Full,
```

```
     AxesLabel→{HoldForm[t], {H, 1/b}}, PlotLegends→
      {LS[H], LS["Kaluza-Klein Scale"]}, Evaluate[opts2]]*)
   ϵplot=ParametricPlot[{{n[t],ϵ[t]}/.bgsols,
      {n[t], 0.1/16}/.bgsols}, {t, t0, tmax},
     PlotStyle→{{}, Dashed},PlotRange→Full, AxesLabel→
      {HoldForm[N],ϵ},PlotLegends→Placed[{LS[HoldForm[ϵ][t]],
        LS[ϵ==HoldForm[0.1/16]]}, After], Evaluate[opts2]]
   ηplot=ParametricPlot[{n[t],Log10[Abs[η[t]]]}/.bgsols,
     {t, t0, tmax},PlotRange→Full,AxesLabel→
      {HoldForm[N],Log[HoldForm[Abs[η]]]}, Evaluate[opts2]]
   alltermplot=LogLogPlot[{ϕ'[t]^2/2/.bgsols, ψ'[t]^2/2/.bgsols,
      FF[t]/.bgsols, (4*π*bmin^2*Exp[-ψ[t]](V[ϕ[t]]+Λ))/.bgsols,
      1/bmin^2*Exp[-2*ψ[t]]/.bgsols}, {t, t0, tmax},
     PlotLegends→{LS[ϕ'[t]^2/2], LS[ψ'[t]^2/2],LS["Flux Term"],
       LS["V-term"], LS["Curv. Term"]}, Evaluate[opts2]]
*)
```

In[88]:=
```
(* *)
```

In[89]:=
```
(*folder=FileNameJoin[{"..", "Plots", "Attractor_Max_E_Folds"}];
Export[FileNameJoin[{NotebookDirectory[],folder,"phi.pdf"}], ϕplot]
 Export[
  FileNameJoin[{NotebookDirectory[],folder,"psi.pdf"}], ψplot]
 Export[FileNameJoin[{NotebookDirectory[],folder,"H.pdf"}], Hplot]
 Export[
  FileNameJoin[{NotebookDirectory[],folder,"epsilon.pdf"}], ϵplot]
 Export[FileNameJoin[{NotebookDirectory[],folder,"eta.pdf"}],
  ηplot]
 Export[FileNameJoin[{NotebookDirectory[],
    folder,"parameters.pdf"}], parameters]
 Export[FileNameJoin[{NotebookDirectory[],folder,
    "energy_terms.pdf"}], alltermplot]*)
```

```
In[90]:= (*
         p2plot=
           LogLinearPlot[{ψ'[t]*t/.bgsols,α}, {t, t0, tmax}, PlotRange→Full,
            PlotLegends→{ψ'[t]*t, HoldForm[α]},Evaluate[opts]]
          p1plot=LogLogPlot[{ϕ'[t]*t/.bgsols, λ*α,ϕ'[t]*t^2/.bgsols},
            {t, t0, tmax}, PlotRange→Full, PlotLegends→
             {ϕ'[t]*t, HoldForm[λ*α], ϕ'[t]*t^2},Evaluate[opts]]*)

In[91]:= (*ϵ[10^13]/.bgsols[[1]]*)

In[92]:= (*ϕdotplot=LogLogPlot[{ϕ'[t]/.bgsols, 1/λ/t, 10^19.55/t^2},
           {t, t0, tmax}, AxesLabel→{t, ϕ'[t]},PlotRange→Full,PlotLegends→
            {ϕ'[t], HoldForm[1/λ/t], 10^19.55/t^2}, Evaluate[opts]]*)

In[93]:= (*ϵPlotTab=
          Table[Plot[{-H'[t]/H[t]^2/.bgsols, 1}, {t, 10^i,10^(i+1)},
            PlotRange→{0,3}, AxesLabel→{t,HoldForm[ ϵ[t]]},
            Evaluate[opts], PlotLegends→{HoldForm[ϵ[t]], ϵ==1}],
           {i, Log10[t0], Log10[tmax],1}] *)

In[94]:= (*ϵ[10^23]/.bgsols*)

In[95]:= (**)

In[96]:= (*HTabPlot=
          Table[LogPlot[{3*H[t]/.bgsols, 1/t, Θϕ}, {t, 10^i,10^(i+1)},
            Evaluate[opts], PlotLegends→{HoldForm[3*H[t]], 1/t, Γ}],
           {i, Log10[t0], Log10[tmax],1}] *)

In[97]:= (*LogLogPlot[{ϕ'[t]^2/2/.bgsols, ψ'[t]^2/2/.bgsols, ρ[t]/.bgsols},
           {t, t0, tmax}, PlotLegends→"Expressions"]
          VTermplot=LogLogPlot[{FF[t]/.bgsols,
              λ*(4*π*bmin^2*Exp[-ψ[t]](V[ϕ[t]]+Λ))/.bgsols,
              (* 1/b[t]^2/.bgsols,*) 1/bmin^2*Exp[-2*ψ[t]]/.bgsols,
              1/t^2}, {t, t0, tmax}, PlotLegends→
              {"Flux Term", "V-term", "Curv. Term", "1/t"}, Evaluate[opts]]
          alltermplot=LogLogPlot[{ϕ'[t]^2/2/.bgsols,
              ψ'[t]^2/2/.bgsols, ρ[t]/.bgsols,FF[t]/.bgsols,
              (4*π*bmin^2*Exp[-ψ[t]](V[ϕ[t]]+Λ))/.bgsols,
              1/bmin^2*Exp[-2*ψ[t]]/.bgsols}, {t, t0, tmax},
            PlotLegends→{ϕ'[t]^2/2, ψ'[t]^2/2, ρ[t],"Flux Term",
              "V-term", "Curv. Term"}, Evaluate[opts]]*)
```

```
In[98]:= (*qγtermplot=
         LogLogPlot[{t^2*ϕ'[t]/.bgsols,t^3*ρ[t]/.bgsols}, {t, t0, tmax},
          PlotLegends→{ϕ'[t]^2/2, ψ'[t]^2/2, ρ[t],"Flux Term",
            "V-term", "Curv. Term"}, Evaluate[opts]]*)

In[99]:= (*(3*α)/(θϕ)*)

In[100]:= (*{θϕ, 3*H[10^23]}/.bgsols*)

In[101]:= (*Plot[{1/t, Exp[1/t]/t}, {t, -1, 1}]*)

In[102]:= (**)

In[103]:= (*folder:="Friction Plots"
          Export[FileNameJoin[
            {NotebookDirectory[],folder,"all_term_plot.pdf"}], alltermplot]
          Export[FileNameJoin[{NotebookDirectory[],folder,
             "3H_Gamma_plot_table.pdf"}], HTabPlot]
          Export[FileNameJoin[{NotebookDirectory[],folder,
             "epsilon_plot_tab.pdf"}], ϵPlotTab]*)

In[104]:= (**)

In[105]:= (*opts2:={AxesStyle→Large, AspectRatio→1/2,
            ImageSize→Large(*, LabelStyle→Large*)}
         LS[x_]:=Style[x, Large]*)

In[106]:= (*Hplot=ParametricPlot[
          {{n[t],Log10[H[t]]}/.bgsols,{n[t],Log10[KK[t]]}/.bgsols},
          {t, t0, tmax},PlotStyle→{{}, Dashed},PlotRange→Full,
          AxesLabel→{HoldForm[N], Log[{H, 1/b}]},
          PlotLegends→{LS[H], LS["Kaluza-Klein Scale"]}, Evaluate[opts2]]*)

In[107]:= (*ϵplot=ParametricPlot[{n[t],Log10[ϵ[t]]}/.bgsols,
            {t, t0, tmax},PlotStyle→{{}, Dashed},PlotRange→Full,
            AxesLabel→{HoldForm[N],Log[ϵ]}, Evaluate[opts2]]
         ηplot=ParametricPlot[{n[t],Log10[Abs[η[t]]]}/.bgsols,
            {t, t0, tmax},PlotRange→Full,AxesLabel→
             {HoldForm[N],Log[HoldForm[Abs[η]]]}, Evaluate[opts2]]*)

In[108]:= (*LogLogPlot[{V0(Exp[-ϕ[t]/A])/.bgsols,
          V0*Exp[-ϕ[t]/B]/.bgsols,V0*(Exp[-ϕmin/A]+Exp[-ϕmin/B])},
         {t, t0, tmax}, PlotRange→Full, PlotLegends→{a,bb,c}]*)
```

In[109]:=
```
(*ψplot=(*ParametricPlot[{{n[t],ψ[t]}/.bgsols,
   {n[t],ψmin[t]}/.bgsols, {n[t],ψstar[t]}/.bgsols},
  {t,t0, tmax},PlotStyle→{{}, Dashed, Dotted},
  PlotRange→Full, AxesLabel→{HoldForm[N], ψ},
  PlotLegends→{LS[ψ],LS[ψmin], LS[ψmax]} ,Evaluate[opts2]]*)
 LogLinearPlot[{ψ[t]/.bgsols}, {t,t0*10, tmax},
  PlotStyle→{{}, Dashed, Dotted},
  PlotRange→Full, AxesLabel→{HoldForm[t], ψ},
  PlotLegends→{LS[ψ],LS[ψmin], LS[ψmax]} ,Evaluate[opts2]]*)
```

Unstable.nb

This file numerically solved (and generated plots for) the unstable Slow-roll Power-law solution.

Definitions

Here we have the definitions of our potentials, their derivatives, and some constants within them:

In[1]:=
```
(*Quit[]*)
```

In[2]:=
```
V[ϕ_] := V0 * (Exp[-ϕ / A])
Vtot[ϕ_, ψ_] :=
 4 * π * bmin^2 * Exp[-ψ] (V[ϕ] + Λ) - 1 / bmin^2 * Exp[-2 * ψ]

Vϕ[ϕ_] := (D[V[x], x]) /. x → ϕ
Vtotϕ[ϕ_, ψ_] := (D[Vtot[x, ψ], x]) /. x → ϕ
Vtotψ[ϕ_, ψ_] := (D[Vtot[ϕ, x], x]) /. x → ψ

H[t_] := Sqrt[1 / 3 (ϕ'[t]^2 / 2 + ψ'[t]^2 / 2 + Vtot[ϕ[t], ψ[t]])]
ϵ[t_] := (ϕ'[t]^2 / 2 + ψ'[t]^2 / 2) / H[t]^2;
η[t_] := (ϕ''[t] * ϕ'[t] + ψ''[t] * ψ'[t]) / (H[t]^3 * ϵ[t]) + 2 * ϵ[t]

Λ := (*1/(8*π*bmin^4)*)0
ϕmin := A * B / (B - A) * Log[B / A]
X := B / A

ψmin[t_] := Log[3] - Log[2 + Sqrt[1 - 24 * bmin^4 * π * V[ϕ[t]]]]
ψstar[t_] := Log[3] - Log[2 - Sqrt[1 - 24 * bmin^4 * π * V[ϕ[t]]]]
```

Useful Quantities

Here, we define some of the quantities that may be useful to compute:

In[15]:=
```
(*b*)
b[t_] := bmin * Exp[ψ[t] / 2]

(*Total Cosmological Constant*)
CC := V0 * (-Exp[-ϕmin / A] + Exp[-ϕmin / B]) + Λ

(*Scaling lambda: λ*)
λ := 1 / A

(*Total Flux*)
flux[t_] := (1 / Sqrt[4 * π]) (1 / bmin^2) * Exp[-ψ[t]]

(*Initial Radius*)
(*b0:=bmin*Exp[ψ0/2]*)

(*Kaluza Klein Scale*)
KK[t_] := bmin / b[t]^2
```

Dials

These are the dials we are free to tune in our models. We have defined the A and B parameters in our potential in terms of X and $\phi_{\min}$, as above, for numerical convenience.

In[20]:=
```
bmin := 10^28.
A := 18.23
B := 36.16
V0 := V0sc

(*ψ0>*)
N[ Log[1 / (4 * Sqrt[π] * bmin)]]
```

Scaling Solutions:

Here we encode the intial conditions revealed by our scaling solution so that our numerics begin in the unstable solution.

In[25]:=
```
p1 := 1 / λ
p2 := 1

α := (1 + λ^2) / (2 * λ^2)

U0 := 2 * Exp[-2 * ψ0] / (bmin^2 * (1 - λ^2));
V0sc := U0 / (4 * π * bmin^2) * Exp[λ * ϕ0 + ψ0]
t0sc := Sqrt[(1 - λ^2) * (λ^2 + 3) * bmin^2 * Exp[2 * ψ0] / (4 * λ^4)]
```

Initial Conditions

Here, we define our initial conditions.

In[31]:=
```
t0 := t0sc
tmax := 100 * t0

ϕ0 := -30.
ϕdot0 := p1 / t0

b0 := bmin * Exp[ψ0 / 2](*0.2*bmin*)
ψ0 := -30.(*2*Log[b0/bmin]*)(*0.5*)(*-19*)
ψdot0 := p2 / t0

ρ0 := 0

parameters = Multicolumn[{
    HoldForm[b_min] == N[bmin],
    HoldForm[ϕ_min] == ϕmin,
    HoldForm[X] == X,
    HoldForm[V_0] == N[V0],

    HoldForm[ϕ_diss] == N[ϕdiss],
    HoldForm[θ_ϕ] == N[θϕ],
    HoldForm[θ_ψ] == N[θψ],
    HoldForm[σ] == N[σ],

    HoldForm[t_0] == N[t0],
    HoldForm[t_max] == N[tmax],
    HoldForm[b_0] == N[b0],
```

```
  HoldForm[ρ0] == N[ρ0],

  HoldForm[ϕ0] == N[ϕ0],
  HoldForm[ϕ̇0] == N[ϕdot0],
  HoldForm[ψ0] == N[ψ0],
  HoldForm[ψ̇0] == N[ψdot0],

  HoldForm[ta] == N[ta],
  HoldForm[A] == N[A],
  HoldForm[α] == N[α],
  HoldForm[1 / α] == N[ϵexp]
 }, {4, Automatic}]
```

Physical Checks

Here we install an internal check that our numerics satisfy physical limits:
(1) Extra Dimensions (now) ≥ 1 μm
(2) Extra dimensions (start) sub-Plackian
(3) $V(\phi)$ + Λ needs to be sub-Planckian

If any one of these conditions fail, the computation stops.

In[40]:=
```
(*1*)If[bmin ≤ 6 * 10^28 / Sqrt[8 * π], "bmin ≤ 1μm ✓" , Quit[]]
(*2*)If[ψ0 ≥ Log[1 / (4 * Sqrt[π] * bmin)],
 "b initial is sub-Planckian ✓" , Quit[]]
(*3*)(*If[V[ϕ]+Λ≤1/(8*π^(3/2)*bmin^3),
 "V(ϕ) is sub-Planckian ✓" , Quit[]]*)
(*3*)Plot[{V[ϕ] + Λ, 1 / (8 * π^(3 / 2) * bmin^3)},
 {ϕ, ϕ0, ϕmin}, PlotLabel → Text[Style[Planck Scale, Orange]] >
   Text[Style[Potential, Blue]], PlotStyle → {Blue, Orange}]
```

Here we plot our potential terms to check on the relative sizes of the various terms in $V(\varphi)$.

In[43]:=
```
Plot[V[ϕ], {ϕ, ϕmin - 10, ϕmin + 10}]
```

In[44]:=
```
LogPlot[{V0 * Exp[-ϕ / A], V0 * Exp[-ϕ / B]},
 {ϕ, ϕ0, ϕmin + 5}, PlotLabel → ϕmin, GridLines → {{ϕmin}, {}}]
```

Differential Equations

Here, we numerically solve the EOMs for the above initial conditions.

In[45]:=
```
bgsols = NDSolve[{
    ϕ''[t] + 3 * H[t] * ϕ'[t] + Vtotϕ[ϕ[t], ψ[t]] == 0,
    ψ''[t] + 3 * H[t] * ψ'[t] + Vtotψ[ϕ[t], ψ[t]] == 0,
    H[t] == n'[t],
    ϕ[t0] == ϕ0, ϕ'[t0] == ϕdot0,
    ψ[t0] == ψ0, ψ'[t0] == ψdot0, n[t0] == 0}, {ϕ, ψ, n},
  {t, t0, tmax}, MaxSteps → Infinity]
```

Plots

Here we generate the plots.

In[46]:=
```
ta := 2.95 * 10^17
tb := 3 * 10^17
tc := 10^15

opts := {ImageSize → Full, GridLines → {{ta(*, tb, tc*)}, {}}}
fontsize := Large
opts2 := {AxesStyle → fontsize, AspectRatio → 1,
  ImageSize → Large, FrameStyle → fontsize,
  PlotTheme → "Scientific"(*, RotateLabel→False*)}
LS[x_] := Style[x, fontsize]

p1plotzoom = LogLogPlot[{ϕ'[t] * t /. bgsols, 1 / λ},
  {t, t0, tb}, FrameLabel → {HoldForm[t "(M_p^-1)"], p1},
  PlotStyle → {{}, Dashed}, PlotLegends →
   Placed[{LS[ϕ̇[t] t], LS[HoldForm[1 / λ]]}, {0.2, 0.85}],
  PlotRange → {18.225, 18.235}, Evaluate[opts2]]
p2plotzoom = LogLogPlot[{ψ'[t] * t /. bgsols, 1}, {t, t0, tb},
  FrameLabel → {HoldForm[t "(M_p^-1)"], p2}, PlotStyle → {{}, Dashed},
  PlotLegends → Placed[{LS[ψ̇[t] t], LS[1]}, {0.2, 0.85}],
  PlotRange → {0.99, 1.01}, Evaluate[opts2]]
p1plot = LogLogPlot[{ϕ'[t] * t /. bgsols, 1 / λ, 2 * λ / (1 + λ^2)},
  {t, t0, 20 * tb}, FrameLabel → {HoldForm[t "(M_p^-1)"], p1},
  PlotStyle → {{}, Dashed, Dotted},
  PlotLegends → Placed[{LS[ϕ̇[t] t], LS[HoldForm[1 / λ]],
     LS[HoldForm[λ α]]}, {0.7, 0.5}], Evaluate[opts2]]
p2plot = LogLogPlot[{ψ'[t] * t /. bgsols, 1, 2 / (1 + λ^2)},
  {t, t0, 20 * tb}, FrameLabel → {HoldForm[t "(M_p^-1)"], p2},
```

```
  PlotStyle → {{}, Dashed, Dotted},
  PlotLegends → Placed[{LS[ψ̇[t] t], LS[HoldForm[1]],
     LS[HoldForm[α]]}, {0.7, 0.85}], Evaluate[opts2]]
Hplot = ParametricPlot[{{n[t], Log10[H[t]]} /. bgsols,
   {n[t], Log10[KK[t]]} /. bgsols}, {t, t0, tmax},
  PlotStyle → {{}, Dashed}, PlotRange → Full,
  FrameLabel → {HoldForm[N_e]}, PlotLegends →
   Placed[{LS[Log[H / M_p]], LS[HoldForm[Log[m_KK / M_p]]]}, {0.2, 0.2}],
  AspectRatio → 1 / 2, ImageSize → 1200, Evaluate[opts2]]
ϵplot = ParametricPlot[{{n[t], Log10[ϵ[t]]} /. bgsols,
   {n[t], Log10[0.006]} /. bgsols}, (*{n[t], Log[0.5]}/.bgsols},*)
  {t, t0, tb}, PlotStyle → {{}, Dashed, Dotted},
  PlotRange → {{0, 15}, {Log10[0.005999], Log10[0.006001]}},
  AxesLabel → {HoldForm[N], Log[ê]},
  PlotLegends → Placed[{LS[HoldForm[ê]], LS[HoldForm[0.006]]
     (*, LS[ê==0.5]*)}, After], Evaluate[opts2]]
ηplot = ParametricPlot[{n[t], Abs[η[t]]} /. bgsols,
  {t, t0, tb}, PlotRange → {{0, 15}, {-0.001, 0.001}},
  AxesLabel → {HoldForm[N], HoldForm[Abs[η̂]]}, Evaluate[opts2]]

(*ϕplot=
 LogLinearPlot[{{ϕ[t]}/.bgsols, ϕmin}, {t, t0, tmax}, PlotStyle→
     {{}, Dashed},PlotRange→Full, AxesLabel→{HoldForm[t], φ},
    PlotLegends→{LS[φ], LS[φ_min]}, Evaluate[opts2]]
   ψplot=LogLinearPlot[ψ[t]/.bgsols, {t,t0, tmax},
     AxesLabel→{t, ψ}, AxesStyle→Medium, Evaluate[opts2]]
    Hplot=LogLogPlot[{H[t]/.bgsols,KK[t]/.bgsols},
      {t, t0, tmax},PlotStyle→{{}, Dashed},PlotRange→Full,
      AxesLabel→{HoldForm[t], {Ĥ, m_KK}}, PlotLegends→
       {LS[Ĥ], LS["4D Kaluza-Klein Scale"]}, Evaluate[opts2]]
     (*nplot=LogLinearPlot[n[t]/.bgsols, {t, t0, tmax},
       AxesLabel→{t, N[t]}, Evaluate[opts], PlotLabel→
        (n[ta]-n[t0]/.bgsols[[1]])"e-folds", PlotRange→Full]*)
     (*LogLogPlot[ρ[t]/.bgsols, {t, t0, tmax},
      AxesLabel→{t,ρ[t]},PlotRange→Full, Evaluate[opts]]*)
     ϵplot=(*LogLinearPlot[{ϵ[t]/.bgsols, 1},
     {t, t0, tmax},PlotRange→{0,3},
```

```
 AxesLabel→{t,HoldForm[ ϵ[t]]}, Evaluate[opts]]*)
ParametricPlot[{{n[t],Log10[ϵ[t]]}/.bgsols,
    {n[t], Log10[0.006]}/.bgsols, {n[t], Log10[0.5]}/.bgsols},
   {t, t0, tmax},PlotStyle→{{}, Dashed, Dotted},
   PlotRange→Full, AxesLabel→{HoldForm[N],Log[ê]},
   PlotLegends→Placed[{LS[HoldForm[ê]],LS[ê==HoldForm[0.006]],
      LS[ê==0.5]}, After], Evaluate[opts2]]
 ηplot=(*LogLinearPlot[Abs[η[t]]/.bgsols,
 {t, t0, tmax}, PlotRange→{0,1},
 AxesLabel→{t,HoldForm[ Abs[η[t]]]}, Evaluate[opts]]*)
ParametricPlot[{n[t],Abs[η[t]]}/.bgsols,
   {t, t0, tmax},PlotRange→Full,
   AxesLabel→{HoldForm[N],HoldForm[Abs[η̂]]}, Evaluate[opts2]]


 VTermplot=LogLogPlot[{(4*π*bmin^2*Exp[-ψ[t]](V[ϕ[t]]))/.
   bgsols, 1/bmin^2*Exp[-2*ψ[t]]/.bgsols}, {t, t0, tmax},
 PlotLegends→{ "V-term", "Curv. Term"}, Evaluate[opts]]*)

(*VTermplot2=
 LogLogPlot[{(4*π*bmin^2*Exp[-ψ[t]](V[ϕ[t]]+Λ))/.bgsols,
   1/bmin^2*Exp[-2*ψ[t]]/.bgsols,
   (4*π*bmin^2*Exp[-ψ[t]](Λ))/.bgsols}, {t, t0, tmax},
  PlotLegends→{ "V-term", "Curv. Term"}, Evaluate[opts]]*)

(*EmitSound[Sound[{SoundNote["C", 0.5],SoundNote["G", 0.5]}]]*)
```

Finally, we export the figures.

In[60]:=
```
folder = FileNameJoin[{"..", "..", "Figures", "Plots",  "Unstable"}];
Export[
 FileNameJoin[{NotebookDirectory[], folder, "p1.pdf"}], p1plot]
Export[FileNameJoin[{NotebookDirectory[], folder, "p2.pdf"}],
 p2plot]
Export[FileNameJoin[{NotebookDirectory[], folder, "p1zoom.pdf"}],
 p1plotzoom]
Export[FileNameJoin[{NotebookDirectory[], folder, "p2zoom.pdf"}],
 p2plotzoom]
Export[FileNameJoin[{NotebookDirectory[], folder, "epsilon.pdf"}],
 ϵplot]
Export[FileNameJoin[{NotebookDirectory[], folder, "eta.pdf"}],
 ηplot]
Export[FileNameJoin[{NotebookDirectory[], folder, "H.pdf"}], Hplot]
```

Appendix F

Stability of Scaling Solutions

In this appendix, we study the stability of the two scaling solutions of interest introduced in the main text. We show in particular how one of these is stable, which makes it an attractor for a wide array of initial conditions, while the other solution has a growing unstable mode that limits the amount of time the unstable solution can dominate in our numerical evolution.

We start by taking

$$\begin{aligned} \varphi &\to \varphi_\star + \delta\varphi, \\ \psi &\to \psi_\star + \delta\psi, \text{ and} \\ H &\to H_\star + \delta H, \end{aligned} \tag{F.1}$$

where (in this appendix only) $\varphi_\star, \psi_\star$, and $H_\star$ are time-dependent solutions to the zeroth order equations of motion. The equations of motion (2.26) to first order in these perturbations are:

$$\begin{aligned} \delta\ddot{\varphi} + 3\left(H_\star\delta\dot{\varphi} + \delta H\dot{\varphi}_\star\right) + \frac{\lambda U(t)}{M_p^2}\left(\lambda\delta\varphi + \delta\psi\right) &= 0 \\ \delta\ddot{\psi} + 3\left(H_\star\delta\dot{\psi} + \dot{\psi}_\star\delta H\right) + \left(\frac{U(t)}{M_p^2} - \frac{4}{b_\star^2}\, e^{-2\psi_\star/M_p}\right)\delta\psi + \frac{\lambda U(t)}{M_p^2}\,\delta\varphi &= 0 \\ 6H_\star M_p^2\,\delta H = \dot{\varphi}_\star\delta\dot{\varphi} + \dot{\psi}_\star\delta\dot{\psi} - \frac{\lambda U(t)}{M_p}\,\delta\varphi + \left(\frac{2M_p}{b_\star^2}\, e^{-2\psi_\star/M_p} - \frac{U(t)}{M_p}\right)\delta\psi & \end{aligned} \tag{F.2}$$

where $U(t) = 4\pi b_\star^2 V_0 \exp[-(\lambda\varphi_\star + \psi_\star)/M_p]$ and we have assumed a potential of the form (4.1). We then proceed to solve for δH from the last of these and use it in

the previous two equations of (F.2). Next, we substitute our power-law assumptions of the form (4.2). This yields:

$$\begin{aligned}
&\delta\ddot{\varphi} + \left(3\alpha + \frac{p_1^2}{2\alpha}\right)\frac{\delta\dot{\varphi}}{t} + \frac{\lambda U_0}{M_p^2}\left(\lambda - \frac{p_1}{2\alpha}\right)\left(\frac{t}{t_0}\right)^{-\lambda p_1 - p_2}\delta\varphi + \left(\frac{p_1 p_2}{2\alpha}\right)\frac{\delta\dot{\psi}}{t} \\
&\quad + \left[\frac{U_0}{M_p^2}\left(\lambda - \frac{p_1}{2\alpha}\right)\left(\frac{t}{t_0}\right)^{-\lambda p_1 - p_2} + \frac{p_1}{\alpha b_\star^2}\, e^{-2\psi_0/M_p}\left(\frac{t}{t_0}\right)^{-2p_2}\right]\delta\psi = 0\,, \\
&\delta\ddot{\psi} + \left(3\alpha + \frac{p_2^2}{2\alpha}\right)\frac{\delta\dot{\psi}}{t} + \left(\frac{p_1 p_2}{2\alpha}\right)\frac{\delta\dot{\varphi}}{t} + \frac{\lambda U_0}{M_p^2}\left(1 - \frac{p_2}{2\alpha}\right)\left(\frac{t}{t_0}\right)^{-\lambda p_1 - p_2}\delta\varphi \qquad \text{(F.3)} \\
&\quad + \left[\frac{U_0}{M_p^2}\left(1 - \frac{p_2}{2\alpha}\right)\left(\frac{t}{t_0}\right)^{-\lambda p_1 - p_2} + \frac{(p_2 - 4\alpha)}{\alpha b_\star^2}\, e^{-2\psi_0/M_p}\left(\frac{t}{t_0}\right)^{-2p_2}\right]\delta\psi = 0\,,
\end{aligned}$$

where U_0 is as previously defined in the main text.

We now proceed to solve these equations in the attractor and slow-roll cases to show that these cases are, indeed, an attractor and unstable, respectively.

F.1 Attractor Solution

Here, we again drop the terms that arise from perturbation in the curvature terms (in (F.3), these are the terms containing $1/b_\star^2$) and substitute our power-law solutions for this case, which are given by (4.8) and (4.9). This produces:

$$\begin{aligned}
&\delta\ddot{\varphi} + \frac{6 + \lambda^2}{1 + \lambda^2}\frac{\delta\dot{\varphi}}{t} + \frac{\lambda^2(5 - \lambda^2)}{(1 + \lambda^2)^2}\frac{\delta\varphi}{t^2} + \frac{\lambda}{1 + \lambda^2}\frac{\delta\dot{\psi}}{t} + \frac{\lambda(5 - \lambda^2)}{(1 + \lambda^2)^2}\frac{\delta\psi}{t^2} = 0\,, \qquad \text{(F.4)} \\
&\delta\ddot{\psi} + \frac{7}{1 + \lambda^2}\frac{\delta\dot{\psi}}{t} + \frac{5 - \lambda^2}{(1 + \lambda^2)^2}\frac{\delta\psi}{t^2} + \frac{\lambda}{1 + \lambda^2}\frac{\delta\dot{\varphi}}{t} + \frac{\lambda(5 - \lambda^2)}{(1 + \lambda^2)^2}\frac{\delta\varphi}{t^2} = 0\,.
\end{aligned}$$

We model the perturbations as power-law solutions of the form

$$\delta\varphi = t^n, \qquad \text{and} \qquad \delta\psi = A t^m\,. \qquad \text{(F.5)}$$

Substituting these into (F.4) gives us two equations in m and n:

$$\begin{aligned}
&\left[(\lambda^2+1)^2 n^2 + 5(\lambda^2+1)n + (5-\lambda^2)\lambda^2\right] t^n \\
&\qquad + A\lambda\left[(\lambda^2+1)m + (5-\lambda^2)\right] t^m = 0\,, \qquad \text{(F.6)}\\
&\lambda\left[(\lambda^2+1)n + (5-\lambda^2)\right] t^n \\
&\qquad + A\left[(\lambda^2+1)^2 m^2 - 5(\lambda^2+1)(\lambda^2-6)m + (5-\lambda^2)\right] t^m = 0\,.
\end{aligned}$$

If we assume $m \neq n$, then each polynomial in square brackets must vanish independently. However, since the polynomials for n and m are identical, they will have the same solution. We are left with $m = n$ and the following two equations which we then solve for n and A:

$$\begin{aligned}
n^2 + \frac{5 + A\lambda}{\lambda^2+1} n - \frac{\lambda(\lambda^2-5)(A+\lambda)}{(\lambda^2+1)^2} &= 0\,,\\
n^2 + \frac{\lambda - A(\lambda^2-6)}{A(\lambda^2+1)} n - \frac{(\lambda^2-5)(A+\lambda)}{A(\lambda^2+1)^2} &= 0\,. \qquad \text{(F.7)}
\end{aligned}$$

This system has solutions

$$n = (0,\, -1)\,, \qquad \text{with} \qquad A = \left(-\lambda,\, \frac{1}{\lambda}\right). \qquad \text{(F.8)}$$

The other two linearly independent solutions are given by $\delta\varphi = t^n,\ \delta\psi = 0$, and $\delta\varphi = 0,\ \delta\psi = t^n$, where n is given by $n = (\lambda^2-5)/(\lambda^2+1)$ in each case. (These cases amount to $A = 0, \infty$, respectively.) Since $|\lambda| < 1$, none of the perturbations grow with time (i.e., $n \leq 0\ \forall\lambda$), hence this solution is stable.

F.2 Slow-roll Solution

As in the main text, we do not drop any term that arose from perturbations in the curvature terms for this case. Substituting our power-law solutions for this case,

which are given by (4.16) and (4.17), we produce:

$$\begin{aligned}
&\delta\ddot{\varphi} + \frac{3\lambda^4+8\lambda^2+3}{2\lambda^2(1+\lambda^2)}\frac{\delta\dot{\varphi}}{t} + \frac{3+\lambda^2}{2(1+\lambda^2)}\frac{\delta\varphi}{t^2} + \frac{\lambda}{1+\lambda^2}\frac{\delta\dot{\psi}}{t} + \frac{3+\lambda^2}{2\lambda^3(1+\lambda^2)}\frac{\delta\psi}{t^2} = 0,\\
&\delta\ddot{\psi} + \frac{5\widetilde{\lambda}^4+6\lambda^2+3}{2\lambda^2(1+\lambda^2)}\frac{\delta\dot{\psi}}{t} + \frac{(\lambda^2+3)(\lambda^4+\lambda^2-1)}{2\lambda^4(1+\lambda^2)}\frac{\delta\psi}{t^2}\\
&\qquad\qquad + \frac{\lambda}{1+\lambda^2}\frac{\delta\dot{\varphi}}{t} + \frac{3+\lambda^2}{2\lambda^3(1+\lambda^2)}\frac{\delta\varphi}{t^2} = 0\,.
\end{aligned} \tag{F.9}$$

Again, we model the perturbations as power-law solutions of the form given in (F.5). We arrive at another two equations for m and n:

$$\begin{aligned}
&\lambda\left[2\lambda(\lambda^2+1)^2n^2 + (\lambda^4+6\lambda^2+3)n + (\lambda^2+3)\lambda^2\right]t^n\\
&\qquad + A\lambda\left[2\lambda^4 m + (\lambda^2+3)\right]t^m = 0\,,\\
&\lambda\left[2\lambda^4 n + (\lambda^2+3)\right]t^n\\
&\qquad + A\left[2\lambda^4(\lambda^2+1)m^2 + \lambda^2(3\lambda^4+4\lambda^2+3)m + \lambda^6+4\lambda^4-3\right]t^m = 0\,.
\end{aligned} \tag{F.10}$$

As before, these solutions are inconsistent if $m \neq n$, so, for the case where $m = n$, we have another two equations in n and A:

$$\begin{aligned}
&2\lambda^3(\lambda^2+1)n^2 + \lambda(2A\lambda^3+\lambda^4+6\lambda^2+3)n + (\lambda^2+3)(A+\lambda^3) = 0\,,\\
&2A\lambda^4(\lambda^2+1)n^2 + \lambda^2(A(3\lambda^4+4\lambda^2+3)+2\lambda^3)n\\
&\qquad + (\lambda^2+3)(A(\lambda^4+\lambda^2-1)+\lambda) = 0\,.
\end{aligned} \tag{F.11}$$

This system has solutions:

$$\begin{aligned}
n &= \left(-1, -\frac{\lambda^2+3}{2\lambda^2}, -\frac{3+\lambda^2 \pm \sqrt{(11-7\lambda^2)(\lambda^2+3)}}{4\lambda^2}\right), \quad \text{with}\\
A &= \left(\lambda, \lambda, -\frac{1}{\lambda}, -\frac{1}{\lambda}\right).
\end{aligned} \tag{F.12}$$

Since $\lambda^2 < 1$ the negative root of the third solution for n is greater than zero indicating we have one growing mode for n: hence, this solution is unstable.